Copy No. _____

Defence Research and Development Canada
Recherche et développement pour la défense Canada

DEFENCE R&D DÉFENSE

Modelling and Simulating Unsteady Six Degrees-of-Freedom Submarine Rising Maneuvers

George D. Watt

Defence R&D Canada – Atlantic

Technical Report
DRDC Atlantic TR 2007-008
February 2007

Canada

This page intentionally left blank.

Modelling and Simulating Unsteady Six Degrees-of-Freedom Submarine Rising Maneuvers

George D. Watt

Defence R & D Canada – Atlantic

Technical Report
DRDC Atlantic TR 2007-008
February 2007

Author

Original signed by George D. Watt

George D. Watt

Approved by

Original signed by Neil Pegg

Neil Pegg
Head, Warship Performance

Approved for release by

Original signed by J.L. Kennedy

K. Foster
Chair, Document Review Panel

Abstract

DRDC Atlantic is collaborating with ANSYS Canada and the University of New Brunswick to develop an unsteady, six degrees-of-freedom, Reynolds Averaged Navier-Stokes (RANS) submarine maneuvering simulation capability. Initially, this is being used to evaluate emergency rising maneuvers. During these maneuvers, high negative angles of attack can occur which result in a roll instability not previously predicted by quasi-steady modelling. The objective of the RANS simulation is to reproduce the instability and investigate mitigation strategies.

Models for weight and buoyancy when blowing, high incidence propulsion, and appendage and propulsion activation are presented and tested. A high incidence, quasi-steady, coefficient based hydrodynamic model used in previous stability analyses is also presented. These models are used for evaluating stability, testing the system models, and investigating different maneuvering scenarios in preparation for carrying out the computationally intensive RANS simulations. These preliminary investigations suggest the initial roll angle prior to blowing ballast, coupled with the roll instability and low pitch angles, plays an important role in the emergence roll angle.

Résumé

RDDC Atlantique, en collaboration avec ANSYS Canada et l'Université du Nouveau-Brunswick (UNB), développe une capacité de simulation de manœuvres instables d'un sous-marin à six degrés de liberté par l'application d'équations de Navier-Stockes à moyenne de Reynolds (RANS). Initialement, cette capacité est utilisée pour évaluer les manœuvres de remontée d'urgence. Au cours de ces manœuvres, des angles d'attaque négatifs élevés peuvent être obtenus, entraînant une instabilité du roulis qui n'était pas prévue antérieurement par la modélisation quasi-stable. L'objectif de la simulation RANS est de reproduire l'instabilité et d'en étudier les possibilités d'atténuation.

Les modèles de poids et de flottabilité lors du délestage, la propulsion à haute incidence et l'activation de l'appendice et de la propulsion sont présentés et vérifiés. On présente également un modèle hydrodynamique de haute incidence, quasi-stable et basé sur les coefficients qui est utilisé dans des analyses antérieures de stabilité. Ces modèles sont utilisés pour évaluer la stabilité, vérifier les modèles de systèmes et étudier les différents scénarios de manœuvre en préparation à l'exécution de simulations exigeant un grand nombre de calculs RANS. Les études préliminaires révèlent que l'angle de roulis initial avant le délestage, jumelé à l'instabilité du roulis et aux faibles angles de tangage, joue un rôle important dans l'angle du roulis d'émersion.

This page is intentionally blank.

Executive Summary

Introduction

DRDC Atlantic is collaborating with ANSYS Canada and the University of New Brunswick (UNB) to develop an unsteady, six degrees-of-freedom (DOF), Reynolds Averaged Navier-Stokes (RANS) simulation of a maneuvering submarine. This capability is initially being used to evaluate emergency rising maneuvers. In a typical rising scenario, ballast is blown at depth, the nose of the boat is pitched up, and speed is increased to minimize large negative angles of attack. Despite these precautions, full scale trials show that an underwater roll instability still can occur and can result in excessive roll when the boat surfaces. Quasi-steady modelling has not previously predicted satisfactorily the roll angles resulting from the instability. The objective of the collaboration is to develop the unsteady RANS simulation capability, use it to reproduce the instability and, if successful, investigate mitigation strategies.

This report presents the 6 DOF equations of motion, a coefficient based quasi-steady hydrodynamic model (a stand-in for the RANS model), and several system models required to support the simulations. It uses these models to investigate various rising scenarios, showing how blowing, the sternplanes, propulsion, control, and the initial heel angle of the boat effect the rising maneuver.

Significance

The unsteady RANS simulation capability is a step towards improving our ability to predict and understand operational limitations. It can be used in many maneuvering scenarios. The system models presented (blowing, control, and propulsion models) are used in both the RANS and coefficient based simulations. The coefficient based simulations provide an efficient test bed for preliminary investigations that will minimize the number of computationally intensive RANS simulations required later.

Principal Results

The models are described, successfully implemented, and preliminary rising simulations carried out using the coefficient based hydrodynamic model. This exercises the models and establishes suitable scenarios for the RANS simulations. Unexpectedly, this preliminary work has shown that initial heel, together with the roll instability and low pitch angles, significantly increases roll angles while rising.

Further Work

ANSYS Canada has completed development of the unsteady 6 DOF RANS simulation capability. The capability is being transferred to UNB where rising simulations will be carried out and compared with the coefficient based simulations presented herein. This will provide an opportunity to validate the current results and further investigate the role of the initial heel angle. This work should be supplemented by full scale trials to see what heel angles occur in practice and to see if mitigation strategies suggested by the simulations are realistic.

G.D. Watt, 2007. Modelling and Simulating Unsteady Six Degrees-of-Freedom Submarine Rising Maneuvers. DRDC Atlantic TR 2007–008. Defence R & D Canada – Atlantic.

Sommaire

Introduction

RDDC Atlantique, en collaboration avec ANSYS Canada et l'Université du Nouveau-Brunswick, développe une capacité de simulation de manœuvres instables d'un sous-marin à six degrés de liberté par l'application d'équations de Navier-Stockes à moyenne de Reynolds (RANS). Initialement, cette capacité est utilisée pour évaluer les manœuvres de remontée d'urgence. Dans un scénario typique de remontée, le ballast est délesté en profondeur, le devant du sous-marin est déplacé vers le haut et la vitesse est accrue pour réduire les angles d'attaque négatifs élevés. Malgré ces précautions, les essais complets démontrent que le roulis sous-marin peut encore être instable et atteindre un niveau excessif lors de l'émersion du sous-marin. La modélisation quasi-stable ne permet pas encore de prédire de façon satisfaisante l'angle de roulis causé par l'instabilité. L'objectif de la collaboration est de mettre sur pied la capacité de simulation RANS instable, de l'utiliser pour reproduire l'instabilité et, le cas échéant, d'en étudier les possibilités d'atténuation.

Le présent rapport présente les équations de mouvement à six degrés de liberté, un modèle hydrodynamique quasi-stable basé sur les coefficients (remplaçant le modèle RANS), et plusieurs autres modèles requis pour appuyer les simulations. Le rapport utilise ces modèles pour exposer différents scénarios de remontée afin de démontrer comment le ballast, les tableaux arrière, la propulsion, le contrôle et l'angle de gîte initial du sous-marin ont un impact sur la manœuvre de remontée.

Portée

La capacité de simulation RANS quasi-stable est une étape vers l'amélioration de notre habileté à prédire et comprendre les limites opérationnelles. Cette capacité peut être utilisée dans de nombreux scénarios de manœuvres. Les modèles de système présentés (modèles de délestages, de contrôle et de propulsion) sont utilisés dans les simulations basées sur RANS et les coefficients. Les simulations basées sur les coefficients fournissent un banc d'essai éventuel pour des recherches préliminaires qui réduiront les simulations à grand nombre de calculs RANS, qui seront nécessaires plus tard.

Résultats

Les modèles sont décrits et appliqués avec succès, et des simulations préliminaires de remontée sont effectuées à l'aide d'un modèle hydrodynamique basé sur les coefficients. Les modèles sont ainsi mis à l'épreuve et servent à établir des scénarios adaptés aux simulations RANS. Contre toute attente, ce travail préliminaire a démontré que le gîte initial, jumelé à l'instabilité du roulis et aux faibles angles de tangage, augmente de façon significative les angles du roulis lors de la remontée du sous-marin.

Recherches futures

ANSYS Canada a terminé le développement de la capacité de simulation RANS instable à six degrés de liberté. La capacité est transférée à l'UNB où des simulations de remontée seront effectuées et comparées avec les simulations basées sur les coefficients qui sont présentées ici. Il sera donc possible de valider les résultats actuels et de pousser l'étude sur le rôle de l'angle de gîte initial. Ce travail devrait être enrichi par des essais complets visant à déterminer les angles de gîte réels et à vérifier si les possibilités d'atténuation suggérées par les simulations sont réalistes.

G.D. Watt, 2007. Modélisation et simulation de manœuvres instables de remontée d'un sous-marin à six degrés de liberté. RDDC Atlantique TR 2007–008. R & D pour la défense Canada – Atlantique.

Table of Contents

Nomenclature

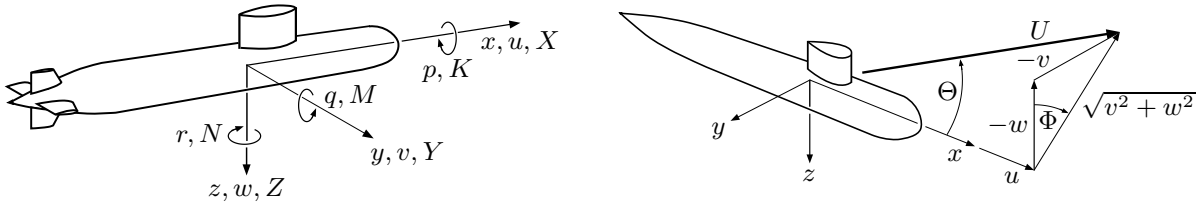

CB, CG	Centers of buoyancy and gravity.
d	Maximum hull diameter.
D	Propeller diameter.
$B = \rho V g$	Buoyancy.
$\overline{BG} = z_G - z_B$	Height of the CB above the CG.
g	Gravitational constant.
I	Moments of inertia in body axes.
J, J_b	Propeller advance ratio and behind-the-boat advance ratio.
K, M, N	Body axis moments.
K', M', N'	Body axis moments nondimensionalized by $\rho U^2 \ell^3/2$.
K_P	Effect of propeller torque on rolling moment K.
K_T, K_Q	Propeller thrust and torque coefficients.
ℓ	Overall length of the hull.
m, m_o	Mass, initial mass within V.
MBT	Main Ballast Tank; several at different axial locations.
n	Propeller revolutions per second, rps.
N	Number of MBTs.
p_a	Atmosperic pressure.
p, q, r	Body axis angular velocities.
Q	Propeller torque.
R	Gas constant for air.
$\mathbf{R} = U\ell/\nu$	Reynolds number.
t, t_e	Time, time of emergence.
t	Propeller thrust deduction (in §4).
T	Thrust (in §4).
T	Temperature (in §5).
u, v, w	Body axis velocities.
w_T, w_{T0}	Taylor wake fraction, generally and at zero incidence.
$U = \sqrt{u^2 + v^2 + w^2}$	Overall speed of vehicle.
U_S	Roll stability index, m/s.
V	Volume of the external hydrodynamic envelope, including main ballast tanks.

V_a, V_{ai}	Volume of air in all MBTs, and in tank i.
V_A	Speed of advance of propeller.
V_T, V_{Ti}	Volume of all MBTs, and of tank i.
$W = mg$	Weight within V.
x, y, z	Body fixed axes.
x_0, y_0, z_0	Inertial (earth-fixed) axes.
x_B, y_B, z_B	Coordinates of CB (centroid of V) in body axes.
x_G, y_G, z_G	Coordinates of CG (center of mass m) in body axes.
x_{Ti}, z_{Ti}	Coordinates of the centroid of MBT i; $y_{Ti} \equiv 0$.
x_μ, z_μ	Coordinates of the centroid of the blown mass fraction; $y_\mu \equiv 0$.
X, Y, Z	Body axis forces.
X', Y', Z'	Body axis forces nondimensionalized by $\rho U^2 \ell^2/2$.
X_P	Effect of propeller thrust on axial force X.
z_{wi}	Depth below the ocean surface of the water level in MBT i.
$\alpha = \tan^{-1}(w/u)$	Angle of attack.
$\beta = \tan^{-1}(-v/u)$	Angle of drift.
$\delta_r, \delta_s, \delta_b$	Rudder, stern, and foreplane deflections; direction is found from the right hand rule using body axes.
$\Theta = \tan^{-1}(\sqrt{v^2 + w^2}/u)$	Flow incidence, always positive.
μ, μ_i	Blown mass fraction, overall and for tank i.
ν	Kinematic viscosity of water.
ρ	Density of sea water.
$\Phi = \tan^{-1}(-v/-w)$	Flow orientation.
ψ, θ, ϕ	Yaw, pitch, and roll Euler angles giving body axes orientation relative to inertial axes.
ϕ_o	Initial heel, the roll angle prior to blowing ballast.

Subscripts

a	The blown air in the MBTs.
c	A command.
o	The condition immediately prior to blowing the MBTs.
t	The trim component.
T	Main ballast tank.
U	Value at which the vehicle becomes unstable (when $U_S = 0$).

A dot over a symbol indicates differentiation with respect to time; eg, $\dot{u} = du/dt$. The following relations are useful:

$$u = U\cos\Theta \qquad v = -U\sin\Theta\sin\Phi$$
$$w = -U\sin\Theta\cos\Phi \qquad \sqrt{v^2 + w^2} = U\sin\Theta$$

Acknowledgment

The author very much appreciated feedback from Mr. Mark Bettle, graduate student, University of New Brunswick, which enabled important corrections to be made to this report.

1 Introduction

6 DOF RANS Simulation

DRDC Atlantic is collaborating with ANSYS Canada and the University of New Brunswick (UNB) to develop an unsteady, six degrees-of-freedom (DOF), Reynolds Averaged Navier-Stokes (RANS) submarine maneuvering simulation capability. This capability is needed to validate fast, coefficient based simulations used to investigate maneuvering limitations and establish safe operating envelopes for underwater vehicles. Several countries (eg, the US, UK, France) use a free swimming scale model for such validations which, according to the US [1], "is currently the best predictor of full scale submarine maneuvering performance." These facilities cost tens of millions of dollars to develop, maintain, and use. A computational fluid dynamics (CFD) validation is much cheaper and capable of providing better detail. The disadvantage to a CFD capability is that its predictions are not as reliable as experiments. But CFD technology is evolving quickly so it is worth developing and evaluating this capability. By collaborating with a successful commercial CFD vendor, there is potential for commercializing the capability thereby minimizing ongoing maintenance and development costs.

ANSYS Canada has developed a basic capability for use with its commercial RANS code CFX [2]. It requires that the flow field be discretized with a rigid, body fixed mesh extending from the surface of the vehicle out to the far field. The mesh and boat move together controlled by the same 6 DOF solid body equations of motion used by the DRDC Submarine Simulation Program (DSSP) [3]. Unlike DSSP, which inputs quasi-steady hydrodynamic information and solves the equations of motion, CFX solves the unsteady RANS equations for the fluid flow about the submarine, calling the solid body equations of motion for information on how to change the flow boundary conditions at each time step. CFX passes the unsteady hydrodynamic forces to the solid body equations which account for inertia, buoyancy, propulsion, and control forces using the models presented below. The CFX simulation is at best second order accurate in space and time while DSSP is fourth order accurate in time. However, the CFX time steps are much smaller than those used by DSSP since they are determined by the complex, unsteady hydrodynamic flow being modelled.

Currently, the CFX simulation can model any maneuver in which the boat is deeply submerged and isolated from any other vehicle or boundary. In developing the current model, an alternative approach using a moving mesh formulation [2] was investigated. This would allow the mesh to deform with time as the boat moves toward or away from a boundary or other vehicle, as would be the case for littoral or two-body problems. Further development is required to complete implementation of the moving mesh capability in the 6 DOF simulation.

The CFX simulation has been passed to UNB for evaluation. It will use the DRDC generic submarine shape for which extensive experimental data are available. The maneuver to be evaluated is a submarine rising maneuver that results in an instability conventional quasi-steady coefficient based hydrodynamic models so far have not satisfactorily reproduced [4,5]. It is a good test case as the submarine can be modelled as an isolated deeply submerged body throughout the maneuver (the underwater roll instability develops before the boat surfaces).

Emergency Rising Maneuver

In emergencies, submarines can blow ballast at depth to get to the surface fast. In a typical scenario, ballast is blown while the boat is proceeding ahead in straight and level flight. Sternplane control is used to immediately pitch up the nose of the boat and speed is increased to minimize large negative angles of attack resulting from buoyancy. Propulsion and the buoyancy component in the axial direction accelerate the boat towards the surface (Figure 1).

The buoyancy component normal to the hull axis generates a crossflow ($-w$ in Figure 1) which results in large flow incidence (Θ) angles. In trials with small to medium sized submarines, this flow incidence can result in a roll instability [4,5]. The instability occurs because the sail is pointing into the crossflow. With small submarines (around 1000 t), underwater roll angles as large as 25 degrees are seen. With large diesel boats (2000 to 3000 t), the underwater roll angle is less than half that but still large enough to instigate excessive roll when the boat surfaces and temporarily loses static stability (until flood water drains from its sail and deck casing). The problem is most severe in small boats because the instability is caused by the destabilizing hydrodynamic force on the sail (proportional to sail size) overcoming static stability (proportional to boat mass). And sail size tends not to diminish as boats get smaller whereas, of course, boat mass does.

The objective of the evaluation is to reproduce through simulation the underwater roll instability of a 3000 t boat and, if successful, to investigate mitigation strategies. This report:

1) develops the solid body model that CFX will call for its unsteady boundary conditions,
2) develops a fast, quasi-steady, coefficient based hydrodynamic model as a stand-in for the RANS model and uses it to establish preliminary rising scenarios.

The first step is to present the solid-body equations of motion for the vehicle. These are six, second order, ordinary differential equations (ODEs) adapted from Feldman's standard equations [6]. The coefficient based hydrodynamic model is then presented followed by a high incidence propulsion model. A weight and buoyancy model accounting for high pitch angles and a variable $\overline{BG}$ value during the blow is developed and, finally, a control model is presented that is used for changing appendage deflection and propulsion states in the simulations.

The report finishes by carrying out several simulations using the coefficient model. This exercises all but the RANS modelling and establishes suitable scenarios for the RANS simulations to follow. This is an invaluable aid in understanding the complex interplay between the many parameters, allowing wise use to be made of the extensive computational resources the RANS simulations will require.

The coefficient based simulations show a roll instability is present and, surprisingly, generates significant roll angles if an appreciable initial heel angle (≈ 2 degrees) is present. This is a new result and reflects the fact that several key characteristics are, for the first time, being modelled simultaneously. If the RANS simulations can validate these results, the rising stability problem may be solved.

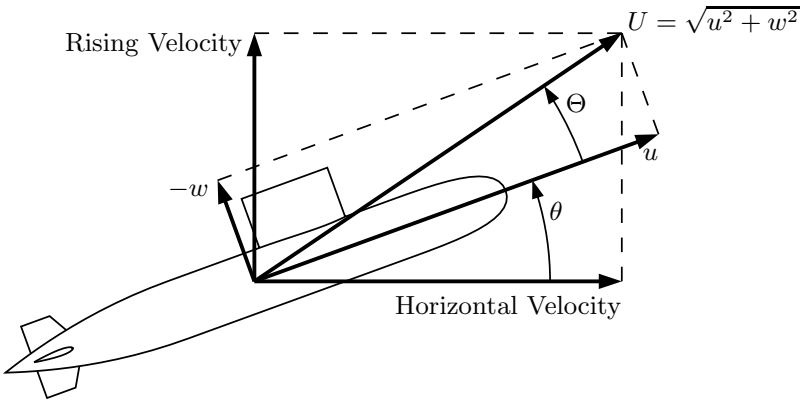

Figure 1 *A buoyant rise with no roll ($\Phi, \phi = 0$).*

2 The Solid Body Equations of Motion

The standard submarine equations of motion [6] are well known, extensively used in underwater vehicle simulations, and readily integrated numerically using a standard ODE solver. The equations describe the time dependency in 12 defining vehicle states:

$$\mathbf{y} = u, v, w, p, q, r, x_0, y_0, z_0, \phi, \theta, \psi \tag{1}$$

The first six states are the translational and rotational vehicle velocities in body fixed axes. The next three are the coordinates of the origin of the body fixed axes in inertial space. The final three are the Euler angles orienting the body fixed axes relative to inertial space. The Euler angles must be applied in a consistent order: if the x, y, z body axes are initially aligned with the x_0, y_0, z_0 inertial axes, the body axes are oriented by yawing about the z axis through an angle ψ, pitching about the y axis through an angle θ, and then rolling about the x axis through an angle ϕ.

The six equations of motion follow. They are known as the 'solid body' equations in the current collaboration as they describe the motion of a rigid, solid body through a fluid, as opposed to the equations of motion for the fluid itself which are solved by the RANS solver. The LHS of the equations, the 'rate of change of momentum' terms expressed in body fixed coordinates, are exact for a rigid body. The RHS terms describe the forces on the vehicle: the hydrodynamic forces F_H, the static weight W and buoyancy B forces, and where applicable the appendage control forces F_C and propulsor forces F_P.

Axial Force

$$m\Big[\dot{u} - vr + wq - x_G(q^2 + r^2) + y_G(pq - \dot{r}) + z_G(pr + \dot{q})\Big] = X_H(t, \mathbf{y}) - (W - B)\sin\theta + X_C(t, \mathbf{y}) + X_P(t, \mathbf{y}) \tag{2a}$$

Lateral Force

$$m\Big[\dot{v} - wp + ur - y_G(r^2 + p^2) + z_G(qr - \dot{p}) + x_G(qp + \dot{r})\Big] = Y_H(t, \mathbf{y}) + (W - B)\cos\theta\sin\phi + Y_C(t, \mathbf{y}) \tag{2b}$$

Normal Force

$$m\Big[\dot{w} - uq + vp - z_G(p^2 + q^2) + x_G(rp - \dot{q}) + y_G(rq + \dot{p})\Big] = Z_H(t, \mathbf{y}) + (W - B)\cos\theta\cos\phi + Z_C(t, \mathbf{y}) \tag{2c}$$

Rolling Moment

$$I_x\dot{p} + (I_z - I_y)qr - (\dot{r} + pq)I_{zx} + (r^2 - q^2)I_{yz} + (pr - \dot{q})I_{xy} + m\Big[y_G(\dot{w} - uq + vp) - z_G(\dot{v} - wp + ur)\Big] = K_H(t, \mathbf{y}) + (y_G W - y_B B)\cos\theta\cos\phi - (z_G W - z_B B)\cos\theta\sin\phi + K_P(t, \mathbf{y}) \tag{2d}$$

Pitching Moment

$$I_y\dot{q} + (I_x - I_z)rp - (\dot{p} + qr)I_{xy} + (p^2 - r^2)I_{zx} + (qp - \dot{r})I_{yz} + m\Big[z_G(\dot{u} - vr + wq) - x_G(\dot{w} - uq + vp)\Big] = M_H(t, \mathbf{y}) - (x_G W - x_B B)\cos\theta\cos\phi - (z_G W - z_B B)\sin\theta + M_C(t, \mathbf{y}) \tag{2e}$$

Yawing Moment

$$I_z\dot{r} + (I_y - I_x)pq - (\dot{q} + rp)I_{yz} + (q^2 - p^2)I_{xy} + (rq - \dot{p})I_{zx} + m\Big[x_G(\dot{v} - wp + ur) - y_G(\dot{u} - vr + wq)\Big] = N_H(t, \mathbf{y}) + (x_G W - x_B B)\cos\theta\sin\phi + (y_G W - y_B B)\sin\theta + N_C(t, \mathbf{y}) \tag{2f}$$

The m and W parameters here refer to the total mass/weight enclosed by the hydrodynamic envelope, including any free flooding water enclosed by this envelope and forced to move with the vehicle (eg, ballast tank flood water). The I_{ij} terms are the moments and products of inertia of this mass and x_G, y_G, z_G locate its center, all in body fixed coordinates. The equations assume that the mass m, including the flood water, translates and rotates as a rigid body. The center of buoyancy coordinates x_B, y_B, z_B locate the centroid of the hydrodynamic envelope. The buoyancy B is the volume within this envelope multiplied by the water density.

The equations of motion assume the mass is rigid and constant. They neglect the contribution of dm/dt and dI/dt terms in the momentum equation which occur when ballast is blown. This is justified on the basis that the overall mass change is small (less than 10%) and takes place slowly. The simulations do model the change of mass with time but only in a quasi-steady manner. (The RANS hydrodynamic model is a true unsteady model.)

Equations (2) are first order ODE's in the body axes velocities but, implicitly, are second order in positional coordinates. Body axis positional coordinates are not of interest so the following 'auxiliary' first order ODE's are integrated simultaneously with (2) to give the inertial coordinates and Euler angles:

$$\dot{x}_0 = u\cos\theta\cos\psi + v(\sin\phi\sin\theta\cos\psi - \cos\phi\sin\psi) + w(\sin\phi\sin\psi + \cos\phi\sin\theta\cos\psi) \tag{3a}$$

$$\dot{y}_0 = u\cos\theta\sin\psi + v(\cos\phi\cos\psi + \sin\phi\sin\theta\sin\psi) + w(\cos\phi\sin\theta\sin\psi - \sin\phi\cos\psi) \tag{3b}$$

$$\dot{z}_0 = -u\sin\theta + v\cos\theta\sin\phi + w\cos\theta\cos\phi \tag{3c}$$

$$\dot{\phi} = p + (r\cos\phi + q\sin\phi)\tan\theta \tag{3d}$$

$$\dot{\theta} = q\cos\phi - r\sin\phi \tag{3e}$$

$$\dot{\psi} = \frac{r\cos\phi + q\sin\phi}{\cos\theta} \tag{3f}$$

Note that (3d) and (3f) make the equations singular at pitch angles of ± 90 degrees.

Equations (2) and (3) define 12 nonlinear, coupled, first order ordinary differential equations in the 12 states (1). To integrate the equations numerically, they must be in the form:

$$\dot{\mathbf{y}} = f(t, \mathbf{y})$$

Equations (3) are already in this form but (2) are not. They are put in the correct form by inverting the coefficient matrix in the following reformulation of (2):

$$\begin{pmatrix} m & 0 & 0 & 0 & mz_G & -my_G \\ 0 & m & 0 & -mz_G & 0 & mx_G \\ 0 & 0 & m & my_G & -mx_G & 0 \\ 0 & -mz_G & my_G & I_x & -I_{xy} & -I_{zx} \\ mz_G & 0 & -mx_G & -I_{xy} & I_y & -I_{yz} \\ -my_G & mx_G & 0 & -I_{zx} & -I_{yz} & I_z \end{pmatrix} \begin{pmatrix} \dot{u} \\ \dot{v} \\ \dot{w} \\ \dot{p} \\ \dot{q} \\ \dot{r} \end{pmatrix} = \begin{pmatrix} f_X(t,\mathbf{y}) \\ f_Y(t,\mathbf{y}) \\ f_Z(t,\mathbf{y}) \\ f_K(t,\mathbf{y}) \\ f_M(t,\mathbf{y}) \\ f_N(t,\mathbf{y}) \end{pmatrix} \tag{4}$$

where $f_F(t, \mathbf{y})$ contains all the terms from both the right and left hand sides of (2) that have no explicit $\dot{\mathbf{y}}$ terms.

For simulations in which the mass, mass centroid, and moments of inertia do not change with time, the coefficient matrix in (4) need only be inverted once. For simulations in which the mass terms change with time, as they do when blowing ballast, matrix inversion must occur

at each time step. This is a straightforward calculation that can be carried out quickly using efficient, compiled algorithms readily available in many scientific utility software packages.

In the RANS simulations, F_H in (2) is modelled in its entirety by the RANS solver. This is accomplished using a body fitted mesh about DRDC's generic submarine shape which consists of an axisymmetric hull, a sail, and four identical tail fins in a symmetric '+' configuration. There is no propeller and so propulsion forces are accounted for separately. Similarly, the appendages do not deflect so control forces must be accounted for separately. Hence the separate F_C and F_P terms in (2). Keeping propulsion and appendage deflection out of the RANS model will considerably reduce computation time and complexity; these capabilities can be added in future if required. Of course, the hydrodynamic stability provided by the appendages is present in the RANS model because the appendages are present.

Submarine tailfins in a + configuration typically do not deflect differentially. Thus, there are no appendage control forces in the rolling moment equation of motion.

Using Hydrodynamic Coefficients With the Solid Body Equations

For rapid, preliminary simulations, F_H in (2) is replaced with a coefficient based model. This model accounts for 'added mass' (see Watt [7]) using acceleration coefficients. This approach is suggested by potential flow theory where the unsteady component of the forces exerted on a vehicle moving through an inviscid fluid can be written exactly as:

$$\text{Unsteady component of } F_H = \begin{pmatrix} X_{\dot{u}} & X_{\dot{v}} & X_{\dot{w}} & X_{\dot{p}} & X_{\dot{q}} & X_{\dot{r}} \\ Y_{\dot{u}} & Y_{\dot{v}} & Y_{\dot{w}} & Y_{\dot{p}} & Y_{\dot{q}} & Y_{\dot{r}} \\ Z_{\dot{u}} & Z_{\dot{v}} & Z_{\dot{w}} & Z_{\dot{p}} & Z_{\dot{q}} & Z_{\dot{r}} \\ K_{\dot{u}} & K_{\dot{v}} & K_{\dot{w}} & K_{\dot{p}} & K_{\dot{q}} & K_{\dot{r}} \\ M_{\dot{u}} & M_{\dot{v}} & M_{\dot{w}} & M_{\dot{p}} & M_{\dot{q}} & M_{\dot{r}} \\ N_{\dot{u}} & N_{\dot{v}} & N_{\dot{w}} & N_{\dot{p}} & N_{\dot{q}} & N_{\dot{r}} \end{pmatrix} \begin{pmatrix} \dot{u} \\ \dot{v} \\ \dot{w} \\ \dot{p} \\ \dot{q} \\ \dot{r} \end{pmatrix} \tag{5}$$

The coefficient matrix here is the added mass matrix. It is symmetric. When divided by ρ it is a function only of vehicle geometry. Potential flow predictions of these coefficients agree well with measurements made in simple acceleration (oscillation) experiments in water. On the other hand, potential flow predictions of the steady state forces do not agree well with experiment because they cannot predict vorticity nor, therefore, lift on a moving body. Vortical flows also result in unsteady forces that are not modelled by (5) and which may be a contributing factor to the failure of coefficient based models to predict the rising instability [5].

The diagonal added mass matrix coefficients have the largest magnitudes. The following off-diagonal coefficients are identically zero when the vehicle has a vertical plane of symmetry as the current geometry does:

$$X_{\dot{v}}, X_{\dot{p}}, X_{\dot{r}},\ Y_{\dot{u}}, Y_{\dot{w}}, Y_{\dot{q}},\ Z_{\dot{w}}, Z_{\dot{p}}, Z_{\dot{r}},\ K_{\dot{u}}, K_{\dot{w}}, K_{\dot{q}},\ M_{\dot{v}}, M_{\dot{q}}, M_{\dot{r}},\ N_{\dot{u}}, N_{\dot{w}}, N_{\dot{q}} = 0 \tag{6}$$

The reason for introducing the coefficient model in this section is that its added mass model necessitates changes to (4). Explicit acceleration terms in F_H in (2) must be combined with

similar terms on the LHS so that (2) becomes:

$$\begin{pmatrix} m-X_{\dot{u}} & 0 & -X_{\dot{w}} & 0 & mz_G-X_{\dot{q}} & -my_G \\ 0 & m-Y_{\dot{v}} & 0 & -mz_G-Y_{\dot{p}} & 0 & mx_G-Y_{\dot{r}} \\ -Z_{\dot{u}} & 0 & m-Z_{\dot{w}} & my_G & -mx_G-Z_{\dot{q}} & 0 \\ 0 & -mz_G-K_{\dot{v}} & my_G & I_x-K_{\dot{p}} & -I_{xy} & -I_{zx}-K_{\dot{r}} \\ mz_G-M_{\dot{u}} & 0 & -mx_G-M_{\dot{w}} & -I_{xy} & I_y-M_{\dot{q}} & -I_{yz} \\ -my_G & mx_G-N_{\dot{v}} & 0 & -I_{zx}-N_{\dot{p}} & -I_{yz} & I_z-N_{\dot{r}} \end{pmatrix} \begin{pmatrix} \dot{u} \\ \dot{v} \\ \dot{w} \\ \dot{p} \\ \dot{q} \\ \dot{r} \end{pmatrix}$$

$$= \begin{pmatrix} f_X(t,\mathbf{y}) - \text{unsteady } X_H \text{ component} \\ f_Y(t,\mathbf{y}) - \text{unsteady } Y_H \text{ component} \\ f_Z(t,\mathbf{y}) - \text{unsteady } Z_H \text{ component} \\ f_K(t,\mathbf{y}) - \text{unsteady } K_H \text{ component} \\ f_M(t,\mathbf{y}) - \text{unsteady } M_H \text{ component} \\ f_N(t,\mathbf{y}) - \text{unsteady } N_H \text{ component} \end{pmatrix} \equiv \begin{pmatrix} g_X(t,\mathbf{y}) \\ g_Y(t,\mathbf{y}) \\ g_Z(t,\mathbf{y}) \\ g_K(t,\mathbf{y}) \\ g_M(t,\mathbf{y}) \\ g_N(t,\mathbf{y}) \end{pmatrix} \tag{7}$$

As for (4), the coefficient matrix in (7) must be inverted at each timestep of the numerical integration if the mass terms change. The added mass coefficients do not change as long as the external vehicle shape does not change.

3 The Quasi-Steady, Coefficient Based Hydrodynamic Model

This model is used for preliminary calculations, to explore the effects of the modelling parameters on the simulation and select values which reproduce maneuvers with the desired characteristics. It is based on Feldman's standard equations [6]. Differences are:

- except for added mass, Feldman's unsteady model is not used,
- translation hydrodynamics are modelled using high incidence experimental data acquired at up to 30 degrees incidence at $\mathbf{R} = 23$ million with the same generic submarine shape used in the RANS model; this data is presented in Figure 8 in Reference [5] and referred to below as the F_{uvw} function,
- a high incidence propulsion model is used based, again, on experiments with our generic submarine shape,
- simple tailplane control models are used which allow the desired maneuver to be achieved; the effect of propulsive state on tailplane control is not modelled.

The subsections below present the g_F functions from (7), isolating the quasi-steady terms from the LHS of (7) on the first line, and the F_C functions from the RHS of (2) so they are easily identified for use in the RANS simulation. The propulsion and weight and buoyancy models are discussed in detail in subsequent sections.

The last lines in the g_F functions below contain special functions and the weight and buoyancy terms. The middle lines contain constant coefficients multiplying state velocities. The coefficients are either suggested by Feldman, by potential flow analysis [7], and/or result from force estimates made by Mackay's DSSP20 program [8] and converted to first and second order derivatives using the DERIVS program [9].

The F_{uvw} functions are plotted in Figure 2. These functions, all of the coefficients listed below, the mass and added mass coefficients from the LHS of (7), and many other relevant physical constants for the simulations are listed in Appendix A. All of the F_{ij} coefficients below are constants unless a dependency is explicitly indicated.

Axial Force

Feldman's $X_{vv}v^2 + X_{ww}w^2 -$ Drag translation terms are included in the $X'_{uvw}(\Theta, \Phi)$ function. To avoid having to model serious discontinuities, this function ignores the effect of sail stall which occurs when $\Theta > 23$ degrees for $\Phi = 60$ to 120 degrees, a flow regime not expected to be important for the current simulations. The only other force suffering the same restriction is rolling moment.

$$\begin{aligned} g_X(t, \mathbf{y}) = m\big[&vr - wq + x_G(q^2 + r^2) - y_G pq - z_G pr\big] \\ &+ X_{uq}uq + X_{vr}vr + X_{wp}wp + X_{wq}wq + X_{pp}p^2 + X_{rp}rp + X_{qq}q^2 + X_{rr}r^2 + X_{q|q|}q|q| \\ &+ \frac{1}{2}\rho U^2 \ell^2 X'_{uvw}(\Theta, \Phi) + X_C(t, \mathbf{y}) + X_P(t, \mathbf{y}) - (W - B)\sin\theta \end{aligned} \tag{8a}$$

where:

$$X_C(t, \mathbf{y}) = \frac{1}{2}\rho\ell^2 \left(X'_{\delta_s \delta_s}{\delta_s}^2 + X'_{\delta_r \delta_r}{\delta_r}^2\right) u^2 \tag{8b}$$

These latter terms model the drag generated by tailplane deflections.

Lateral Force

A linear model is used for tailplane control derivatives which ignores tailplane stall. The lateral force generated by the rudder is not large but, since the rudder is at the end of the boat, the long moment arm provides good yaw control.

$$\begin{aligned} g_Y(t, \mathbf{y}) = m\big[&wp - ur + y_G(r^2 + p^2) - z_G qr - x_G qp\big] \\ &Y_{up}up + Y_{ur}ur + Y_{wp}wp + Y_{wr}wr + Y_{pq}pq + Y_{qr}qr + Y_{p|p|}p|p| + Y_{r|r|}r|r| \\ &+ \frac{1}{2}\rho U^2 \ell^2 Y'_{uvw}(\Theta, \Phi) + Y_C(t, \mathbf{y}) + (W - B)\cos\theta\sin\phi \end{aligned} \tag{9a}$$

where:

$$Y_C(t, \mathbf{y}) = \frac{1}{2}\rho\ell^2 Y'_{\delta_r} u^2 \delta_r \tag{9b}$$

Normal Force

Sternplane control is to normal force what rudder control is to lateral force. It is a small force that takes advantage of a long moment arm to provide good pitch control.

$$\begin{aligned} g_Z(t, \mathbf{y}) = m\big[&uq - vp + z_G(p^2 + q^2) - x_G rp - y_G rq\big] \\ &+ Z_{uq}uq + Z_{vp}vp + Z_{wp}wp + Z_{wq}wq + Z_{pp}p^2 + Z_{rp}rp + Z_{qq}q^2 + Z_{rr}r^2 + Z_{q|q|}q|q| \\ &+ \frac{1}{2}\rho U^2 \ell^2 Z'_{uvw}(\Theta, \Phi) + Z_C(t, \mathbf{y}) + (W - B)\cos\theta\cos\phi \end{aligned} \tag{10a}$$

where:

$$Z_C(t, \mathbf{y}) = \frac{1}{2}\rho\ell^2 Z'_{\delta_s} u^2 \delta_s \tag{10b}$$

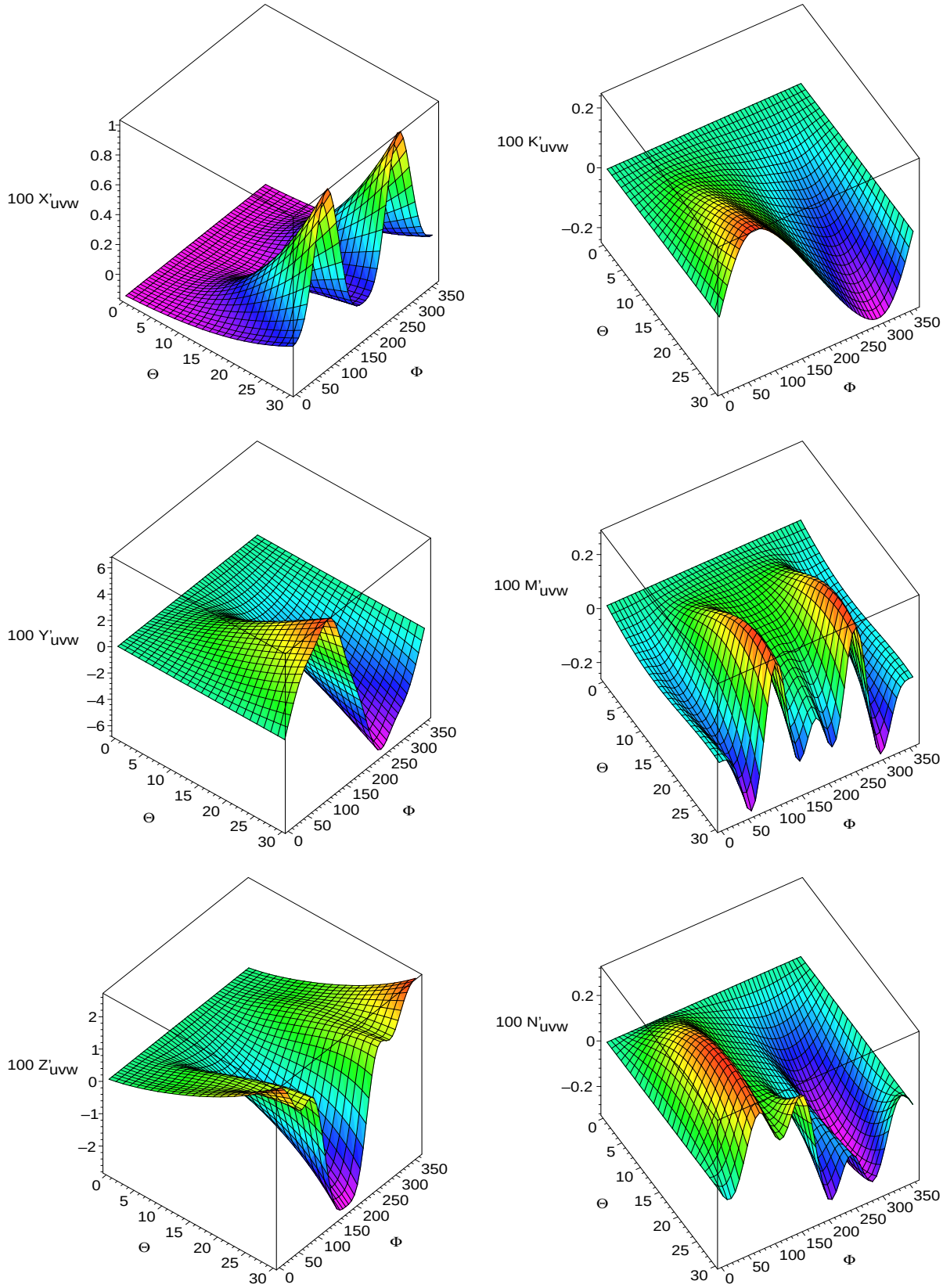

Figure 2 *The six $F_{uvw}(\Theta, \Phi)$ forces used in the coefficient model (angles in degrees).*

Rolling Moment

The K'_{δ_r} term is included for generality but it is zero for our generic shape which has a symmetric rudder centered on a symmetric hull and a body axes origin located on the hull centerline. The propulsion system uses a propeller which uses torque to generate thrust. This generates a moment K_P capable of rolling the boat a fraction of a degree or so. It is useful to model in a rising stability investigation because it introduces a small roll angle, the initial displacement a roll instability needs to take hold. As with axial force, the $K'_{uvw}(\Theta,\Phi)$ function does not model the discontinuity resulting from sail stall which occurs when $\Theta > 23$ degrees for $\Phi = 60$ to 120 degrees.

Heel and stability are controlled by the lateral and vertical locations of the centers of gravity and buoyancy. In general, $y_B \approx 0$ and is fixed by the shape of the hydrodynamic envelope. On the other hand, y_G can be adjusted by moving mass laterally which is typically done to trim the boat in roll. The important $(z_B B - z_G W)\cos\theta\sin\phi$ static stability term is the only mechanism the boat has for remaining upright in the presence of propeller torque and destabilizing hydrodynamic forces. Static stability is proportional to $\overline{BG} = z_G - z_B$, the height of the CB above the CG.

$$\begin{aligned} g_K(t,\mathbf{y}) &= (I_y - I_z)qr + I_{zx}pq - I_{yz}(r^2 - q^2) - I_{xy}pr + m\big[y_G(uq - vp) - z_G(wp - ur)\big] \\ &\quad + K_{up}up + K_{ur}ur + K_{vq}vq + K_{wp}wp + K_{wr}wr + K_{pq}pq + K_{qr}qr + K_{p|p|}p|p| + K_{r|r|}r|r| \\ &\quad + \frac{1}{2}\rho U^2\ell^3 K'_{uvw}(\Theta,\Phi) + K_C(t,\mathbf{y}) + K_P(t,\mathbf{y}) \\ &\quad + (y_G W - y_B B)\cos\theta\cos\phi - (z_G W - z_B B)\cos\theta\sin\phi \end{aligned} \tag{11a}$$

where:

$$K_C(t,\mathbf{y}) = \frac{1}{2}\rho\ell^3 K'_{\delta_r} u^2 \delta_r \tag{11b}$$

Pitching Moment

The important M_{δ_s} coefficient defines linear pitch control and $M_{\delta_s|\delta_s|}$ allows for second order effects in lift which can occur in low aspect ratio appendages; this latter term does not model stall. The $M_{\delta_s\delta_s}, M_{\delta_r\delta_r}$ coefficients account for any moment generated by the drag terms in (8b) not acting through the body axes origin, so they are zero for the generic model with its symmetric tailplanes. Again, the $(z_B B - z_G W)\sin\theta$ static stability term tries to keep the boat level in pitch. Pitch trim is controlled dynamically using δ_s or statically by adjusting the axial location of the CG.

$$\begin{aligned} g_M(t,\mathbf{y}) &= (I_z - I_x)rp + I_{xy}qr - I_{zx}(p^2 - r^2) - I_{yz}qp + m\big[z_G(vr - wq) - x_G(uq - vp)\big] \\ &\quad + M_{uq}uq + M_{vp}vp + M_{vr}vr + M_{wp}wp + M_{wq}wq + M_{pp}p^2 + M_{pr}pr + M_{qq}q^2 + M_{rr}r^2 + M_{q|q|}q|q| \\ &\quad + \frac{1}{2}\rho U^2\ell^3 M'_{uvw}(\Theta,\Phi) + M_C(t,\mathbf{y}) - (x_G W - x_B B)\cos\theta\cos\phi - (z_G W - z_B B)\sin\theta \end{aligned} \tag{12a}$$

where:

$$M_C(t,\mathbf{y}) = \frac{1}{2}\rho\ell^3\left(M'_{\delta_s}\delta_s + M'_{\delta_s|\delta_s|}\delta_s|\delta_s| + M'_{\delta_s\delta_s}{\delta_s}^2 + M'_{\delta_r\delta_r}{\delta_r}^2\right)u^2 \tag{12b}$$

Yawing Moment

The weight and buoyancy terms in yawing moment are zero for a neutrally buoyant, well trimmed boat. They do not interact with yaw angle or yaw control.

Figure 2 shows that pitching and yawing moments both have considerable Φ variation at high incidence. Since these functions result from least squares fits to data taken in Φ increments of 30 degrees, this Φ variation may not be adequately resolved.

$$\begin{aligned} g_N(t,\mathbf{y}) = (I_x - I_y)pq + I_{yz}rp - I_{xy}(q^2 - p^2) - I_{zx}rq + m\big[x_G(wp - ur) - y_G(vr - wq)\big] \\ + N_{up}up + N_{ur}ur + N_{vq}vq + N_{wp}wp + N_{pq}pq + N_{qr}qr + N_{p|p|}p|p| + N_{r|r|}r|r| \\ + \frac{1}{2}\rho U^2\ell^3 N'_{uvw}(\Theta,\Phi) + N_C(t,\mathbf{y}) + (x_G W - x_B B)\cos\theta\sin\phi + (y_G W - y_B B)\sin\theta \end{aligned} \quad (13a)$$

where:

$$N_C(t,\mathbf{y}) = \frac{1}{2}\rho\ell^3 N'_{\delta_r} u^2 \delta_r \quad (13b)$$

4 Propeller Thrust and Torque

A high incidence (up to 30 degrees) propulsion model is developed following Watt [10] by adapting the classic propulsion model [11] so that wake fraction varies with incidence.

A conventional dimensionless representation for open water propeller thrust T and torque Q uses thrust and torque coefficients which depend solely on the advance ratio J:

$$K_T(J) = \frac{T}{\rho n^2 D^4}\,, \qquad K_Q(J) = \frac{Q}{\rho n^2 D^5}\,, \qquad J = \frac{V_A}{nD} \quad (14)$$

V_A is the speed of advance of the propeller through the water, n is propeller revolutions per second, and D is propeller diameter. A stern propeller on a submarine operates in a wake which reduces the average inflow to the propeller relative to the speed of the boat. This is accounted for classically with a one-dimensional correction. The speed of advance of the propeller through the water is approximated by:

$$V_A = (1 - w_T)u \quad (15)$$

where w_T is the Taylor wake fraction and u is, as usual, the forward speed of the boat. The classical model does not account for crossflow and does not distinguish between u and U so (15) is a minor extension to the classical approach. As shown below, a further necessary extension is to allow the wake fraction to vary with incidence, whereas it is constant in the classical model.

In addition, when a propeller generating thrust T operates behind a hull, it also induces negative pressure on the hull afterbody upstream of it. This increases the drag on the hull, negating some propeller thrust. This is accounted for classically using the thrust deduction fraction t, another constant:

$$X_P = (1 - t)T \quad (16)$$

The complimentary fraction $1 - t$ is called the thrust deduction factor.

To use (14), open water experiments with a propeller operating at various advance ratios are required to determine K_T and K_Q. To use (15), a wake survey needs to be conducted behind the hull on which the propeller is to be used. And (16) requires model tests with the

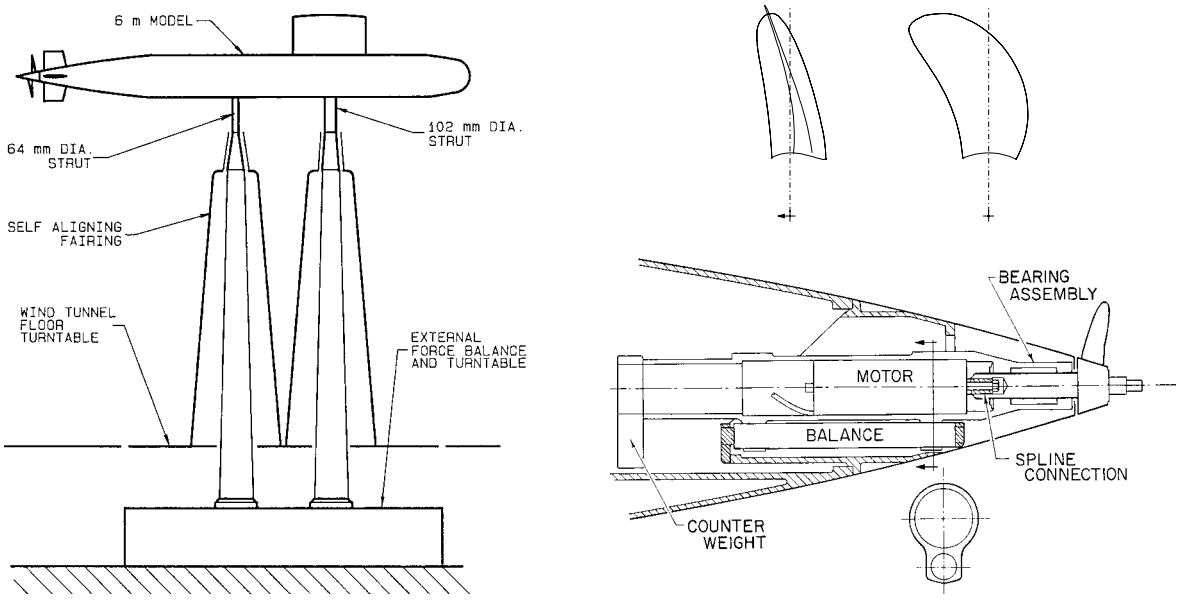

Figure 3 *The DRDC Static Test Rig (STR) generic hull, sail, and tail with propulsion system installed in the Institute for Aerospace Research 9 m wind tunnel. The conventional three bladed propeller is mounted on a six component internal balance. The model is yawed and pitched using a floor turntable with the sail located vertically or horizontally on the axisymmetric hull.*

hull and propeller combination. Herein, a single model setup using the generic hull with a propeller operating behind it is used instead. This is possible only because of the information obtained from testing at incidence and because of the assumptions made in the modelling of incidence, as described below.

The experiments again take place in the wind tunnel (Figure 3) at incidence angles from -30 to 30 degrees at Reynolds numbers over 20 million (based on hull length) [12,13,14]. The propeller diameter is half the hull diameter and operates in dynamic similarity to an imagined full scale prototype. Propeller thrust and torque are measured as well as the overall forces on the vehicle.

Because V_A and w_T are unknown, the effect of propulsion on K_T and K_Q is initially found as a function of:

$$J_b = \frac{u}{nD} = \frac{J}{(1 - w_T)} \tag{17}$$

where J_b is the behind-the-boat advance ratio. The coefficients are obtained by measuring propeller thrust and torque at zero incidence, fitting them with polynomial interpolants, and correcting for minor compressibility effects due to high propeller RPM [13]:

$$\begin{aligned} K_T(J_b) = {} & 0.410758 - 0.115654J_b - 0.107836J_b^2 + 0.0713369J_b^3 - 0.00620451J_b^4 \\ & - 0.0127538J_b^5 + 0.00487893J_b^6 - 0.000678484J_b^7 + 0.0000333463J_b^8 \end{aligned} \tag{18a}$$

$$\begin{aligned} K_Q(J_b) = {} & 0.0690631 - 0.0249658J_b - 0.00623472J_b^2 + 0.00171807J_b^3 + 0.00579169J_b^4 \\ & - 0.00559630J_b^5 + 0.00178950J_b^6 - 0.000246886J_b^7 + 0.0000126029J_b^8 \end{aligned} \tag{18b}$$

These are plotted in Figure 4.

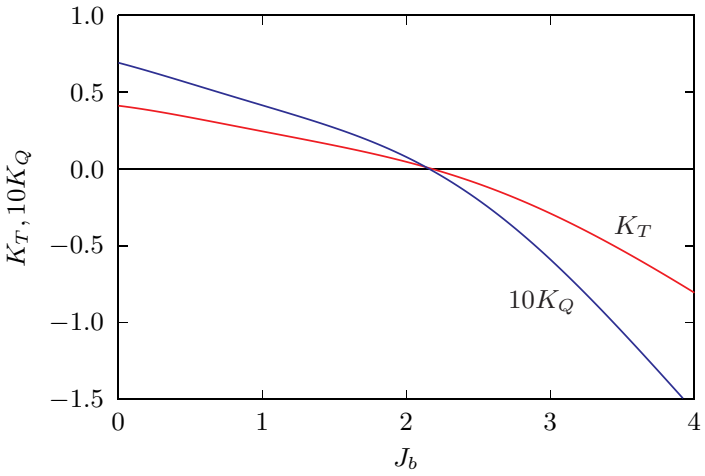

Figure 4 *STR zero incidence thrust and torque coefficients as a function of behind-the-boat advance ratio. Corrected for compressibility effects.* $\boldsymbol{R} > 20$ *million.*

Effect of Incidence

Consider Figure 5 where STR thrust and torque data from two pitch runs at constant propeller RPM are plotted. Two data points are seen at each angle for each run for each of thrust and torque because each run is a sweep from $\alpha = -30$ to 30 degrees. The $\pm\alpha$ pairs are fairly close indicating symmetry about $\alpha = 0$. Yaw sweep data lose some of this symmetry due to, it is thought, the trailing vortex field from the sail; for rising stability, vertical plane incidence is of primary interest and so only the pitch data are used.

The wind tunnel speed is constant for these pitch sweeps. Therefore, as incidence increases, u and J_b reduce as the cosine of the incidence angle, as shown in Figure 5. The solid line fit through the J_b data is the curve:

$$J_{b\text{fit}}(\Theta) = 1.02266 \cos\Theta \tag{19}$$

This $\cos\Theta$ variation in J_b will have negligible effect on thrust and torque at low incidence. However, in Figure 5, thrust and torque initially decrease relatively fast with incidence as it increases from zero. This is thought to result from the crossflow sweeping the wake aside thereby reducing the wake fraction and increasing propeller inflow. This reduces propeller loads. The load reduction is curtailed at 15 to 20 degrees incidence because of the increasingly strong roll-off in $J_{b\text{fit}}$.

Thus, K_T and K_Q vary with Θ independently of J_b, which means the description in (18) is incomplete. From basics, it is known that thrust and torque can be described solely in terms of the conventional advance ratio $J = V_A/nD$ and, therefore, that the functions:

$$K_{T,Q}\left(\frac{J}{1-w_{T0}}\right) \tag{20}$$

are always correct. Here, w_{T0} is w_T at zero incidence where K_T, K_Q (18) were acquired; it is the conventional constant Taylor wake fraction. To use (20), V_A and therefore w_T must be known as a function of incidence. Then (17) allows the thrust and torque coefficients to be generalized:

$$K_{T,Q}(J_b) \rightarrow K_{T,Q}\left(\frac{1-w_T}{1-w_{T0}}J_b\right) \tag{21}$$

In other words, (17) remains valid in the generalized model.

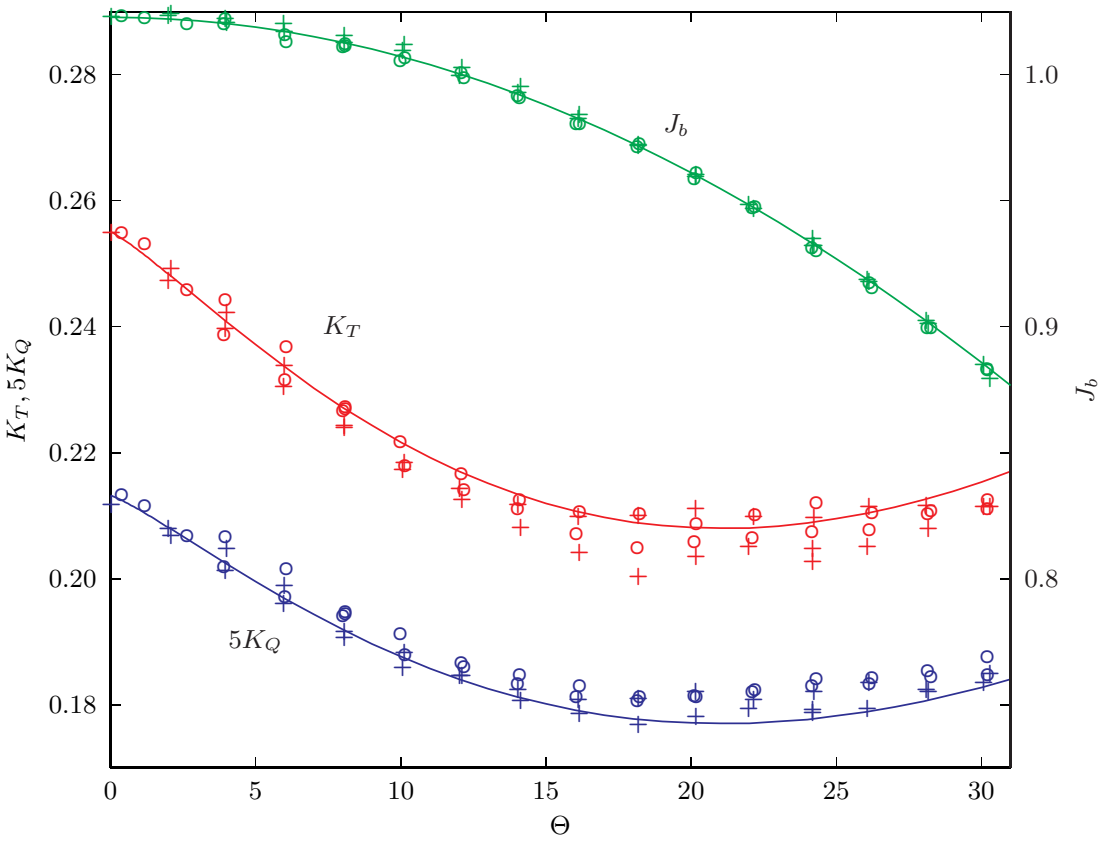

Figure 5 *Propeller thrust, torque, and behind-the-boat advance ratio variation with incidence for $\Phi = 0, 180$ degrees, constant wind speed, and constant propeller RPM nominally set for self propulsion. Not corrected for compressibility effects. ∘ = Run 208 and + = Run 210 from [12].*

The shapes of the curves in Figure 5 suggest the drop in wake fraction might be modelled as:

$$w_T = w_{T0} e^{-(k\Theta)^\gamma} \tag{22}$$

where w_{T0}, k, γ are unknown constants. Using (19) in a least squares fit of (21) and (22) to the K_T, K_Q incidence sweep data (multiplying K_T by 1.063 and K_Q by 1.048 because the data are uncorrected for compressibility effects) gives:

$$w_{T0} = 0.31, \quad k = 3.4, \quad \text{and} \quad \gamma = 1.18 \tag{23}$$

The lines through the K_T, K_Q data in Figure 5 show the fit.

To summarize, the effect of propulsion on axial force and rolling moment is modelled using:

$$\begin{aligned} X_P &= \rho n^2 D^4 (1-t) K_T(J_m) \\ K_P &= -\rho n^2 D^5 K_Q(J_m) \end{aligned} \tag{24a}$$

where J_m is the modified advance ratio:

$$J_m = \frac{u\left(1 - w_{T0} e^{-(k\Theta)^\gamma}\right)}{nD(1-w_{T0})} \tag{24b}$$

and the K_T, K_Q functions in (24a) are given by (18).

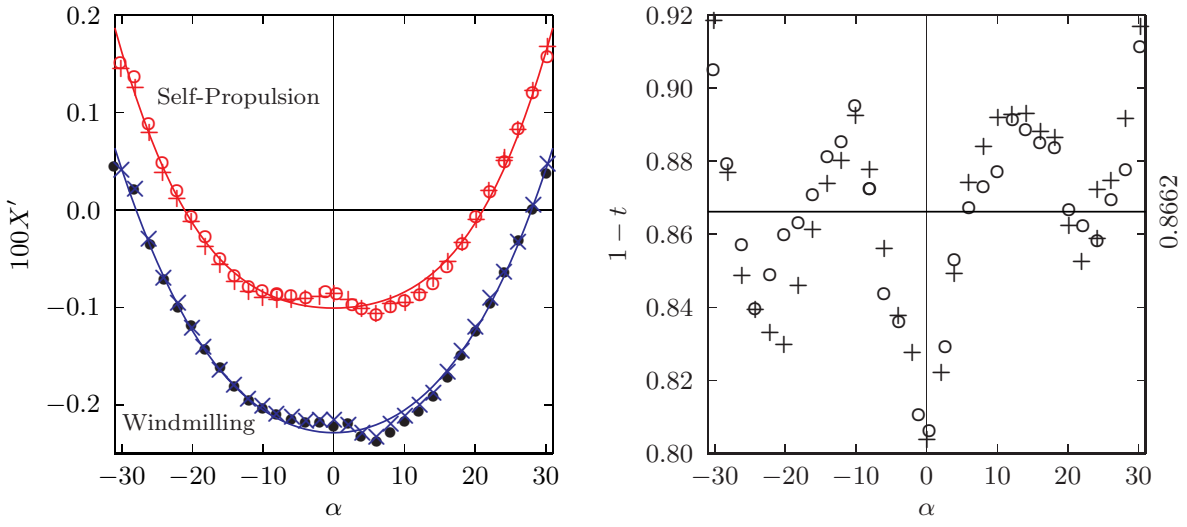

a) *Overall axial force.* **b)** *Thrust deduction factor.*

Figure 6 *The thrust deduction data in (b) are the differences between the fitted curves from (a) normalized by the thrust data from Figure 5.* ∘ *= Run 208,* + *= Run 210,* • *= Run 214,* × *= Run 216 from [12].*

Thrust Deduction

The thrust deduction factor $1-t = X_P/T$ is estimated from the STR experiments by comparing overall axial force and localized propeller thrust measurements. Runs 208 and 210 from [12] give overall axial force X and propeller thrust T measurements for pitch sweeps from $\alpha = -30$ to 30 degrees with the propeller providing self-propulsion at zero incidence. These are the red data points in Figures 5 and 6a. To get the X_P component from the X data, the axial force from similar data acquired with the propeller unpowered and windmilling is subtracted from the X data (propeller thrust for the windmilling condition is effectively zero). The windmilling X data (runs 214 and 216 from [12]) are shown in blue in Figure 6a.

Unlike the yaw data presented in [14], the Figure 6a pitch data are uncorrected for support strut tare and interference effects. This correction would put the self-propulsion zero incidence axial force much closer to zero, as would be expected. However, it is only the difference between the self-propulsion and windmilling X data that is used and this difference is unaffected by the correction which is the same for each data set.

The STR axial force data clearly suffer from some systematic error as the model is pitched through zero degrees. To correct for this, and because the data in the two sets of runs are not all at the same angles, the data are least square fitted with 4^{th} order polynomials in α (even powers only). These fits are shown in Figure 6a. The thrust deduction factor data is then calculated from:

$$\frac{X_{\text{fit}_{208,210}} - X_{\text{fit}_{214,216}}}{\rho n^2 D^4 K_{T_{208,210}}} \tag{25}$$

and is shown in Figure 6b.

Although $1-t$ appears to vary with incidence, the variation is similar in magnitude to the fitting error in Figure 6a and is discounted. Thus, thrust deduction is just a constant, the average of the Figure 6b data:

$$1 - t = 0.8662 \tag{26}$$

Commanded Speed and Trim

It is usually more convenient to command forward speed than RPM. Commanded forward speed u_c is the self-propulsion speed of the boat, the speed achieved when in 'equilibrium' (straight, level, neutrally buoyant, zero incidence, fully trimmed flight). The equilibrium hydrodynamic state is the same at any speed and associated with it is a simple linear relationship between speed and RPM, as given by the advance ratio (17). To use this relationship, the self-propulsion behind-the-boat advance ratio J_{bs} must be known.

Equilibrium implies roll and pitch angles, flow incidence, all accelerations, and all velocities are zero except for the self-propulsion (commanded) speed:

$$u = U \equiv u_c \tag{27}$$

When equilibrium is achieved, only the four X, Z, K, M equations of motion have nonzero terms and these must combine in such a way as to zero each equation:

$$X: \qquad 0 = \frac{1}{2}\rho u_c^2 \ell^2 \left(X'_{uvw}(0,\Phi) + X_{\delta_s\delta_s}{\delta_s}^2 \right) + \rho n^2 D^4 (1-t) K_T(J_{bs}) \tag{28a}$$

$$Z: \qquad 0 = \frac{1}{2}\rho u_c^2 \ell^2 \left(Z'_{uvw}(0,\Phi) + Z'_{\delta_s}\delta_s \right) + W - B \tag{28b}$$

$$K: \qquad 0 = \rho n^2 D^5 K_Q(J_{bs}) + (y_G W - y_B B) \tag{28c}$$

$$M: \qquad 0 = \frac{1}{2}\rho u_c^2 \ell^3 \left(M'_{uvw}(0,\Phi) + M'_{\delta_s}\delta_s \right) - (x_G W - x_B B) \tag{28d}$$

(28d) reflects the fact that $M'_{\delta_s|\delta_s|} = M_{\delta_s\delta_s} = 0$, as given in Appendix A. The expressions for F_{uvw} in Appendix A show that all the horizontal plane Y, K, N hydrodynamic translational forces are zero when $\Theta = 0$. Thus, simply zeroing the rudder deflection zeros the Y and N forces. On the other hand, the vertical plane X, Z, M translational forces reduce to nonzero constants at $\Theta = 0$ because of the hydrodynamic asymmetry associated with the sail.

Equations (28) show that trimming is necessary to achieve equilibrium. The asymmetric hydrodynamic forces are normally countered using hydrodynamic forces generated by the stern and bowplanes; this keeps the trim effective as speed is changed. However, since bowplanes are not present in the current model, trim is achieved instead using a combination of sternplane deflection and weight compensation. A small sternplane deflection is used to trim the boat to zero pitch angle and the weight is adjusted to negate the normal force from the sternplanes. The weight trim W_t is added at $x_{Go} = x_B = 0$ so that the last term in (28d) remains zero. The sternplane trim deflection is therefore independent of speed:

$$\delta_{st} = \frac{-M'_{uvw}(0,\Phi)}{M'_{\delta_s}} \frac{180}{\pi} = 0.813 \text{ degrees.} \tag{29a}$$

while, from (28b), the weight trim is speed dependent:

$$W_t = W - B = -\frac{1}{2}\rho u_c^2 \ell^2 \left(Z'_{uvw}(0,\Phi) + Z'_{\delta_s}\delta_{st} \right) = -543 u_c^2 \text{ Newtons} \tag{29b}$$

At 5 knots, W_t is just 0.01% of B so its speed dependence minimally compromises equilibrium.

The sternplane trim deflection is so small it has only a small effect on the solution of (28a) for J_{bs}:

$$J_{bs} = 0.9783 \tag{30}$$

With the unique constant J_{bs} known, the desired relationship between n and u_c is:

$$n = \frac{u_c}{J_{bs}D} = 0.2555u_c \tag{31}$$

and (24b) can be replaced with:

$$J_m = \frac{uJ_{bs}\left(1 - w_{T0}e^{-(k\Theta)^\gamma}\right)}{u_c(1 - w_{T0})} \tag{32}$$

In other words, the advance ratio is just proportional to the actual forward speed divided by the forward speed that the current propeller RPM achieves in equilibrium conditions.

Finally, consider (28c) which states that propeller torque must be trimmed with a lateral shift in the CG to achieve equilibrium. This will not be done in the current simulations so that a small roll (heel) angle will always be present, as is typical in real life. This should allow any roll instability that is present to develop and grow. If $y_G = y_B$, then propeller torque will generate a small roll angle and (28c) is more properly modelled as:

$$K: \qquad 0 = \rho n^2 D^5 K_Q(J_{bs}) - (z_G W - z_B B)\sin\phi \tag{33}$$

which gives:

$$\phi_o = -0.1044 \text{ degrees.}$$

at a steady forward speed of 5 knots. This increases with n^2 and therefore with u_c^2.

5 Buoyancy, Weight, and Blowing

Buoyancy is fixed by the shape of the external hydrodynamic envelope. With the main ballast tanks (MBTs) flooded, the weight is nominally equal to the buoyancy. However, as noted above, the weight can be adjusted (using small onboard compensation tanks) for each steady state condition at which the operators wish to achieve equilibrium. The simulation initial conditions account for this trim so the simulations begin in equilibrium. Blowing must also be modelled, but it is always activated after a simulation has been started in equilibrium.

Weight is modelled as:

$$W = W_o - \mu B \qquad \text{where} \qquad W_o = B + W_t \tag{34a}$$

Similarly:

$$m = m_o - \frac{\mu B}{g} \qquad \text{and} \qquad m_o = \frac{B}{g} + m_t \tag{34b}$$

The 'o' subscript refers to conditions immediately prior to blowing. W_o is the equilibrium weight which equals the buoyancy plus the trim weight W_t necessary to achieve equilibrium at some initial state. The blown mass fraction μ is zero at submerged equilibrium and about 0.1 with the MBTs empty. As was shown above, the trim weight W_t is approximately $0.0001B$ so W_o is effectively equal to B. Since rotation is zero during equilibrium, the values of the moments of inertia are not critical and any effect W_t has on the moments is ignored. It is assumed that both W_o and W_t have their centroids at x_{Go}, y_{Go}, z_{Go} and that initial equilibrium in straight and level flight is achieved with $x_{Go} = x_B$ and $y_{Go} = y_B$.

Mass Change While Blowing

Submarines have several main ballast tanks distributed along the length of the hull and can blow them independently or all together. The forward tanks are always largest so the nose rises faster than the stern. This, coupled with propulsion, gets the boat to the surface fast in an emergency. Emergency operating procedures may call for the forward tanks to be blown first and the aft tanks only after the nose has begun to rise. However, all tanks are blown simultaneously in the current model. Each tank centroid is assumed to be located on the hull centerline. Since the forward MBT volumes are largest, the blown mass centroid, (x_μ, y_μ, z_μ), will be slightly forward of the CB. There are N main ballast tanks with a total volume $V_T = \sum_{i=1}^{N} V_{Ti}$ with each tank having an axial centroid at x_{Ti}. The blown mass fraction is then:

$$\mu = \frac{W_o - W}{B} = \frac{\rho g V_a}{B} = \frac{\rho g \sum_{i=1}^{N} V_{ai}}{B} = \sum_{i=1}^{N} \mu_i \tag{35}$$

where V_a is the total volume of air in (water expelled from) the MBTs and V_{ai} is the volume of air in tank i. When blowing begins, $V_{ai} = 0$ and it is maximum when all the water is expelled, when $V_{ai} = V_{Ti}$.

The axial centroid of the blown mass fraction is:

$$x_\mu = \frac{\sum_{i=1}^{N} x_{Ti}\mu_i}{\mu} = \frac{\sum_{i=1}^{N} x_{Ti} V_{ai}}{V_a} \tag{36}$$

However, the vertical centroid of the blown mass fraction z_μ is dependent on the local vertical centroids, the z_{μ_i} say, which vary approximately linearly with local blown mass fraction μ_i even though the MBTs have irregular shapes. The z_{μ_i} have an initial value near the top of the hull when $\mu_i = 0$ and end with a value on the centerline when the blow is complete. The initial z_{μ_i} value is taken to be 90% of the maximum hull radius $d/2$:

$$z_\mu = \frac{\sum_{i=1}^{N} z_{\mu_i}\mu_i}{\mu} = \frac{-0.45d \sum_{i=1}^{N} \left(1 - \frac{V_{ai}}{V_{Ti}}\right) V_{ai}}{V_a} \tag{37}$$

This accounts for different levels of water in each MBT, which occurs when the boat is pitched up putting the forward tanks at a different depth, and therefore pressure and blown air density, than the aft tanks.

Expressions for x_G, z_G in terms of x_μ, z_μ are obtained by taking moments about the body axes origin. Remembering that B and x_B do not change when blowing ballast and $x_{Go} = x_B$, $z_{Go} = z_B + \overline{BG}_o$ initially, there results:

$$x_G = \frac{x_B - \frac{\mu B}{W_o} x_\mu}{1 - \frac{\mu B}{W_o}}, \qquad z_G = \frac{z_B + \overline{BG}_o - \frac{\mu B}{W_o} z_\mu}{1 - \frac{\mu B}{W_o}} \tag{38}$$

The $\overline{BG} = z_G - z_B$ value is then:

$$\overline{BG} = \frac{\overline{BG}_o + \dfrac{\mu B}{W_o}(z_B - z_\mu)}{1 - \dfrac{\mu B}{W_o}} = \overline{BG}_o + \frac{\dfrac{\mu B}{W_o}}{1 - \dfrac{\mu B}{W_o}}(z_{Go} - z_\mu) \tag{39}$$

If the vehicle CG is on the hull centerline, and because the vertical centroids of the MBTs are on the hull centerline, then $\overline{BG}$ has the same value before (when $\mu = 0$) and after the blow (when $z_\mu = 0$). During the blow, z_μ is negative so $\overline{BG}$ temporarily increases.

From (2d), static stability in roll is determined by the term $z_G W - z_B B$ which, using (34a) and (38b), becomes:

$$z_G W - z_B B = B\left(\overline{BG}_o - \mu z_\mu\right) = B\,\overline{BG}^* \tag{40a}$$

where:

$$\overline{BG}^* = \overline{BG}_o - \mu z_\mu \tag{40b}$$

When $W \neq B$, $z_G W - z_B B$ is different from $B\,\overline{BG}$ or $W\overline{BG}$ and it is convenient to use the modified $\overline{BG}$ value $\overline{BG}^*$. $\overline{BG}^*$ is the same before and after the blow, regardless of z_{Go}, and differs from $\overline{BG}$ only by $O(\mu z_{Go}, \mu^2 z_\mu)$. The temporary increase in $\overline{BG}^*$ during the blow tends to delay the onset of the roll instability until the MBTs are almost empty. So modelling the vertical variation of z_μ with time is important.

The moments of inertia all vary somewhat with blown mass. These variations are small and often neglected during blowing simulations, primarily so the mass matrix multiplying the 6 accelerations in the equations of motion does not have to be continually inverted during numerical integration of the equations. However, the variation is easy to account for and inverting a 6×6 matrix is not computationally expensive these days. Here, then, are the moments and products of inertia accounting for blown mass by assuming it occurs at a point:

$$\begin{aligned}
I_x &= \int (y^2 + z^2) dm = I_{xo} - \mu m_o z_\mu^2 & I_{xy} &= \int xy\, dm = I_{xy_o} \\
I_y &= \int (z^2 + x^2) dm = I_{y_o} - \mu m_o (z_\mu^2 + x_\mu^2) & I_{yz} &= \int yz\, dm = I_{yz_o} \\
I_z &= \int (x^2 + y^2) dm = I_{zo} - \mu m_o x_\mu^2 & I_{zx} &= \int zx\, dm = I_{zxo} + \mu m_o z_\mu x_\mu
\end{aligned} \tag{41}$$

Blowing Model

The above mass model requires knowledge of V_{ai}, the volume of air in each MBT. This volume is derived here as a function of time, tank location, and the depth and pitch angle of the boat.

The MBTs are blown from a reservoir of very high pressure air (several hundred atmospheres) which discharges through nozzles in the MBTs. One dimensional, isentropic, compressible flow theory [15] predicts the maximum nozzle velocity to be Mach 1. This is maintained if the discharge to reservoir pressure ratio is less than 0.53 which will be the case for most of the duration of any blow. In this case, the reservoir air density ρ_r during the blow, assuming isentropic flow, is:

$$\frac{d\rho_r(t)}{dt} = C_1 \rho_r^{\frac{k+1}{2}} \tag{42}$$

where $k = 1.4$ for air and C_1 is a negative constant that depends only on the properties of the bottled air and nozzle diameter:

$$C_1 = \frac{\left.\frac{d\rho_r}{dt}\right|_o}{{\rho_r}_o^{\frac{k+1}{2}}} \tag{43}$$

Integrating (42) gives the isentropic blowing model:

$$\rho_r(t) = \frac{\rho_{ro}}{\left(1 - \frac{k-1}{2} C_2 (t - t_o)\right)^{\frac{2}{k-1}}} \tag{44}$$

where C_2 is the blowing constant:

$$C_2 = C_1 {\rho_r}_o^{\frac{k-1}{2}} = \frac{\left.\frac{d\rho_r}{dt}\right|_o}{\rho_{ro}} = \frac{\left.\frac{dm_r}{dt}\right|_o}{m_{ro}} \tag{45}$$

m_r is the mass of air in the reservoir and t_o is the time at which the blow is initiated. C_2 can vary from -0.1 to -0.01 s^{-1} depending on nozzle diameter and reservoir size. For a particular boat, reservoir size depends on which and how many reservoir options the operators choose to use.

Some analyses simply assume the mass flow rate from the reservoir is proportional to the mass left in the reservoir [16]. This is equivalent to setting $k = 1$ in (42) which results in:

$$\rho_r(t) = \rho_{ro} e^{C_2 (t - t_o)} \tag{46}$$

This 'exponential' model is compared to the isentropic model in Figure 7. With identical blowing constants, the exponential model empties the reservoir faster then the ideal frictionless isentropic model, which doesn't make sense. However, using a smaller blowing constant with the exponential model provides a time response similar to that of the isentropic model. The model to use depends on how the blowing constant is obtained. If the blowing constant is calculated from a known initial mass and mass flow rate, then the isentropic model should be more accurate. If C_2 is obtained by fitting time response data to the exponential model, then the exponential model should be used. Herein, the exponential model is used in keeping with the precedent set by Mackay [16].

The total mass of air m_a in the MBTs must equal that released by the reservoir and the sum of the air masses m_{ai} in each individual tank:

$$m_a = m_{ro} \left(1 - e^{C_2 (t - t_o)}\right) = \sum_{i=1}^{N} m_{ai} \tag{47}$$

It is now assumed that the air delivery system to the MBTs is tuned so that:

$$m_{ai} = \frac{m_a V_{Ti}}{V_T} \tag{48}$$

The next assumption is questionable and is made to avoid having to use a heat transfer model. It is known that the air jetting into the tanks generates good mixing, creating a

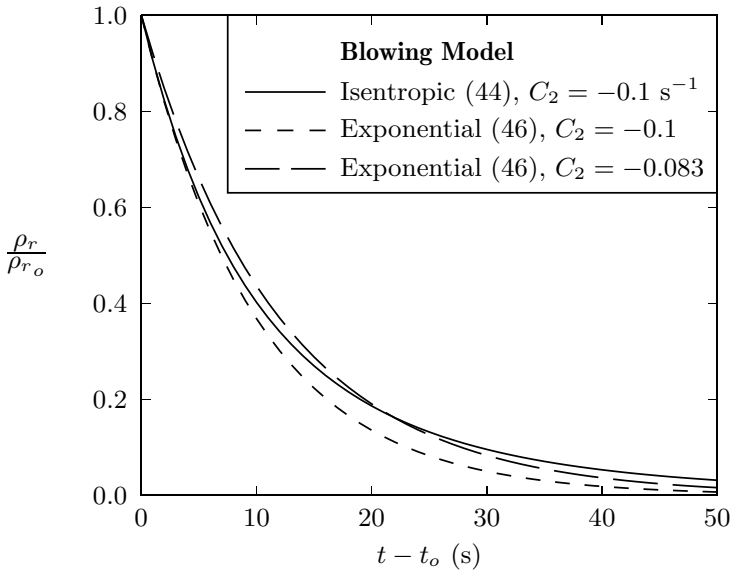

Figure 7 *Two blowing models giving similar blow histories using different blowing constants.*

turbulent and frothy air/water interface. This promotes good heat transfer from the water to the expanding cold air. Therefore, the assumption made is that the air blowing into the MBTs takes on the ambient MBT temperature immediately. This generates buoyancy more quickly than will actually occur and, in the current context, may bring on the rising instability prematurely.

The air pressure in ballast tank i is therefore:

$$p_{ai} = p_{\text{at}} + \rho g z_{wi} = \rho_{ai} RT \tag{49}$$

where p_{at} is atmospheric pressure, z_{wi} is the depth of the water level in tank i below the ocean surface, ρ_{ai} is the density of the air in tank i, R is the gas constant for air, and T is the ambient temperature in the MBTs. (49) ignores the pressure loss through the openings in the bottom of the MBTs through which flood water is expelled during the blow. These openings are large so the MBTs fill quickly when the boat dives; losses for the slower rising maneuver should be small.

The volume of air in each MBT is then:

$$V_{ai} = \frac{m_{ai}}{\rho_{ai}} = \frac{m_{ro}\left(1 - e^{C_2(t-t_o)}\right) RTV_{Ti}}{(p_{\text{at}} + \rho g z_{wi}) V_T} \tag{50}$$

When the boat is pitched at an angle θ, z_{wi} is different for each MBT and is itself dependent on V_{ai}:

$$z_{wi} = z_0 - x_{Ti}\sin\theta - 0.45d\cos\theta\left(1 - \frac{2V_{ai}}{V_{Ti}}\right) \tag{51}$$

This is only valid for $z_{wi} \geq 0$. Substituting (51) into (50) results in an expression quadratic in V_{ai}/V_{Ti}, the solution for which is:

$$\frac{V_{ai}}{V_{Ti}} = A_1 + \sqrt{A_1^2 + A_2} \tag{52}$$

$$A_1 = \frac{-p_{\text{at}} - \rho g\left(z_0 - x_{Ti}\sin\theta - 0.45d\cos\theta\right)}{1.8\rho g d\cos\theta}, \qquad A_2 = \frac{m_{ro}RT\left(1 - e^{C_2(t-t_o)}\right)}{0.9\rho g d V_T\cos\theta}$$

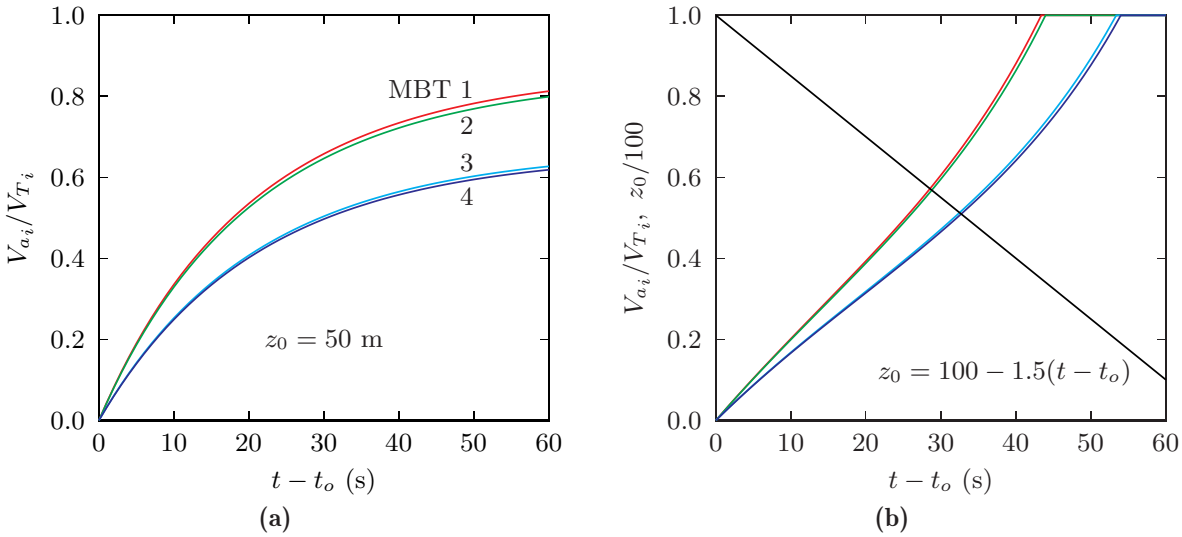

Figure 8 *Blowing ballast (a) at a pitch angle of 20 degrees at a fixed depth of 50 m and (b) while rising to the surface from an initial depth of 100 m.* $C_2 = -0.045\ s^{-1}$, $m_{ro} = 1500$ *kg, the* x_{Ti} *and other parameters are given in Appendix A.*

with the constraint that V_{ai}/V_{Ti} is limited to 1.0. When $V_{ai}/V_{Ti} > 1$, air is expanding out the bottom of the MBT. During a simulation, z_{wi} should be checked to ensure it is positive; a negative z_{wi} value indicates the boat is on the surface.

Figure 8 shows the predictions of the blowing model for a boat with a fixed pitch angle sitting at a fixed depth in one case (unrealistic) and coming to the surface at a constant rate in another. In the latter case, the boat is still 35 m deep when air begins escaping from the forward ballast tank. This figure shows the importance of modelling depth, pitch angle, and ballast tank axial location.

Finally, it is clear that ballast blowing will result in discontinuities in the equations of motion at the times that the MBTs empty. These discontinuities can compromise the efficiency and accuracy of the ODE integrator if they are severe enough. Predicting the times at which discontinuities occur so the integration can be stopped and restarted at these times requires, from (52), knowledge of θ and z_0 at the discontinuities, states which are themselves solutions of the integration and therefore unknown until the discontinuity has been reached. Methods are available for handling this problem but are not implemented at this time. In practice, integrating through the discontinuities has not proven to be a problem; some inaccuracy results but not as much as is present in the modelling assumptions themselves.

6 Control System Modelling

When control surface deflections or propulsion changes are commanded, the changes are implemented through control systems of varying complexity. Following Watt [17], these changes are modelled using a second order differential equation:

$$\frac{d^2\delta}{dt^2} + 2\zeta\omega\frac{d\delta}{dt} + \omega^2\delta = \omega^2\delta_c \tag{53}$$

where δ is the time dependent quantity being modelled (control surface deflection or commanded forward speed), δ_c is the commanded value of δ (ie, the value the control system is trying to implement), ζ is control system damping (assumed sub-critical: $0 < \zeta < 1$), and ω is the response frequency of the control system. The general solution to (53) is:

$$\delta = \delta_c - \frac{\delta_c - \delta_0}{\sin\beta} e^{-\zeta\omega(t-t_0)} \sin\left(\sqrt{1-\zeta^2}\,\omega(t-t_0) + \beta\right) \tag{54}$$

where t_0 is the time at which the new command δ_c is issued, δ_0 is the value of δ at $t = t_0$, and β is a phase shift used to match the rate $d\delta/dt$ at $t = t_0$. Thus, δ_0 and β ensure the model for δ is first order continuous when a new command is issued. The enabling mathematics and some implementation examples are provided in [17].

To use this model, three invariant control system characteristics must be specified for each control system:

ζ	Control system damping as described above. The lower the damping the faster the system achieves δ_c, but at the expense of overshoot. Typical values range from 0.7 to 0.9.
$\omega_{\max}$	The natural response frequency, the maximum frequency at which the system can respond.
$\left.\frac{d\delta}{dt}\right\|_{\mathrm{RL}}$	The rate limit, the maximum rate at which the system can respond.

The response to any given command is determined by first assuming $\omega = \omega_{\max}$ and then checking to see if the response rate $d\delta/dt$ is less than the rate limit. If true, this 'frequency limited' solution is implemented. If false, a 'rate limited' solution is used in which ω is reduced until the maximum $d\delta/dt$ magnitude in the response matches the rate limit.

This algorithm can be implemented using the two FORTRAN subroutines listed in Appendix B. The first, CNSYS2, calculates the $\delta_0, t_0, \beta, \omega$ parameters at the issuance of each new δ_c command for each control system. These are saved and passed to the second subroutine, CSDEFL, which simply calculates (54) at any point in time.

Figure 9 shows the control system model in action. Except for different damping parameters, the invariant control system characteristics are the same in each half of the figure, as is the initial rate $d\delta/dt = 0$ at $t = t_0$. In part (a), the response to $\delta_c = 5$ is frequency limited, with $\omega = \omega_{\max}$ whereas the response to $\delta_c = 10$ is rate limited with $\omega = 1.25$ s^{-1}.

In Figure 9b, new commands are issued every second for the first three seconds to show how the algorithm maintains first order continuity in its response.

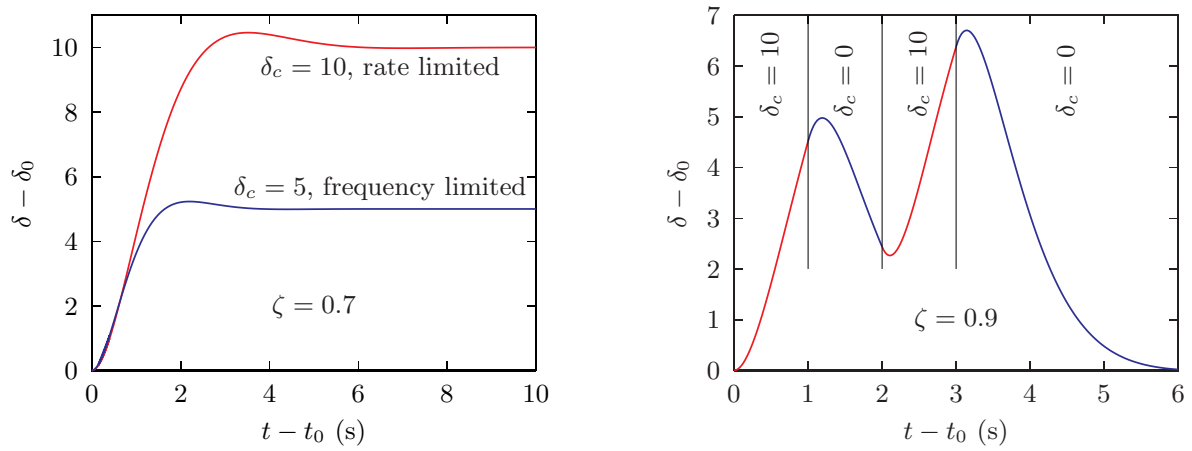

a) *Initial commands* $\delta_c = 5, 10$. **b)** *Changing commands at* $t = 0, 1, 2, 3$ *s.*

Figure 9 *First order continuous control system time responses to different initial commands and a sequentially changing command.* $\omega_{\max} = 2\ s^{-1}$, $(d\delta/dt)_{\mathrm{RL}} = 0.1\ \ \delta$ *units per second.*

7 Estimating Roll Stability

Watt [4] presents a 1 DOF, quasi-steady, linearized stability analysis of ϕ in the rolling moment equation of motion assuming:

- $\dot{\theta}, q, r = 0$ and $p = \dot{\phi}$,
- ϕ is decoupled from θ, Θ, u so these latter parameters that can be arbitrarily large,
- $\overline{BG}$ is constant.

The result is a simple expression giving the balance between the stabilizing static and destabilizing hydrodynamic forces:

$$B\,\overline{BG}\cos\theta - \frac{1}{2}\rho\ell^3 U^2\ \frac{\partial K'}{\partial \Phi}\bigg|_{\Phi=0} > 0 \qquad \text{for stability.} \tag{55}$$

The second term is the destabilizing force and it varies with the dynamic pressure of the flow and so increases with the square of the velocity. It is also proportional to a stability derivative that can be estimated from (A5):

$$100\ \frac{\partial K'_{uvw}}{\partial \Phi}\bigg|_{\Phi=0} = 0.200\cos\Theta\sin\Theta + 0.891\sin^2\Theta + 0.449\sin^3\Theta \tag{56}$$

This is nonlinear in flow incidence Θ, as shown in Figure 10.

Watt [4] discusses how the quasi-steady assumption leads to an underprediction of the stability derivative when this derivative is obtained from a moment measurement in a steady flow with the trailing vortex field from the sail fully developed. This trailing wake interacts with the tailplanes reducing the rolling moment generated by the sail alone. The problem with the steady flow data is that when a boat starts to roll, the trailing vortex field is not fully developed; indeed, it is just beginning to develop. Hence, there is some justification for using stability derivatives from steady state measurements with the tail removed. Reference [4] compares the two methods. Herein, (56) is used for simplicity.

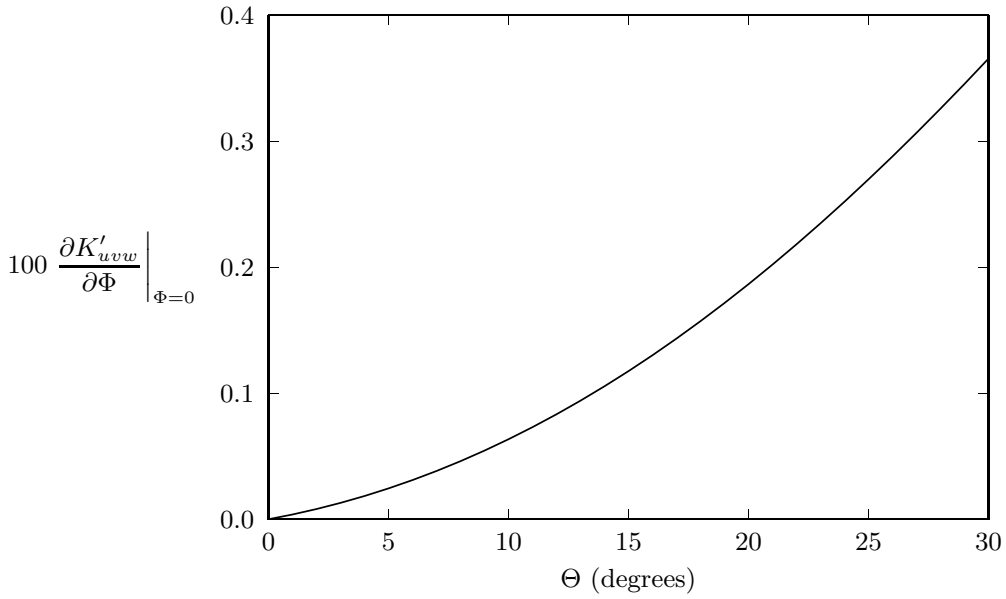

Figure 10 *The nonlinear hydrodynamic stability derivative.*

Watt and Bohlmann [5] also show how q and $\dot{q}$ effect the roll stability limit. For simplicity again, this effect is neglected here.

In the simulations presented in the next section, (55) provides a simple way to estimate stability. Stability is monitored using a velocity stability 'index':

$$U_S = \sqrt{\frac{B\,\overline{BG}^*\cos\theta}{\frac{1}{2}\rho\ell^3\ \frac{\partial K'_{uvw}}{\partial \Phi}\Big|_{\Phi=0}}} - U > 0 \qquad \text{for stability} \tag{57}$$

This gives physical meaning to nonzero U_S values: when $U_S = 1$ m/s, say, then the boat would be unstable if U were 1 m/s larger, everything else being the same. Note that $\overline{BG}$ has been replaced with $\overline{BG}^*$ from (40) so the stability index accounts for the temporary increase in static stability while the tanks are being blown.

It is worth examining the impact of two conventional remedies for the rising instability on the stability index. The first remedy suggests that increasing speed is beneficial because it reduces flow incidence Θ (see Figure 1). This may have a net benefit, even though the destabilizing hydrodynamic force increases as the square of the speed, since from (56) when Θ is large, $\partial K/\partial\Phi$ can decrease as the cube of $\Theta \sim -w/U$. Thus, in (55) the highest order term in $U^2(\partial K/\partial\Phi)$ is $O(1/U)$. This remedy's dependence on a third order term in the stability derivative suggests that any benefit is likely to be both marginal and geometry dependent.

The second remedy suggests that increasing pitch angle is beneficial because it reduces Θ by shifting the impact of buoyancy away from increasing $-w$ towards increasing u and therefore speed. If $-w$ falls off as $\cos\theta$, then the highest order term in $U^2(\partial K/\partial\Phi)$ is $O(\cos^3\theta/U)$ and the second order term would also decrease as $O(\cos^2\theta)$. This effect is moderated by the reduction of static stability with $\cos\theta$ in (55), so that the net effect on the second and third terms is $O(\cos\theta)$ and $O(\cos^2\theta/U)$ which is still better than that provided by the first remedy. Because this benefit is seen at lower order, it is more likely to be generally useful.

8 Simulations Using the Coefficient Based Model

Rising simulations are now presented using the coefficient based hydrodynamic model in place of the RANS model. Various scenarios are examined to see how they effect the roll angle of the boat immediately before surfacing (the emergence roll angle). A typical scenario is given in Figure 1 from Watt and Bohlmann [5] and is reproduced here as Figure 11.

The boat in Figure 11 is at depth when it uses sternplane control to pitch up to the desired angle θ for the rising maneuver. It then blows only half of its MBTs. The downward force from the sternplanes and the forward momentum of the boat initially generate a positive w velocity before the blow progresses enough that buoyancy makes w negative; this accounts for the early jump of π in Φ, shown in the figure as a change of sign in Θ^*. Although propeller rpm is constant throughout the maneuver, the axial velocity u increases because of the buoyancy component in the axial direction, and from the thrust resulting from the hull 'sailing' in the crossflow. Flow incidence Θ increases as the blowing progresses but tapers off after blowing stops. The air continues to expand in the ballast tanks, but incidence is kept in check by the increasing forward speed. The maneuver was nominally carried out in a vertical plane (the rudder was fixed) but the heading ψ still varies.

Roll angle ϕ is small through most of the rise, until just after the MBTs empty and expanding air in the tanks has begun escaping and possibly interacting with the sail. The boat begins to roll and emerges through the surface with a small to moderate roll angle. As it surfaces, the submarine immediately loses static stability which is regained gradually as floodwater drains from the sail and deck casing. This loss of stability, combined with the emergence roll angle and roll rate, result in an excessive roll angle before the boat recovers.

Despite the care taken conducting this maneuver (pitch up attitude prior to blowing, moderate blowing), an uncomfortably large roll angle still occurred on the surface. The temporary loss of hydrostatic stability a submarine experiences when surfacing is well understood and normally not a problem; however, this surface instability is aggravated by emergence roll which is the result of the underwater roll instability that previous computer simulations have not been able to predict.

With this scenario in mind, nine simulations with the present model have been carried out and are presented in detail in Appendix C. The differences between the simulations are summarized in Table 1, significant values for some states are listed in Table 2, and the roll histories are all compared in Figure 12.

The equations of motion are formulated and solved using Maple.[1] Within Maple, the ODEs are numerically integrated using RKF45, a Runge-Kutta integrator that chooses its own step size Δt based on local error, the difference between the 4^{th} and 5^{th} order accurate solutions it propagates simultaneously. Time steps are about half a second for most of the integration but are typically scaled back to half that to get past discontinuities associated with the ballast tanks emptying.

Simulation 1

This first simulation provides a baseline rising maneuver with which subsequent simulations are compared. The procedure is typical of that used by some of the larger diesel boats. Unlike the procedure used in Figure 11, Simulation 1 (S1) increases commanded speed when ballast is blown, a common practice intended to both reduce flow incidence and get the boat to the surface quickly.

[1] `www.maplesoft.com`

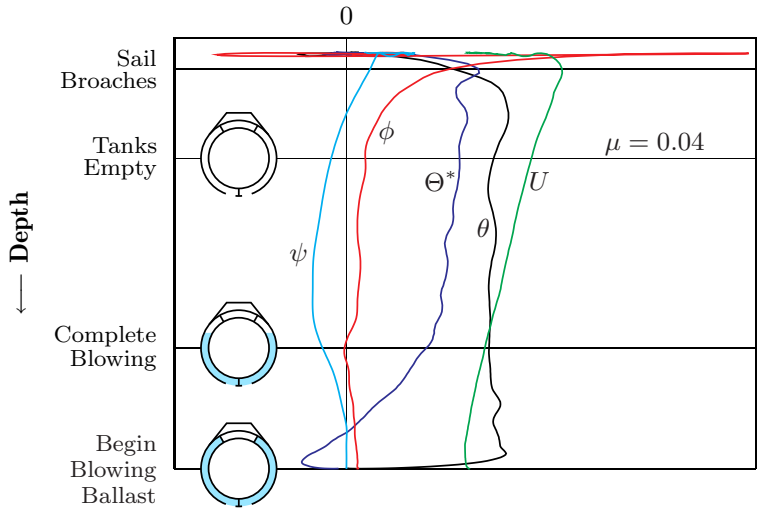

Figure 11 *Full scale rising trial for a 2000–3000 t boat blowing limited ballast at depth.* Θ^* *is* Θ *allowed to go negative (for display purposes only) when* Φ *jumps by* π.

S1 is displayed in Figure C1 in Appendix C (the first page of this appendix explains how to read the figure). It begins with the boat in equilibrium in straight and level flight with a speed of 3 m/s (just under 6 knots) at a depth of 100 m. At $t = 0$, the sternplanes are activated to pitch the nose up, ballast is blown using normal air only, and a speed of 6 m/s is requested. As the large forward MBTs empty, the sternplane deflection is reduced to keep the pitch angle at about 20 degrees.

Figure C1a shows that u initially decreases. This is because of increased drag from the deflecting sternplanes. After 10 to 15 seconds u increases quickly as u_c and the pitch angle and net buoyancy increase. At the end of the maneuver, u is still increasing because of buoyancy and the nose up pitch angle. The crossflow $-w$ increases steadily as the buoyancy increases.

The pitch rate q (Figure C1b) initially increases because of the sternplane deflection but levels off as sternplane control is countered by static stability in pitch. It suddenly decreases when the sternplane deflection is reduced to maintain the pitch angle. q eventually increases again, forcing the sternplanes to stay active, because of increasing buoyancy in the nose MBTs which, as well as being larger, are under less pressure than the stern tanks. This stops suddenly when the forward tanks empty, after which increasing buoyancy in the aft MBTs reduces q.

As the commanded speed u_c in Figure C1a increases from 3 to 6 m/s, p in Figure C1b and ϕ in C1d increase in magnitude as propeller torque increases (J_b decreases). ϕ is more clearly seen in Figure 12. Since buoyancy does more to accelerate the boat than propulsion, J_b begins to increase at about $t = 18$ s and this will cause propeller torque to decrease as well. Despite decreasing torque, both p and ϕ steadily increase in magnitude for the rest of the maneuver as the boat responds to the increasing moment on the sail.

The mass characteristics are shown in Figure C1e. The discontinuity that results from the forward ballast tanks emptying generates discontinuities in all the mass characteristics but does not cause the ODE integrator much trouble, probably because the effect is small relative to the overall mass of the vehicle. As discussed earlier, the static stability $\overline{BG}^*$ increases steadily through the maneuver and then falls relatively quickly at the end, just as the tanks empty, to its original value. The discontinuity as the tanks empty is an artifact of the current model and could be eliminated by refining the model.

Simulation	**Initial Conditions:** unless otherwise noted, equilibrium flight at $u_c = 3$ m/s, $\phi = \phi_o$, $\delta_s = \delta_{s_t}$, $z_0 = 100$ m, $x_G, y_G = 0$; additional parameters as per Appendix A.			
	δ_s commanded (deg.)	u_c commanded (m/s)	Blow	Characteristics
S1	-20 @ $t = 0$ -1 @ $t = 17$ 3 @ $t = 38$	6 @ $t = 0$	normal	Baseline simulation: $\phi_o = -0.142$ degrees, $\delta_{s_t} = 0.813$ degrees, $y_{G_o} = 0$, $W_t = 1.64(10^{-4})B$.
S2	-20 @ $t = 0$ -1 @ $t = 17$ 3 @ $t = 38$	3	normal	S1 without the speed increase.
S3	-11 @ $t = 0$ -1 @ $t = 17$ 1 @ $t = 33$	4.5 @ $t < 0$ 9 @ $t = 0$	normal	S1 with 50% more speed, twice the dynamic pressure. Initial equilibrium at $u_c = 4.5$ m/s $\Rightarrow \phi_o = 0.320$ deg., $W_t = 3.69(10^{-4})B$.
S4	δ_{s_t}	6 @ $t = 0$	normal	S1 without using the sternplanes.
S5	-20 @ $t = 0$ 1 @ $t = 16.5$ 3 @ $t = 35$	6 @ $t = 0$	emergency	S1 except the MBTs are blown using the emergency air which provides twice the mass of air as for a normal blow.
S6	-20 @ $t = 0$ -1 @ $t = 17$ 25 @ $t = 37.7$	6 @ $t = 0$	normal	S1 except when the boat reaches a depth of 50 m, the sternplanes are used to reduce the pitch angle to about 5 degrees on surfacing.
S7	-25 @ $t = 0$ 1 @ $t = 25$	6 @ $t = 0$	normal	S1 except the boat is surfaced at a higher pitch angle of 35 instead of 20 degrees.
S8	-20 @ $t = 0$ -1 @ $t = 17$ 3 @ $t = 38$	6 @ $t = 0$	normal	S1 except the magnitude of the initial heel angle ϕ_o is increased to 2 degrees by setting $y_{G_o} = -0.0114$ m.
S9	-9 @ $t = 0$ 0 @ $t = 16$ 3 @ $t = 40$	6 @ $t = 0$	normal	S8 except the sternplanes limit the pitch angle to about 10 degrees throughout the maneuver.

Table 1 *Eight variations on a baseline simulation (S1). The simulations are shown in Appendix C and use the coefficient based hydrodynamic model from Appendix A.*

The normal velocity w, while it is never positive, has a maximum at about $t = 4$ s because of the downward force from the sternplanes and forward momentum of the boat. Because v is also small, Φ is very sensitive to this (Figure C1f) but eventually settles down as w becomes decisively negative.

The stability index U_S is initially high and positive but drops rapidly as speed and flow incidence increase. Stability is lost just before the forward tanks empty, when $\overline{BG}^*$ is decreasing. This timing is consistent with that of the trial in Figure 11. Despite the instability, roll magnitudes are not large enough to be of concern.

Simulation	$\frac{\overline{BG}^*_{\max}}{\overline{BG}_o}$	$U_S = 0$		Emergence States (at $t = t_e$)				
		$\frac{\overline{BG}^*_U}{\overline{BG}_o}$	$\frac{t_U}{t_e}$	t_e (s)	U_S (m/s)	Roll Angle ϕ (deg.)	Pitch Angle θ (deg.)	Flow Incidence Θ (deg.)
S1	1.213	1.15	0.92	47.4	−1.81	−2.0	20.5	17.1
S2	1.213	1.17	0.91	48.6	−1.75	0.3	21.5	19.4
S3	1.213	1.08	0.94	43.0	−1.46	−3.6	20.4	12.0
S4	1.217	1.21	0.86	62.1	−2.24	−3.9	9.5	21.5
S5	1.215	1.16	0.83	43.6	−2.68	−4.1	20.1	17.7
S6	1.213	1.19	0.86	49.2	−2.58	−3.4	5.4	29.7
S7	1.209	1.08	0.97	42.5	−0.55	−1.3	35.8	12.1
S8	1.213	1.15	0.91	47.5	−1.82	−9.2	20.1	17.2
S9	1.216	1.20	0.86	55.0	−2.26	−16.4	10.2	21.1

Table 2 *Some simulation results: The maximum $\overline{BG}^*$ value is virtually constant. $\overline{BG}^*_{\max}$ and $\overline{BG}^*_U$, the $\overline{BG}^*$ value just as the boat becomes unstable, are shown relative to $\overline{BG}_o = 0.35$ m. The time at which the boat becomes unstable, t_U, is normalized by the time taken to surface. The remaining values are those at the end of the maneuver, at $t = t_e$.*

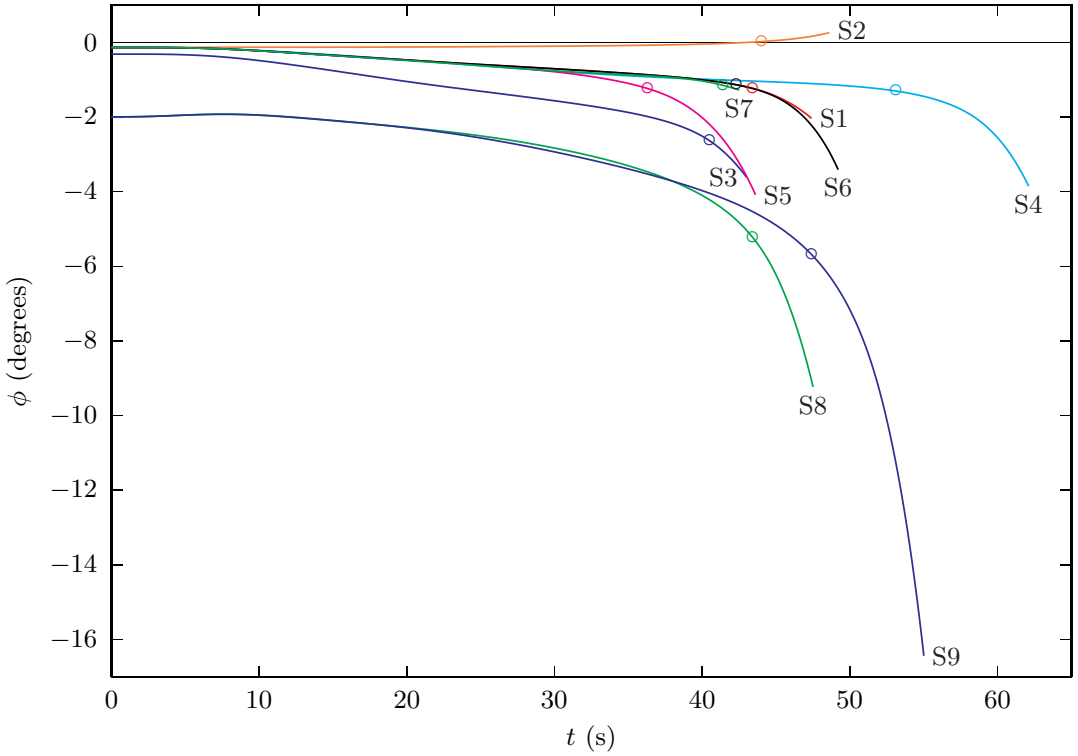

Figure 12 *Roll angle $\phi(t)$ for each of the simulations. $U_S = 0$ at each '$\circ$' symbol.*

Simulation 2

S2 differs from S1 only by maintaining a constant commanded speed of 3 m/s throughout the maneuver. This reduces u by only about 10% at the end of the maneuver since u is strongly influenced by buoyancy and the pitch angle. Flow incidence at the surface is increased from 17 to 19 degrees (Table 2). The net effect is slightly detrimental. There is a slight decrease in stability: $\overline{BG}_U^*$ is slightly larger so instability has occurred sooner in the blow (t_U relative to the time at which the V_{a1}/V_{T1} reaches 1.0). As well, there is slightly more time for the boat to respond to the instability (t_U/t_e is slightly smaller).

The most interesting difference between S1 and S2 is the effect on p and ϕ. Since u_c is constant, the advance ratio J_b initially increases (it initially decreases in S1) and eventually increases by a factor of three as u increases. This results in decreasing torque and a decreasing heel angle; p magnitudes are always positive and so the boat rolls in the opposite direction than in S1. Thus, while propeller thrust has only a minor effect on this maneuver, torque can influence the direction of roll. One wonders if the propeller could be used to maintain a constant roll angle.

Again, the roll magnitudes here are not significant.

Simulation 3

S3 differs from S1 by increasing the commanded speeds by 50% which doubles the dynamic pressure (hydrodynamic forces) throughout the maneuver. Sternplane control is adjusted to keep about the same maximum pitch angle of 20 degrees. Despite the faster speed, the boat reaches the surface only 4.4 s sooner than in S1. This is because little depth change occurs in the first half of either maneuver and $-w$, about half of the rising velocity (cf, Figure 1), is slightly reduced in S3 relative to S1.

A substantial reduction in Θ occurs over most of this maneuver because of the large increase in u and slight decrease in $-w$. Although this is countered to a large extent by the increase in dynamic pressure, $\overline{BG}_U^*$ shows that instability has been delayed. This is also seen in the increased t_U/t_e ratio.

S3 brings to light a disturbing new parameter that needs to be considered. Despite the fact that S3 is the shorter, more stable maneuver, it achieves a roll angle 80% greater than in S1. This is attributed to the larger initial heel angle ($\phi_o = -0.32$ versus -0.14 degrees in S1) which results from the higher initial propulsion torque required for the S3 maneuver. Clearly, initial heel is an important factor in this analysis.

The S3 emergence roll angle is, nevertheless, not large enough to be of concern.

Simulation 4

S4 differs from S1 in that sternplane control is not used to pitch the nose up. This results in a much longer maneuver. The crossflow $-w$ is primarily determined by the buoyancy; it develops earlier in the absence of downwards force from the sternplanes but not as quickly as in S1 because the ballast tanks empty slower. However, $-w$ achieves a higher magnitude because it has more time to develop. This, combined with a lower axial velocity, results in substantially larger flow incidence throughout the maneuver.

The net effect is a measurable decrease in stability, as seen by the larger $\overline{BG}_U^*$ value and substantially lower t_U/t_e ratio. Figure 12 shows that the lower pitch angle in the S4 maneuver has little effect on the roll time history prior to the S1 maneuver becoming unstable. The big difference between the simulations is the extra time the S4 maneuver gives the boat to respond to the instability once it occurs. This results in a roll angle almost twice that of S1.

The S4 emergence roll angle is still not large. The Figure 11 emergence roll angle is much larger without the aggravating factor of an extremely low pitch angle.

Simulation 5

S5 is the same as S1 except that emergency ballast blowing is used instead of normal blowing. This means that twice the mass of air is blown in S5 than in S1, resulting in both fore and aft tanks emptying before the boat surfaces. Slightly different sternplane control is used to maintain a pitch angle of 20 degrees. The maneuver occurs about 4 s faster than S1 because full buoyancy is achieved faster. Although $-w$ grows faster than in S1, it is largely countered by higher u magnitudes so Θ is only slightly larger. $\overline{BG}_U^*$ is little changed but t_U/t_e is the smallest of all the maneuvers, even though t_e is also small. Thus, the extra buoyancy gets the boat to the surface in 92% of the time of the S1 maneuver but also gives the boat twice as much time to react to the instability, resulting in twice the roll angle.

Simulation 6

S6 is the same as S1 except the sternplanes are used to curtail the pitch angle as the boat passes the 50 m depth mark so the boat can surface on a relatively even keel. This generates higher flow incidence at the end of the maneuver which is partially countered by lower dynamic pressure. It brings on the instability somewhat earlier and delays completion of the maneuver, increasing the time during which the boat is unstable by 80%. This results in a 70% increase in the final roll angle although, again, the final roll angle is not large.

Full scale maneuvers suggest that last minute pitch curtailment can result in substantial roll.

Simulation 7

S7 is the same as S1 except the sternplanes are kept deflected longer so the boat surfaces at a pitch angle of 35 degrees. This action is opposite in nature to the pitch curtailment used in S6. This is the fastest maneuver, even beating S3. Flow incidence is substantially reduced and instability is much delayed. The final roll angle is substantially less than for S1.

Simulation 8

S8 is the same as S1 except that the CG is moved laterally off the centerline by 11 cm generating an initially large heel (ϕ_o) of 2 degrees. This results in little or no change to most time histories, including flow incidence, speed, and the stability index. However, flow incidence now generates a much larger force on the rolled sail (cf, Figure 10) which produces higher roll rates and an emergence roll angle of 9 degrees.

Both the initial heel and final roll angles here are similar to those in Figure 11. The final roll clearly occurs as a result of the relatively large initial heel angle.

Simulation 9

S9 is S8 with the pitch angle limited to about 10 degrees throughout the maneuver. This brings on instability sooner (larger $\overline{BG}_U^*$ value) and the time during which the boat is unstable $(1-t_U)$ is doubled, resulting in an 80% larger emergence roll angle. This is very much a concern given the consequences upon surfacing shown in Figure 11.

Discussion

Simulations 1 through 7 result in roll angles that are small enough to be significantly influenced by propeller torque changes. This complicates the interpretation of the simulations. Since the roll angles are too small to be of concern, the conclusions drawn from these simulations are tentative; they are:

- increasing propeller speed has a small beneficial effect on roll stability and is important for minimizing the duration of the rise.
- propeller torque has the potential for growing or reducing the initial heel angle.
- buoyancy is necessary but excessive buoyancy unnecessarily aggravates the roll instability.
- increasing pitch is the best way to increase both speed and roll stability.
- pitch curtailment when surfacing aggravates the roll instability.

S8 shows that a large (but still realistic) initial heel angle has the greatest effect on the emergence roll angle. It does not effect stability because static stability and the destabilizing hydrodynamic force both increase linearly with ϕ. However, the rolling moment induced by the crossflow grows with the heel angle, and the additional heel needed to offset this additional moment grows as well. This is easily seen from a simplified quasi-steady analysis of the rolling moment equation. If Φ is small so $\Phi \sim \phi$, Q is propeller torque, and $y_B = z_G = 0$, then the K equation can be written as:

$$\text{small terms} = K_\Phi \phi - Q + y_G W + z_B B \phi \tag{58a}$$

so that:

$$\phi = \frac{Q - y_G W + (\text{small terms})}{K_\Phi + z_B B} \tag{58b}$$

Thus, heel grows as the magnitude of the denominator in (58b) decreases; that is, as stability decreases. This is why ϕ grows in the simulations even though the boat is still stable — new equilibria are being sought to offset the increasing rolling moment. However, the growth in ϕ is also proportional to the numerator which increases with the initial heel angle (determined by $Q - y_G W$). So S3 and S8 see greater roll changes prior to instability than does S1. When the boat goes unstable in S3 and S8, it does so with a higher roll rate and rolling moment so subsequent roll is more severe than for S1. (Note that (58) becomes invalid when instability occurs because the dynamics are no longer quasi-steady.)

S9 confirms the finding with the lower amplitude roll simulations that decreased pitch does not substantially alter the roll time history prior to instability. Decreased pitch decreases stability and provides increased time for the boat to react to the instability. This increases the emergence roll angle and roll rate which, in turn, aggravate roll as the boat surfaces and temporarily loses static stability.

9 Concluding Remarks

Propulsion, blowing, and control system models have been presented and tested prior to use in an unsteady 6 DOF RANS simulation. The models were tested using a high incidence, quasi-steady, coefficient based hydrodynamic model and several submarine emergency rising scenarios were explored.

The coefficient based simulations show that the boat consistently becomes unstable just before the ballast tanks empty, several seconds before surfacing. The best way of dealing with the roll instability is to use speed, induced by moderate buoyancy and a substantial pitch angle so instability is not aggravated, to get the submarine to the surface before it has time to respond to the instability.

When the initial heel angle is small (much less than a degree), emergence roll angles are also small. However, when the initial heel angle is appreciable (eg, 2 degrees), emergence roll angles are a concern; combined with low pitch angles, emergence roll angles large enough to instigate excessive roll after surfacing can result.

Further investigations are needed to validate these preliminary findings. The unsteady RANS simulations to follow will be important in this regard. Full scale trials are necessary to validate the suggested mitigation strategies and to see what kind of heel angles boats typically run with. The isothermal blowing model, which assumes the blown air temperature immediately warms to ambient temperatures, needs further investigation.

References

1. D.E. Hess, T.C. Fu, J.P. Feldman (2004), Naval Maneuvering Research and the Need for Shear Stress Measurements, *24th AIAA Aerodynamic Measurement Technology and Ground Testing Conference*, AIAA Paper 2004-2605, Portland, June.
2. ANSYS Canada Ltd. (2007), Software Design Document for a Six DOF Unsteady Simulation Capability in ANSYS-CFX, DRDC Atlantic CR 2007-020, in review, DISTRIBUTION LIMITED.
3. M. Mackay (2006), DSSP21 Build 061102 User Guide, DRDC Atlantic TM 2006-252, in review.
4. G.D. Watt (2001), A Quasi-Steady Evaluation of Submarine Rising Stability: The Stability Limit, *RTO-AVT Symposium on Advanced Flow Management*, Loen, Norway, May.
5. G.D. Watt and H.J. Bohlmann (2004), Submarine Rising Stability: Quasi-Steady Theory and Unsteady Effects, *25th Symposium on Naval Hydrodynamics*, St. John's, 6–18 August.
6. J. Feldman (1979), DTNSRDC Revised Standard Submarine Equations of Motion, DTNSRDC/SPD-0393-09, June.
7. G.D. Watt (1988), Estimates for the Added Mass of a Multi-Component, Deeply Submerged Vehicle, DREA TM 88/213, October.
8. M. Mackay (1999), DSSP20 (Beta Edition) User Guide to the Preprocessing Modules, DREA TM 1999-108, August.
9. G.D. Watt (1998), Estimating Underwater Vehicle Stability and Control Derivatives Using ESAM and a Preliminary Version of DSSP20, DREA TM 98/224, September, DISTRIBUTION LIMITED.
10. G.D. Watt (1998), A Propulsion Model for Submerged Vehicle Maneuvering Simulations, DREA TM 98/231, August, DISTRIBUTION LIMITED.
11. J.D. van Manen and P. van Oossanen (1988), Propulsion, Volume II, Chapter 6 of Principles of Naval Architecture, edited by E.V. Lewis, SNAME.
12. E. Fournier and V.D. Nguyen (1993), Wind Tunnel Investigation of the DREA Powered Mk I Submarine Model, DREA CR/93/459 (also NRC LTR-HA-30/6130), Volumes 1 and II, June, DISTRIBUTION LIMITED.
13. G.D. Watt (1995), Re-Evaluating the Thrust and Torque Measurement Capability of the Mark I Propulsion System for the DREA Static Test Rig, DREA TM 95/209, April.
14. G.D. Watt and E.Y. Fournier (1995), Submarine Propulsion Testing in the IAR 9 m Wind Tunnel, *Third Canadian Marine Hydrodynamics and Structures Conference*, Halifax, August.
15. R.L. Daugherty and J.B. Franzini (1977), Fluid Mechanics with Engineering Applications, McGraw-Hill.
16. M. Mackay (1992), DREA Submarine Simulation Program Version 0.2 (DSSP02) – Release Notes, DREA TC 92/308, April, DISTRIBUTION LIMITED.
17. G.D. Watt (1990), Modelling Submarine Control Surface Deflection Dynamics, DREA TM 90/203, March.

Appendix A: Simulation Constants, Functions, and Coefficients

Constants

The following constants are used in the simulations:

$k2mps = 0.514\dot{}$	Convert knots to m/s.
$g = 9.81$	Gravitational constant, m/s^2.
$\ell = 70$	Overall length of boat, m.
$d = \ell/8.75$	Maximum hull diameter, m.
$D = d/2$	Propeller diameter, m.
$\rho = 1025$	Density of sea water, kg/m^3.
$V = 0.008645\ell^3$	Volume displaced by the hydrodynamic envelope, m^3.
$\overline{BG}_o = 0.005\ell$	Initial height of CB above CG, m.
$x_B, y_B, z_B = 0, 0, -\overline{BG}_o$	CB coordinates, m.
$x_{Go}, y_{Go}, z_{Go} = x_B, y_B, z_B + \overline{BG}_o$	Initial CG coordinates, m.
$I_{xo} = 3\left(10^{-5}\right)\left(\frac{1}{2}\rho\ell^5\right)$	Initial moment of inertia about x axis, kg m^2.
$I_{y_o} = 10^{-3}\left(\frac{1}{2}\rho\ell^5\right)$	Initial moment of inertia about y axis, kg m^2.
$I_{zo} = I_{y_o}$	Initial moment of inertia about z axis, kg m^2.
$I_{xy_o}, I_{yz_o}, I_{zxo} = 0, 0, 0$	Initial products of inertia, kg m^2.
$N = 4$	Number of main ballast tanks.
$V_{T1}, V_{T2}, V_{T3}, V_{T4} = 100, 60, 60, 30$	MBT volumes, m^3.
$V_T = V_{T1} + V_{T2} + V_{T3} + V_{T4} = 250$	Total volume of all MBTs, m^3.
$x_{T1}, x_{T2}, x_{T3}, x_{T4} = 22, 19, -29, -32$	Axial location of MBT centroids, m.
$T = 278.16$	MBT temperature, degrees Kelvin, K.
$p_a = 101325$	Atmospheric pressure, N/m^2.
$R = 287$	Gas constant for air, J/kg/K.
$C_2 = -0.06, -0.03$	Normal, emergency blowing constants, s^{-1}
$m_{ro} = 1000, 2000$	Normal, emergency air mass for blowing, kg.
$\zeta, \omega_{\max}, d\delta/dt\|_{\mathrm{RL}} = 0.9, 2.0\,\mathrm{s}^{-1}, 0.1\,\mathrm{s}^{-1}$	Sternplane control parameters.
$\zeta, \omega_{\max}, d\delta/dt\|_{\mathrm{RL}} = 0.7, 0.1\,\mathrm{s}^{-1}, 0.5\,\mathrm{m/s}^2$	Propulsion (u_c) control parameters.

Coefficient Model Translational Hydrodynamic Functions

The $F_{uvw}(\Theta, \Phi)$ functions used in the coefficient model and plotted in Figure 2 in the main text are listed below.

$$\begin{aligned}
100X'_{uvw} = &-0.1460444814\cos^2(\Theta) + 2.092727148\sin^2(\Theta) \\
&+ 0.8822237467\sin^4(\Theta) + 0.1130677803\cos(\Theta)\sin(\Theta)\cos(\Phi) \\
&- \left[0.7378986666\sin^2(\Theta) - 1.657751309\sin^3(\Theta)\right]\cos(\Phi) \\
&- \left[0.8340902069\sin^2(\Theta) + 1.978042538\sin^3(\Theta)\right]\cos(2\Phi) \\
&+ \left[0.04793423102\sin^2(\Theta) - 0.3341608580\sin^3(\Theta)\right]\cos(3\Phi) \\
&- \left[0.2580423873\sin^2(\Theta) - 1.195335953\sin^3(\Theta)\right]\cos(4\Phi) \qquad \text{(A1)}
\end{aligned}$$

$$
\begin{aligned}
100Y'_{uvw} = {} & 6.742784020\cos(\Theta)\sin(\Theta)\sin(\Phi) \\
& + \left[11.01008861\sin^2(\Theta) + 4.193261671\sin^3(\Theta)\right]\sin(\Phi) \\
& - \left[12.89386476\sin^2(\Theta) - 20.17874874\sin^3(\Theta)\right]\sin(2\Phi) \\
& - \left[0.3810901693\sin^2(\Theta) - 2.091386770\sin^3(\Theta)\right]\sin(3\Phi) \\
& - \left[2.870012312\sin^2(\Theta) - 8.508595821\sin^3(\Theta)\right]\sin(4\Phi) \\
& - \left[0.08969245281\sin^2(\Theta) + 1.145093633\sin^3(\Theta)\right]\sin(5\Phi)
\end{aligned} \tag{A2}
$$

$$
\begin{aligned}
100Z'_{uvw} = {} & 0.05545234430\cos^2(\Theta) + 5.718214158\sin^2(\Theta) \\
& - 16.10350880\sin^4(\Theta) + 1.984938259\cos(\Theta)\sin(\Theta)\cos(\Phi) \\
& + \left[11.33288282\sin^2(\Theta) - 33.70003698\sin^3(\Theta) + 47.14241947\sin^4(\Theta)\right]\cos(\Phi) \\
& - \left[9.210462863\sin^2(\Theta) - 15.58771719\sin^3(\Theta) + 6.913780522\sin^4(\Theta)\right]\cos(2\Phi) \\
& - \left[4.447468749\sin^2(\Theta) - 30.70824244\sin^3(\Theta) + 36.56417687\sin^4(\Theta)\right]\cos(3\Phi) \\
& + \left[3.004351162\sin^2(\Theta) - 15.78083491\sin^3(\Theta) + 23.80409862\sin^4(\Theta)\right]\cos(4\Phi) \\
& + \left[2.393554689\sin^2(\Theta) - 10.88133361\sin^3(\Theta) + 9.034353557\sin^4(\Theta)\right]\cos(5\Phi)
\end{aligned} \tag{A3}
$$

$$
\begin{aligned}
100K'_{uvw} = {} & 0.2004601495\cos(\Theta)\sin(\Theta)\sin(\Phi) \\
& + \left[0.9563341051\sin^2(\Theta) - 0.7780718288\sin^3(\Theta)\right]\sin(\Phi) \\
& + \left[0.2673488329\sin^2(\Theta) - 0.1491263433\sin^3(\Theta)\right]\sin(2\Phi) \\
& - \left[0.01868084765\sin^2(\Theta) - 0.1247368635\sin^3(\Theta)\right]\sin(3\Phi) \\
& - \left[0.1360269435\sin^2(\Theta) - 0.2877553519\sin^3(\Theta)\right]\sin(4\Phi)
\end{aligned} \tag{A4}
$$

$$
\begin{aligned}
100M'_{uvw} = {} & 0.01548372486\cos^2(\Theta) + 1.024848874\sin^2(\Theta) \\
& - 4.832975106\sin^4(\Theta) - 0.4018487745\cos(\Theta)\sin(\Theta)\cos(\Phi) \\
& - \left[0.1346352455\sin^2(\Theta) - 1.278018136\sin^3(\Theta)\right]\cos(\Phi) \\
& - \left[1.930064018\sin^2(\Theta) - 3.352906727\sin^3(\Theta)\right]\cos(2\Phi) \\
& + \left[0.2547988257\sin^2(\Theta) + 0.5809402243\sin^3(\Theta)\right]\cos(3\Phi) \\
& + \left[0.6306394660\sin^2(\Theta) - 0.5989226878\sin^3(\Theta)\right]\cos(4\Phi) \\
& + \left[0.4984216470\sin^2(\Theta) - 1.729231462\sin^3(\Theta)\right]\cos(5\Phi)
\end{aligned} \tag{A5}
$$

$$
\begin{aligned}
100N'_{uvw} = {} & 1.409218893\cos(\Theta)\sin(\Theta)\sin(\Phi) \\
& - \left[2.020221148\sin^2(\Theta) - 0.7333665071\sin^3(\Theta)\right]\sin(\Phi) \\
& + \left[2.948685948\sin^2(\Theta) - 6.376794178\sin^3(\Theta)\right]\sin(2\Phi) \\
& - \left[0.1218281303\sin^2(\Theta) - 0.2698840669\sin^3(\Theta)\right]\sin(3\Phi) \\
& + \left[0.3267021655\sin^2(\Theta) - 1.560874539\sin^3(\Theta)\right]\sin(4\Phi) \\
& + \left[0.1230668903\sin^2(\Theta) - 0.1030152504\sin^3(\Theta)\right]\sin(5\Phi)
\end{aligned} \tag{A6}
$$

DSSP20/DERIVS Coefficient Estimates

The DERIVS program [5] uses the DSSP20 program to estimate first and second order derivatives for a simplified submarine geometry. The geometry is shown in Figure A1. The control derivative estimates are:

$$\begin{aligned} X'_{\delta_s\delta_s} &= -0.0208151 & X'_{\delta_r\delta_r} &= -0.0208151 \\ Z'_{\delta_s} &= -0.0238569 & Y'_{\delta_r} &= 0.0238569 \\ M'_{\delta_s} &= -0.0109145 & K'_{\delta_r} &= 0 \\ M'_{\delta_s\delta_s} &= 0 & M'_{\delta_r\delta_r} &= 0 \\ M'_{\delta_s|\delta_s|} &= 0 & N'_{\delta_r} &= -0.0109145 \end{aligned} \tag{A7}$$

DERIVS generates the following rotational derivatives. If they are zero or very small, they are replaced with their added mass equivalent if that is appreciable. The numbers shown below are the dimensionless coefficients (eg, $X'_{pp} = -0.0000281$) so that the dimensions of the (A8) coefficients are the same as the dimensions of the terms in brackets (eg, the dimensions of X_{pp} are the same as those of $\rho\ell^4$).

$$\begin{aligned} X_{pp} &= -0.0000281\left(\tfrac{1}{2}\rho\ell^4\right) & K_{up} &= -0.0004229\left(\tfrac{1}{2}\rho\ell^4\right) \\ X_{rr} &= 0.0032739\left(\tfrac{1}{2}\rho\ell^4\right) & K_{p|p|} &= -0.0000002\left(\tfrac{1}{2}\rho\ell^5\right) \\ X_{wp} &= -0.0002454\left(\tfrac{1}{2}\rho\ell^3\right) & K_{wp} &= \text{added mass equivalent} \\ X_{uq} &= 0.0000191\left(\tfrac{1}{2}\rho\ell^3\right) & K_{ur} &= -0.0001373\left(\tfrac{1}{2}\rho\ell^4\right) \\ X_{qq} &= 0.0033202\left(\tfrac{1}{2}\rho\ell^4\right) & K_{r|r|} &= -0.0000002\left(\tfrac{1}{2}\rho\ell^5\right) \\ X_{q|q|} &= 0.0000005\left(\tfrac{1}{2}\rho\ell^4\right) & M_{pp} &= 0.0000026\left(\tfrac{1}{2}\rho\ell^5\right) \\ Y_{up} &= -0.0049919\left(\tfrac{1}{2}\rho\ell^3\right) & M_{rr} &= 0.0000031\left(\tfrac{1}{2}\rho\ell^5\right) \\ Y_{p|p|} &= -0.0000026\left(\tfrac{1}{2}\rho\ell^4\right) & M_{wp} &= -0.0000033\left(\tfrac{1}{2}\rho\ell^4\right) \\ Y_{wp} &= \text{added mass equivalent} & M_{uq} &= -0.0060731\left(\tfrac{1}{2}\rho\ell^4\right) \\ Y_{ur} &= 0.0110609\left(\tfrac{1}{2}\rho\ell^3\right) & M_{qq} &= 0 \\ Y_{r|r|} &= 0.0030937\left(\tfrac{1}{2}\rho\ell^4\right) & M_{q|q|} &= -0.0012988\left(\tfrac{1}{2}\rho\ell^5\right) \\ Z_{pp} &= \text{added mass equivalent} & N_{up} &= -0.0006396\left(\tfrac{1}{2}\rho\ell^4\right) \\ Z_{rr} &= 0 & N_{p|p|} &= -0.0000003\left(\tfrac{1}{2}\rho\ell^5\right) \\ Z_{wp} &= -0.0000128\left(\tfrac{1}{2}\rho\ell^3\right) & N_{wp} &= -0.0000248\left(\tfrac{1}{2}\rho\ell^4\right) \\ Z_{uq} &= -0.0131470\left(\tfrac{1}{2}\rho\ell^3\right) & N_{ur} &= -0.0064560\left(\tfrac{1}{2}\rho\ell^4\right) \\ Z_{qq} &= \text{added mass equivalent} & N_{r|r|} &= -0.0012988\left(\tfrac{1}{2}\rho\ell^5\right) \\ Z_{q|q|} &= -0.0030973\left(\tfrac{1}{2}\rho\ell^4\right) \end{aligned} \tag{A8}$$

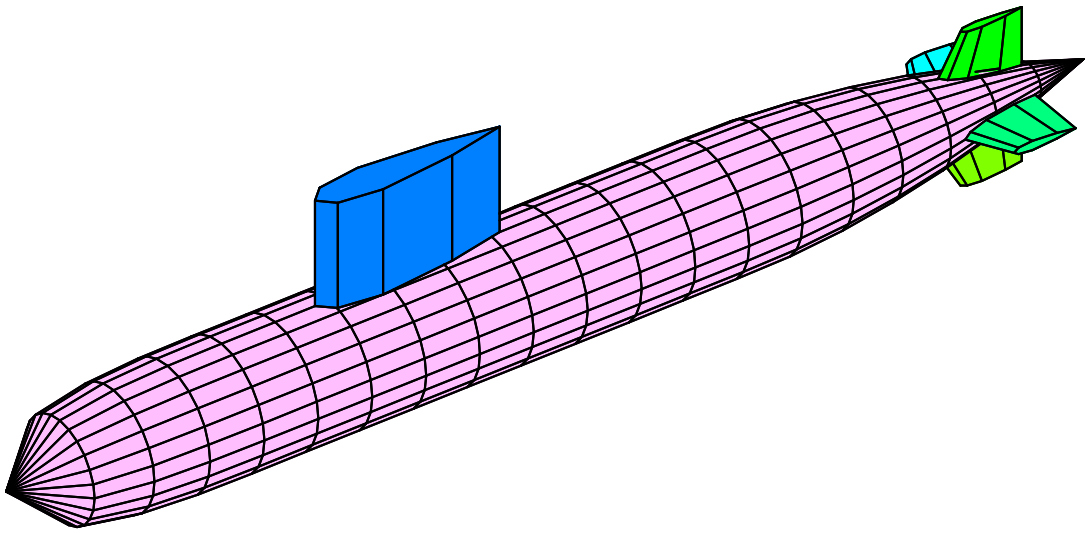

Figure A1 *The simplified geometry used by DSSP20 [4] for estimating vehicle steady state derivatives.*

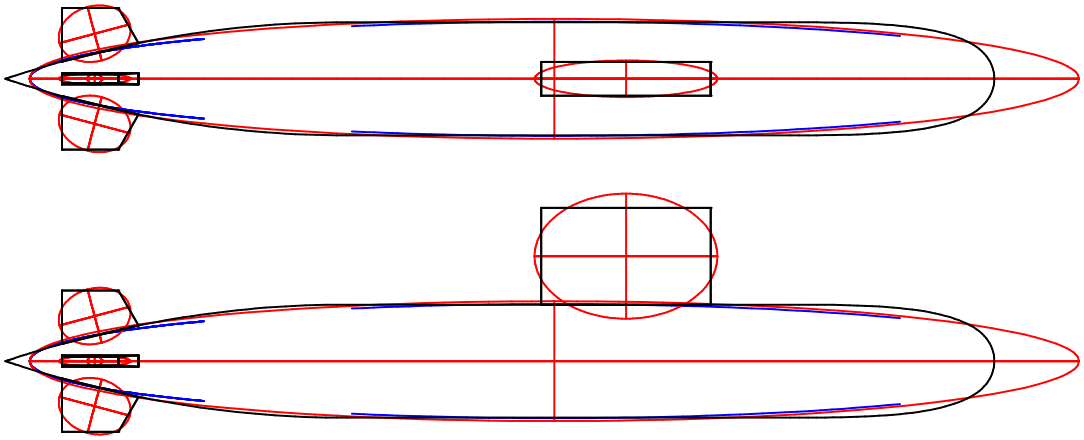

Figure A2 *Planform and elevation views of the generic shape being modelled (black lines) and the component replacement ellipsoids (red and blue lines) used for estimating vehicle added mass, following [3].*

Added Mass Coefficients

Replacing vehicle components with equivalent ellipsoids (Figure A2), for which analytical expressions for the added masses are available, the added mass coefficients for the entire vehicle can be estimated. Interference effects on the appendages, due to the presence of the hull are estimated [3]. The coefficients are (cf, Equations (5) & (6) from the main text):

$$
\begin{aligned}
X_{\dot{u}} &= -5.489\left(10^{-4}\right)\left(\tfrac{1}{2}\rho\ell^3\right) & K_{\dot{v}} &= Y_{\dot{p}} \\
X_{\dot{w}} &= -2.844\left(10^{-6}\right)\left(\tfrac{1}{2}\rho\ell^3\right) & K_{\dot{p}} &= -2.682\left(10^{-5}\right)\left(\tfrac{1}{2}\rho\ell^5\right) \\
X_{\dot{q}} &= 9.443\left(10^{-6}\right)\left(\tfrac{1}{2}\rho\ell^4\right) & K_{\dot{r}} &= -2.051\left(10^{-5}\right)\left(\tfrac{1}{2}\rho\ell^5\right) \\
Y_{\dot{v}} &= -1.959\left(10^{-2}\right)\left(\tfrac{1}{2}\rho\ell^3\right) & M_{\dot{u}} &= X_{\dot{q}} \\
Y_{\dot{p}} &= -2.915\left(10^{-4}\right)\left(\tfrac{1}{2}\rho\ell^4\right) & M_{\dot{w}} &= Z_{\dot{q}} \\
Y_{\dot{r}} &= 2.067\left(10^{-5}\right)\left(\tfrac{1}{2}\rho\ell^4\right) & M_{\dot{q}} &= -9.209\left(10^{-4}\right)\left(\tfrac{1}{2}\rho\ell^5\right) \\
Z_{\dot{u}} &= X_{\dot{w}} & N_{\dot{v}} &= Y_{\dot{r}} \\
Z_{\dot{w}} &= -1.622\left(10^{-2}\right)\left(\tfrac{1}{2}\rho\ell^3\right) & N_{\dot{p}} &= K_{\dot{r}} \\
Z_{\dot{q}} &= -2.575\left(10^{-4}\right)\left(\tfrac{1}{2}\rho\ell^4\right) & N_{\dot{r}} &= -9.392\left(10^{-4}\right)\left(\tfrac{1}{2}\rho\ell^5\right)
\end{aligned}
\tag{A9}
$$

The added mass coefficients also give the steady state potential flow forces on the vehicle. These are only used when there is no estimate available that accounts for viscous effects. The steady state potential flow coefficients used are (see Equation 25, from [3]):

$$
\begin{aligned}
X_{vr} &= -Y_{\dot{v}} & K_{wp} &= -Y_{\dot{p}} \\
X_{rp} &= -Y_{\dot{p}} & K_{pq} &= K_{\dot{r}} \\
X_{wq} &= Z_{\dot{w}} & K_{vq} &= Y_{\dot{r}} + Z_{\dot{q}} \\
Y_{wr} &= X_{\dot{w}} & K_{wr} &= -Y_{\dot{r}} - Z_{\dot{q}} \\
Y_{qr} &= X_{\dot{q}} & K_{qr} &= -M_{\dot{q}} + N_{\dot{r}} \\
Y_{wp} &= -Z_{\dot{w}} & M_{wq} &= X_{\dot{q}} \\
Y_{pq} &= -Z_{\dot{q}} & M_{vr} &= Y_{\dot{p}} \\
Z_{wq} &= -X_{\dot{w}} & M_{vp} &= -Y_{\dot{r}} \\
Z_{qq} &= -X_{\dot{q}} & M_{pr} &= K_{\dot{p}} - N_{\dot{r}} \\
Z_{vp} &= -Y_{\dot{v}} & N_{qr} &= -K_{\dot{r}} \\
Z_{pp} &= Y_{\dot{p}} & N_{vq} &= -X_{\dot{q}} - Y_{\dot{p}} \\
Z_{rp} &= Y_{\dot{r}} & N_{pq} &= -K_{\dot{p}} + M_{\dot{q}}
\end{aligned}
\tag{A10}
$$

Appendix B: Subroutines for Control System Modelling

The FORTRAN 77 program `cs.f` is listed below. It consists of a main program and two subrouines CNSYS2 and CSDEFL. The main program is just a utility for exercising the subroutines. The enabling mathematics for the subroutines is presented in [17].

```
      PROGRAM CS
*************************************************************************
* Front end for SUBROUTINE CNSYS2. Reads the following data from       *
* input file SIMU.INP.                                                  *
*                                                                       *
*          TEND            The end of the simulation.                  *
*          WMAX,DDMX,ZETA  Control system charateristics:response      *
*         <leave no space>         frequency, rate limit, damping.     *
*          NCOM            Number of commands to be issued (max 20).   *
*          TC(1),DC(1)     Time command is issued, Defltn commanded.   *
*          TC(2),DC(2)              ...                    ...         *
*              ...                                                      *
*          TC(NCOM),DC(NCOM)                                            *
*                                                                       *
* Program CS calculates the proper time response to this series of     *
* commands, matching the control surface deflection and rate of        *
* deflection each time a new command is issued (initial conditions are *
* all taken as zero). Data is output to file PLOT.DAT every            *
* approximately 0.05 seconds.                                           *
*************************************************************************

      IMPLICIT DOUBLE PRECISION (A-Z)
      INTEGER I,J,MAXCOM,NCOM
      PARAMETER( MAXCOM = 20,
     +               PI = 3.14159265358979323 85D0,
     +             RTOD = 180.D0/PI,
     +             DTOR = 1./RTOD    )
* A maximum of 20 commands in a series.

      DIMENSION TC(MAXCOM),DC(MAXCOM)
* TC: the time at which a command is issued.
* DC: the commanded deflection angle.

* Computer dependent numbers.
      COMMON /CMPTR/ SMLNUM,SN100,TOL,TL1000,TL1LOG
      SMLNUM = 1.E-5
   22 SMLNUM = 0.5*SMLNUM
           A = SMLNUM+1.0
      IF (A .GT. 1.0) GOTO 22
       SN100 = SMLNUM*100.
C The error tolerance level (normally set by the calling routine).
         TOL = 1E-5
      TL1000 = MAX(TOL/1000.,SN100)
      TL1LOG = LOG(TL1000)

      DATA DELC,AMP,DELTA/3*0.0/
* Zero initial state and command state for control system.
```

```
* Open and read input file SIMU.INP.
      OPEN(50,FILE='SIMU.INP',STATUS='OLD')
      READ(50,*) TEND
      READ(50,*) WMAX,DDMX,ZETA
      READ(50,*) NCOM
      IF (NCOM .GT. MAXCOM) THEN
        WRITE(ITERM,4010) MAXCOM,NCOM
        WRITE(IOUTL,4010) MAXCOM,NCOM
 4010 FORMAT(/' FATAL ERROR: Array dimensioning restricts you to ',
     +I3,' commands.'/' You have specified ',I3,' commands.'/)
        STOP
      ELSE IF (NCOM .LE. 0.0) THEN
        WRITE(ITERM,4020) NCOM
        WRITE(IOUTL,4020) NCOM
 4020 FORMAT(/' FATAL ERROR: It is meaningless to specify ',I3,
     +' commands.'/)
        STOP
      ENDIF
      READ(50,*) (TC(I),DC(I),I=1,NCOM)

      DO 100 I=1,NCOM
  100 DC(I) = DC(I)*DTOR

      IF (TEND .LT. TC(1)) THEN
        WRITE(ITERM,4030) TC(1),TEND
        WRITE(IOUTL,4030) TC(1),TEND
 4030 FORMAT(/' FATAL ERROR: The integration BEGINS when the first ',
     +'command is issued'/' at t =',f7.1,', but you have specified ',
     +'that it ENDS at t =',f7.1,'.'/)
        STOP
      ENDIF

           T = TC(1)
      TSTART = T

* Data is written to specially formatted output file PLOT.DAT.
      OPEN(51,FILE='PLOT.DAT',STATUS='UNKNOWN')
WRITE(51,*) 1,0,0,0,0
WRITE(51,*)
WRITE(51,*)
WRITE(51,*)
WRITE(51,*)
WRITE(51,*)

      I = 1
  200 CONTINUE

      CALL CNSYS2(TC(I),DC(I),DELC,T0,AMP,BETA,OMEGA,WMAX,DDMX,ZETA)
      I = I+1
      IF (I .LE. NCOM) THEN
        TSTOP = min(TC(I),TEND)
```

```
      ELSE
        TSTOP = TEND
      ENDIF

       J = NINT((TSTOP-T)/0.05)
      IF (J .LE. 5) J=J+1
      DT = (TSTOP-T)/J

300   CONTINUE

      CALL CSDEFL(T,DELTA,DELC,T0,AMP,BETA,OMEGA,ZETA)
      IF (T .EQ. TSTART) THEN
        WRITE(51,*) 0,T,DELTA*RTOD
      ELSE
        WRITE(51,*) 1,T,DELTA*RTOD
      ENDIF

      T = T+DT
      IF (T .GT. TEND+TOL)  GOTO 10
      IF (T .GT. TSTOP+TOL) GOTO 200
      GOTO 300

  10  CONTINUE
      WRITE(51,*) -1
      END

      SUBROUTINE CNSYS2(T,D2, DELC,T0,AMP,BETA,OMEGA, WMAX,DELDMX,ZETA)
*************************************************************************
*                                                                       *
* (c) Copyright Her Majesty the Queen in Right of Canada, as            *
*     represented by the Department of National Defence.                *
*                                                                       *
* CNSYS2 accepts a new commanded deflection, D2, for a control surface  *
* at time T and matches a second order response to the current control  *
* surface position and speed characteristics; this response depends on  *
* the control system characteristics WMAX, DELDMX and ZETA. The         *
* parameters describing the response to the previous command, DELC      *
* through OMEGA, are upgraded to the new response parameters.           *
*                                                                       *
*      T - Current time.                                                *
*     D2 - Newly commanded deflection angle, effective at time T.       *
*                                                                       *
*   DELC - Old commanded deflection angle, changed to D2 on output.     *
*     T0 - Time of issuance of old command, changed to T on output.     *
*    AMP - Oscillation amplitude of response at time previous command   *
*          was issued (T=T0), output value is for new command.          *
*   BETA - Phase shift of oscillation of previous response, output      *
*          value is for new command.                                    *
*  OMEGA - Frequency at which control system reacts. Input value is     *
*          for previous command; output value is for new command.       *
*                                                                       *
* Fixed parameters:                                                     *
```

```
*   WMAX - The maxmimum frequency, omega, at which the control system  *
*          can respond; OMEGA = WMAX unless this results in a maximum  *
*          rate of deflection exceeding DELDMX.                        *
* DELDMX - The maximum rate at which the control surface is capable of *
*          deflecting; a positive number.                              *
*   ZETA - The damping of the control system.                          *
*                                                                      *
************************************************************************

      IMPLICIT DOUBLE PRECISION (A-Z)
      PARAMETER(   PI = 3.1415926535897932D0,
     +           RTOD = 180.D0/PI,
     +           ZERO = 0.0,
     +            ONE = 1.0  )
C Relative error used in this subroutine (TL1000) is 1/1000 that used in
C the calling routine so, for practical purposes, this routine is exact.
      COMMON /CMPTR/ SMLNUM,SN100,TOL,TL1000,TL1LOG

      SAVE ZSAVE1,ZSAVE2,Z2,RTZ,ACZ,ACZ2,ZETRTZ,
     +     COF7,TEST,COF6,COF5,COF4,COF3,COF2
      DATA ZSAVE1,ZSAVE2/2*-1./

C Some calculations need not be repeated if ZETA doesn't change from
C call to call.
      IF (ZSAVE1 .NE. ZETA) THEN
        ZSAVE1 = ZETA
            Z2 = ZETA*ZETA
           RTZ = SQRT(1-Z2)
           ACZ = ACOS(ZETA)
          ACZ2 = ACZ+ACZ
        ZETRTZ = ZETA/RTZ
          COF7 = -(Z2*(Z2*(Z2*7.1168-26.0928)-46.0728)-3.0375)/4354.56
          TEST = (TL1000/COF7)**0.142857143
      ENDIF

   50 CONTINUE
      IF (AMP .NE. ZERO) THEN

        WT = OMEGA*(T-T0)
        A1 = -ZETA*WT
C If original amplitude has decayed by a factor of TL1000, AMP = 0.0.
        IF (A1 .GT. TL1LOG) THEN
             A1 = AMP*EXP(A1)
             A2 = RTZ*WT+BETA
           DEL0 = DELC-A1*SIN(A2)
          DELD0 = OMEGA*A1*SIN(A2-ACZ)
        ELSE
          AMP = 0.0
          GOTO 50
        ENDIF

C  If DELD0 is effectively zero, take a shortcut.
```

```
        IF (ABS(DELD0) .LT. TL1000) THEN
           AMP = 0.0
          DELC = DEL0
          GOTO 50
        ENDIF
        DELDEL = D2-DEL0

C  Calculate frequency limited characteristics.

C   Evaluate BETA keeping in mind that DELDEL may be zero.
          A1 = ZETA*DELDEL-DELD0/WMAX
        BETA = ATAN2(RTZ*ABS(DELDEL),A1*SIGN(ONE,DELDEL))
        IF (BETA .GT. 0.7  .AND.  BETA .LT. 2.4) THEN
          AMP = DELDEL/SIN(BETA)
        ELSE
          AMP = A1/RTZ/COS(BETA)
        ENDIF

        DDMAX = AMP*WMAX*RTZ*EXP(ZETRTZ*(BETA-ACZ2))

C  If BETA .LT. ACZ2 and if the maximum rate of deflection is greater
C  than the limit, the solution is rate limited.

        IF (ABS(DDMAX) .GT. DELDMX  .AND.  BETA .LT. ACZ2) THEN

          DDMAX = SIGN(DELDMX,DELDEL)
          RATIO = DELD0/DDMAX

C   See if Beta can be solved for with Taylor series or if Newton-
C   Raphson method should be used.

           A1 = MAX(ZERO,1.-RATIO)
          EPS = SQRT(A1+A1)

          IF (EPS .LE. TEST) THEN

C    Calculate BETA directly using its Taylor series about BETA = ACZ2.
            IF (ZSAVE2 .NE. ZETA) THEN
              ZSAVE2 = ZETA
                COF6 = ZETA*(Z2*(Z2*1.6-15.6)-8.1)/850.5
                COF5 = (Z2*(Z2*6.4+62.4)+8.1)/1728.
                COF4 = -ZETA*(Z2*1.6+2.7)/54.
                COF3 = (Z2*8.+3.)/72.
                COF2 = -ZETA/3.
            ENDIF
            BETA = ACZ2-RTZ*EPS*(EPS*(EPS*(EPS*(EPS*(EPS*
     +             (EPS*COF7+COF6)+COF5)+COF4)+COF3)+COF2)+1.)

          ELSE

C   Calculate BETA using the Newton-Raphson iteration. Guess an initial
C   value for BETA: choose initial value so subsequent iterations march
```

```
C   BETA monotonically towards its correct value without overshooting.

            IF (RATIO .GE. 0.0) THEN
C    a minimum value!
              BETA = ACZ
            ELSE
C    the inflection point or zero!
              BETA = MAX(ACZ2+ACZ-PI,ZERO)
            ENDIF

C   Enter iterative loop.
              A1 = RATIO*RTZ
  100         A2 = BETA-ACZ
              A3 = A2-ACZ
              DB = RTZ/SIN(A3)*(SIN(A2)-A1*EXP(ZETRTZ*A3))
            BETA = BETA+DB
C   Test to see if more accuracy is required (BETA in radians).
            IF (ABS(DB) .GT. TL1000) GOTO 100

          ENDIF

C  The rate limited BETA is now known. Calculate the rate limited OMEGA,
C  saving AMP for later calculation.
            AMP = DELDEL/SIN(BETA)
          OMEGA = DDMAX/AMP/RTZ*EXP(ZETRTZ*(ACZ2-BETA))
C  Note that DELDEL cannot be zero; if it is the solution is
C  necessarily frequency limited.

        ELSE

C  The frequency limited OMEGA.
          OMEGA = WMAX

        ENDIF

      ELSE

C AMP equal zero, a special case.
DELDEL = D2-DELC
        IF (ABS(DELDEL) .LT. TL1000) THEN
          DELC = D2
          RETURN
        ENDIF
         AMP = DELDEL/RTZ
        BETA = ACZ

C The rate limit prediction of OMEGA:
        DDMAX = SIGN(DELDMX,DELDEL)
        OMEGA = DDMAX/DELDEL*EXP(ZETRTZ*ACZ)
C Convert to frequency limit prediction if appropriate.
        OMEGA = MIN(OMEGA,WMAX)
```

```
      ENDIF

C AMP = (D2-DELC)/SIN(BETA), BETA, and OMEGA have now been determined.

      DELC = D2
        T0 = T
write(*,*) ' OMEGA,BETA = ',omega,beta*rtod
write(*,*) ' DDMAX = ',deldel/sin(beta)*omega*rtz
     +                        *exp(zetrtz*(beta-acz2))

      END

      SUBROUTINE CSDEFL(T,DELTA, DELC,T0,AMP,BETA,OMEGA,ZETA)
*********************************************************************
* Calculate the deflection, DELTA, of a control surface at time T. The *
* charateristics of the second order control system for the control    *
* surface are given by:                                               *
*                                                                     *
*  DELC - Commanded deflection angle.                                 *
*    T0 - Time command was issued.                                    *
*   AMP - Amplitude of oscillation of control system at time command  *
*         was issued.                                                 *
*  BETA - Phase shift of oscillation.                                 *
* OMEGA - Response frequency at which oscillation occurs.             *
*  ZETA - Damping of control system.                                  *
*********************************************************************

      IMPLICIT DOUBLE PRECISION (A-Z)
      SAVE ZSAVE,RTZ
C Relative error used in this subroutine (TL1000) is 1/1000 that used in
C the calling routine so, for practical purposes, this routine is exact.
      COMMON /CMPTR/ SMLNUM,SN100,TOL,TL1000,TL1LOG
      DATA ZSAVE/-1./

      IF (AMP .EQ. 0.0) THEN
        DELTA = DELC
      ELSE
         WT = OMEGA*(T-T0)
        ZWT = -ZETA*WT
C If original amplitude has decayed by a factor of TL1000, DELTA = DELC.
        IF (ZWT .GT. TL1LOG) THEN
          IF (ZETA .NE. ZSAVE) THEN
              RTZ = SQRT(1.-ZETA*ZETA)
            ZSAVE = ZETA
          ENDIF
          DELTA = DELC-AMP*EXP(ZWT)*SIN(RTZ*WT+BETA)
        ELSE
          DELTA = DELC
        ENDIF
      ENDIF

      END
```

Appendix C: Simulation Plots

Each of the nine pages following this one contain graphical output from a rising simulation using the coefficient based hydrodynamic model. The first simulation, Figure C1, forms the basis for Simulations 2 through 8 (Figures C2 through C8). Simulation 9 (Figure C9) is based on Simulation 8. Hereafter, Simulation n is referred to as Sn.

To simplify comparisons, the scales on graphs of the same type are the same. The only exceptions are the (b) and/or (d) plots in S6, S7, and S9; however, these contain horizontal dashed lines showing the normal location of the limits.

All variables plotted are listed along the ordinate axis in an order that determines the color of the curve showing that quantity in the plot:

Variable 1	Red
2	Green
3	Blue
4	Black
5	Cyan (light blue)
6	Orange

The exceptions are the V_{ai}/V_{Ti} curves in parts (e) of the figures. These follow the same color scheme used in Figure 8 in the main text:

V_{a1}/V_{T1}	Red
V_{a2}/V_{T2}	Green
V_{a3}/V_{T3}	Cyan
V_{a4}/V_{T4}	Blue

and are easily identified as the only curves in parts (e) which attain a value of 1.0.

All the plots with time along the abscissa axis have vertical black lines marking significant events. Fine dashed vertical lines indicate times at which new sternplane commands are issued. Fine solid vertical lines mark the times when the first and fourth MBTs suddenly empty ($V_{ai}/V_{Ti} = 1$); the fourth tank often does not empty before the boat reaches the surface. These events are also marked in parts (c) of the figures (the trajectory) by the plus (+) symbols.

In addition, a dark vertical line with circles ($\circ$) at its end points marks the time at which the boat becomes unstable in roll. This is determined by when $U_S = 0$ in parts (a). In parts (c), this point is marked by just the circle symbol.

The plots end when the boat emerges through the surface, at $t = t_{\mathrm{e}}$. This is defined as the time at which the top of the forward most MBT is at the ocean surface. This means the simulations finish with the body fixed axes origin at various depths (cf, parts(c) of S6 and S7) because of different surfacing pitch angles.

Parts (f) of the figures show Θ and Φ. As explained in the main text, Φ can jump by π when w changes sign (depending on v), which it does in the first 10 seconds or so of S1 and comes close to doing in several of the other simulations. When this happens, something approaching a discontinuity appears in Θ; it would be a discontinuity if v were exactly zero when w changed sign.

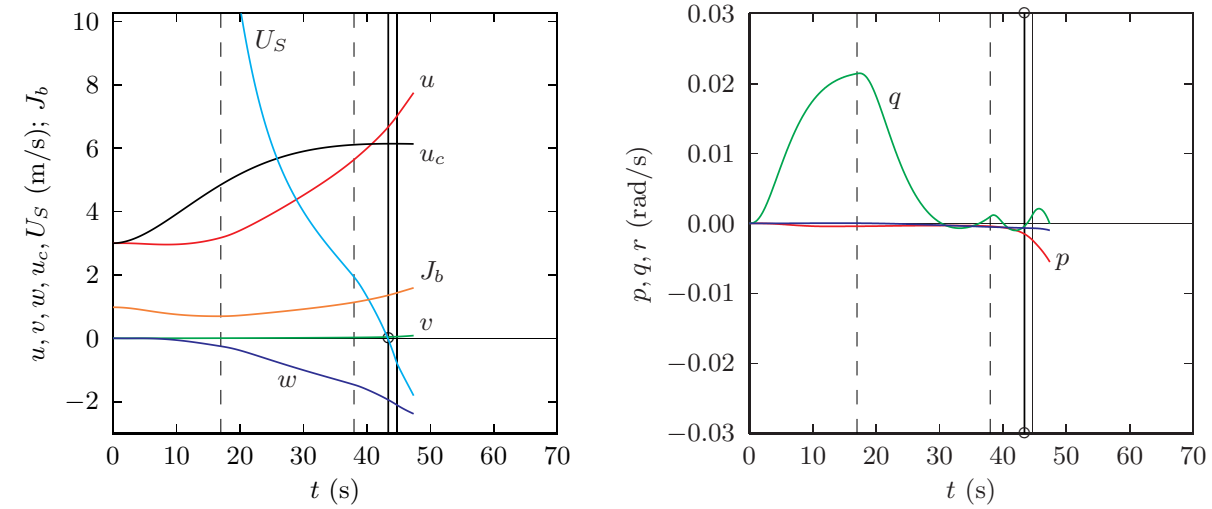

a) *Velocity and propulsion states.*

b) *Rotational velocity states.*

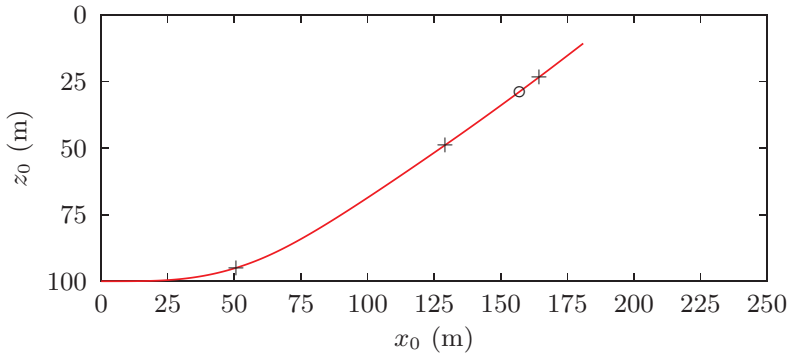

c) *Trajectory, elevation view.*

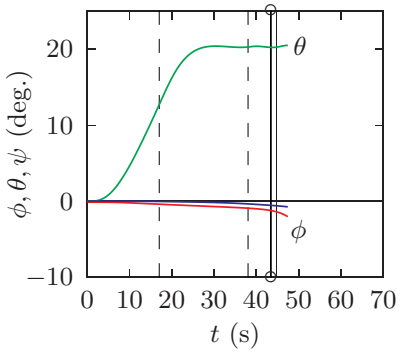

d) *Euler angles.*

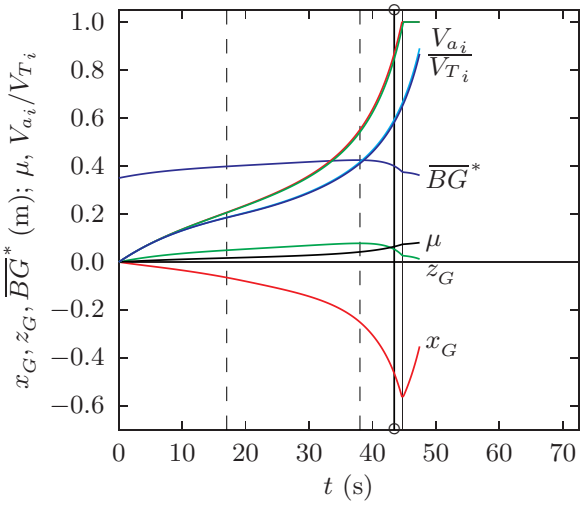

e) *Mass and blow characteristics.*

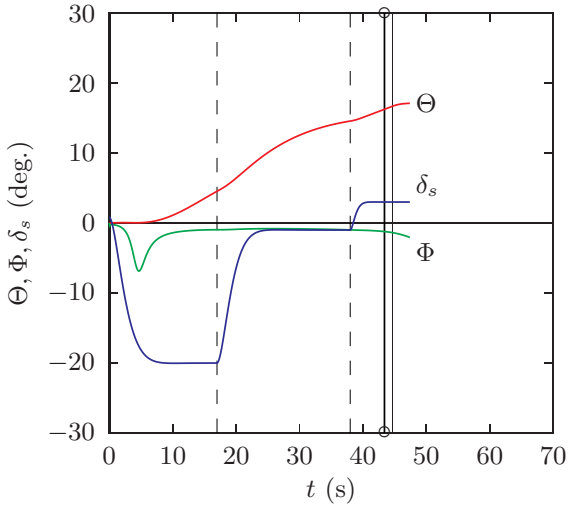

f) *Incidence and sternplane deflection.*

Figure C1 *Simulation 1: The baseline simulation. Start from straight and level flight at 100 m depth and a speed of 3 m/s. At t = 0, command a sternplane deflection of –20 degrees to pitch up. Simultaneously blow ballast normally and command a speed increase to 6 m/s. Adjust the sternplane deflection to limit the pitch angle to 20 degrees.*

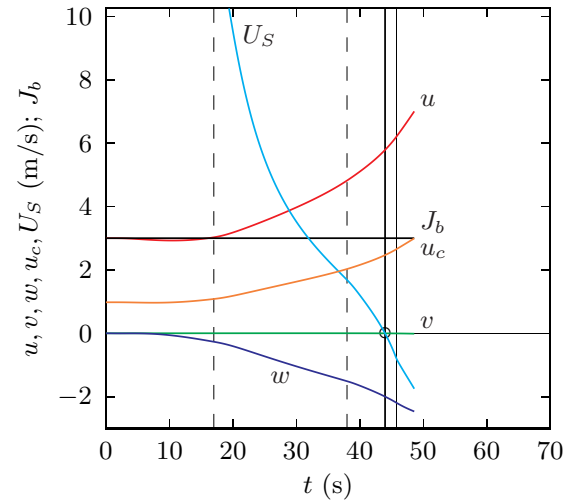

a) *Velocity and propulsion states.*

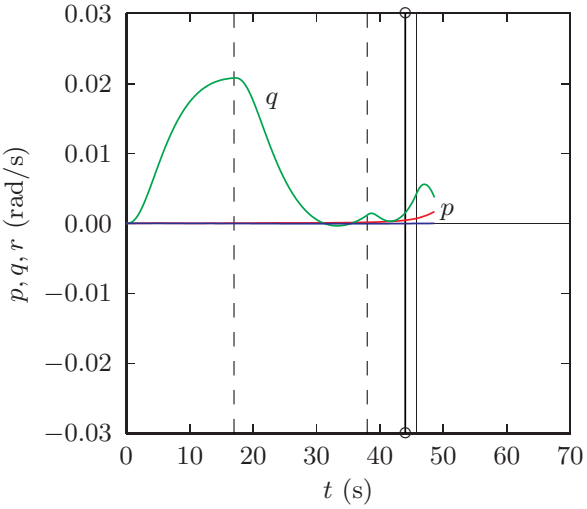

b) *Rotational velocity states.*

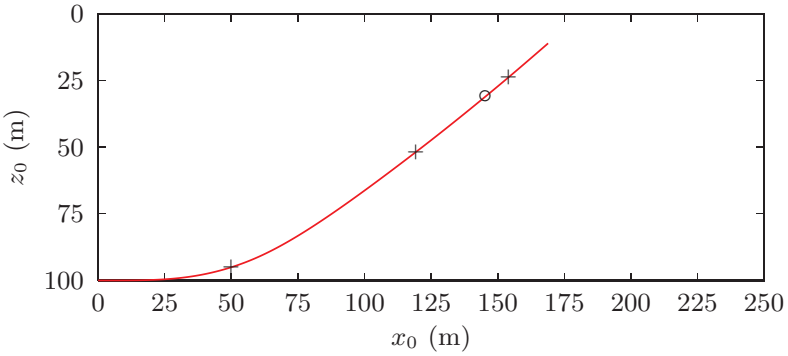

c) *Trajectory, elevation view.*

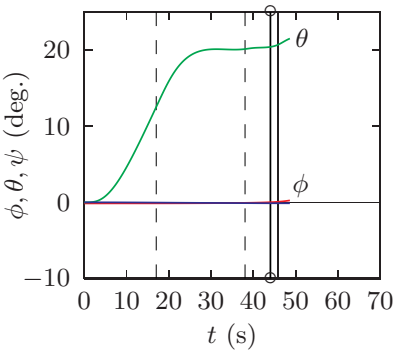

d) *Euler angles.*

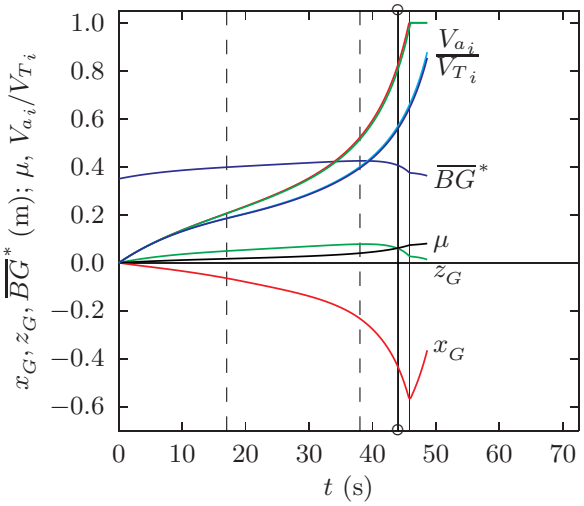

e) *Mass and blow characteristics.*

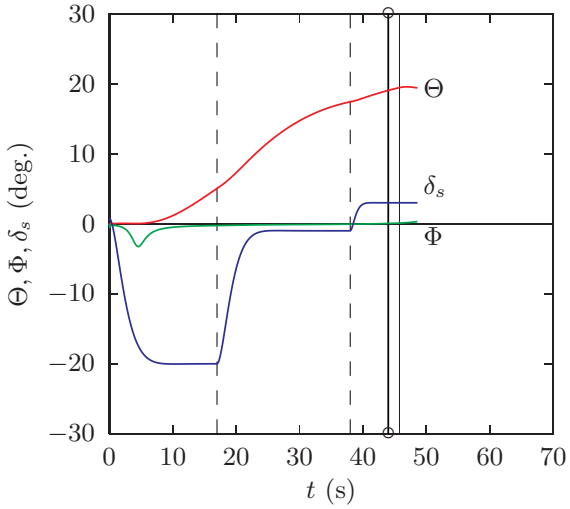

f) *Incidence and sternplane deflection.*

Figure C2 *Simulation 2: The same as S1 except commanded speed is not increased.*

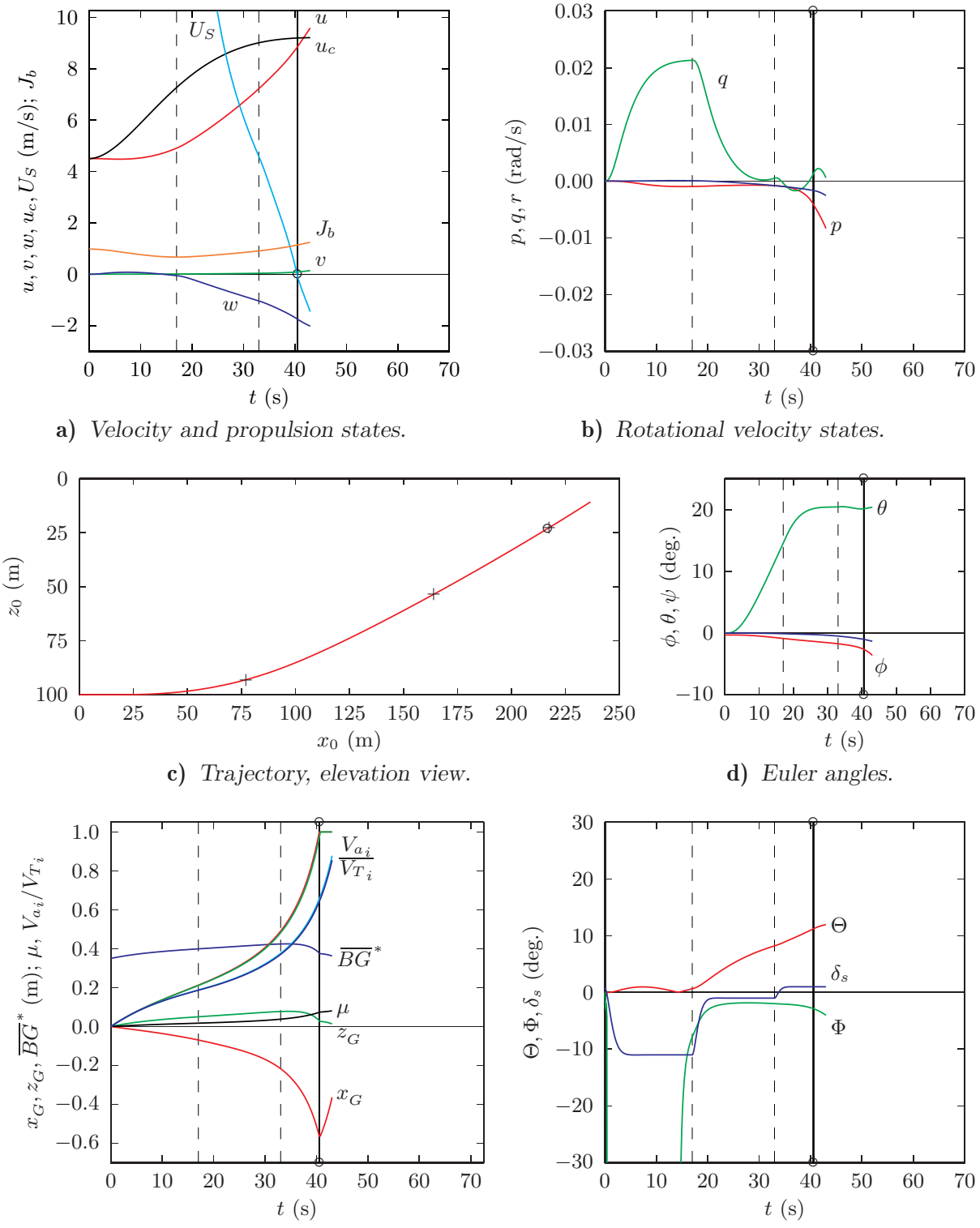

a) *Velocity and propulsion states.*

b) *Rotational velocity states.*

c) *Trajectory, elevation view.*

d) *Euler angles.*

e) *Mass and blow characteristics.*

f) *Incidence and sternplane deflection.*

Figure C3 *Simulation 3: The same as S1 except the initial speed is 4.5 m/s, increased to 9 m/s beginning at $t = 0$; that is, the speeds are increased by 50%, approximately doubling the dynamic pressure.*

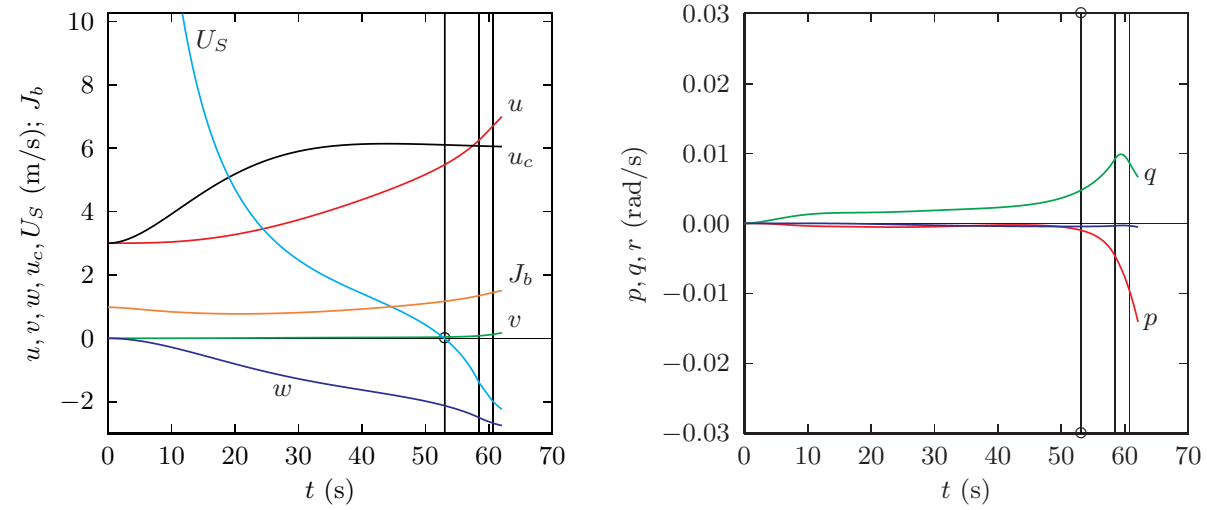

a) *Velocity and propulsion states.*

b) *Rotational velocity states.*

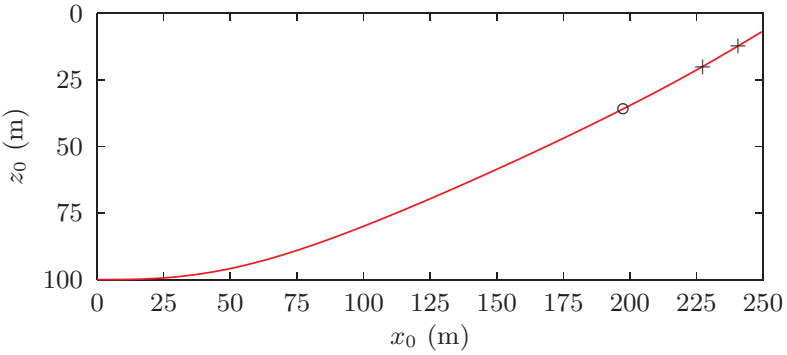

c) *Trajectory, elevation view.*

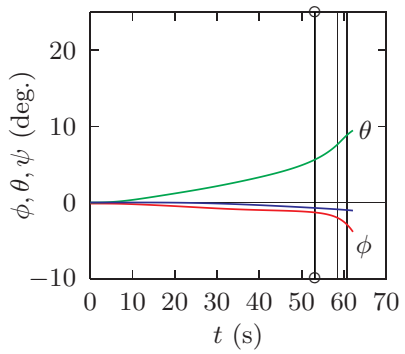

d) *Euler angles.*

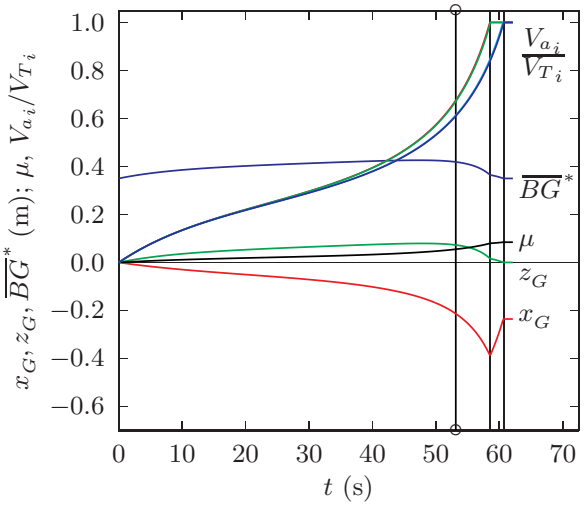

e) *Mass and blow characteristics.*

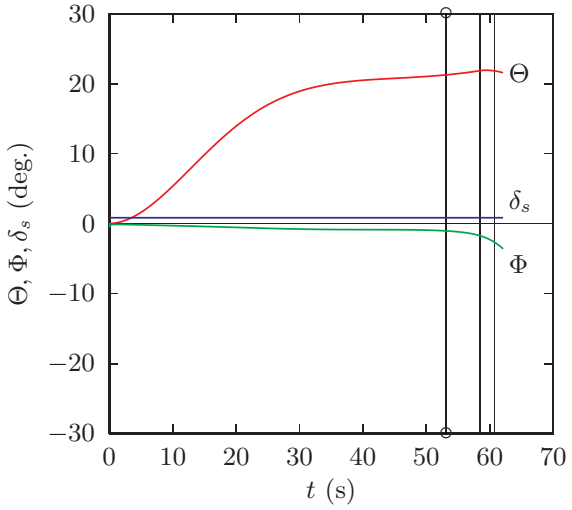

f) *Incidence and sternplane deflection.*

Figure C4 *Simulation 4: The same as S1 except sternplane control is not used to pitch the nose up.*

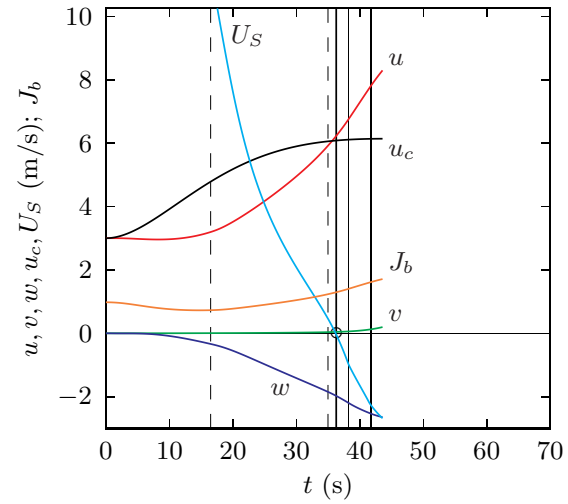

a) *Velocity and propulsion states.*

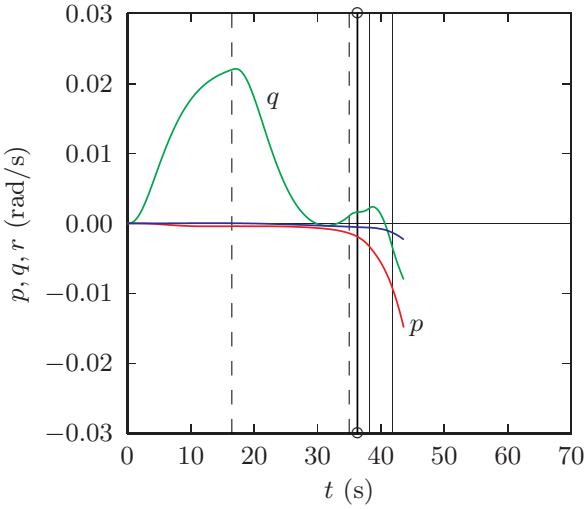

b) *Rotational velocity states.*

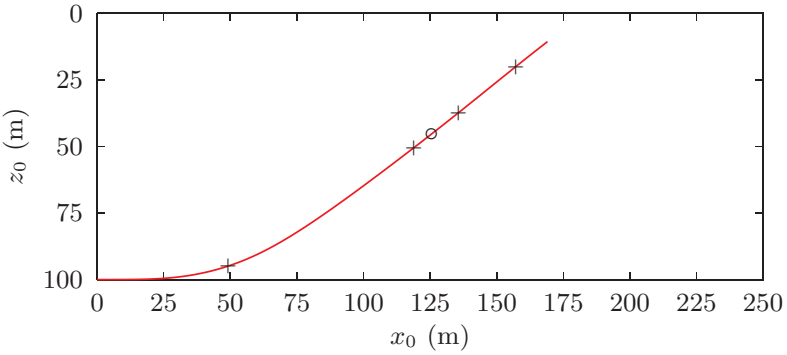

c) *Trajectory, elevation view.*

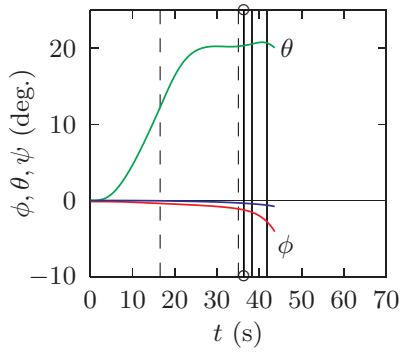

d) *Euler angles.*

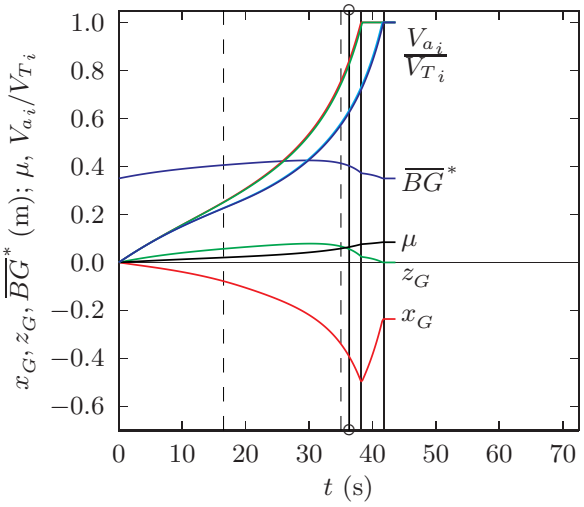

e) *Mass and blow characteristics.*

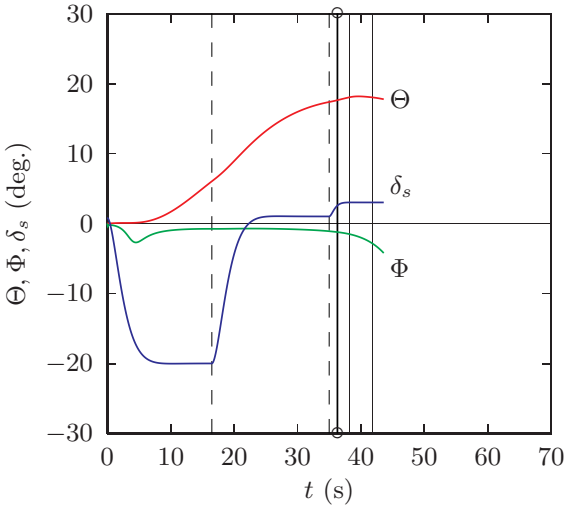

f) *Incidence and sternplane deflection.*

Figure C5 *Simulation 5: The same as S1 except the MBTs are blown using the emergency air supply which provides twice the mass of air as for normal blowing.*

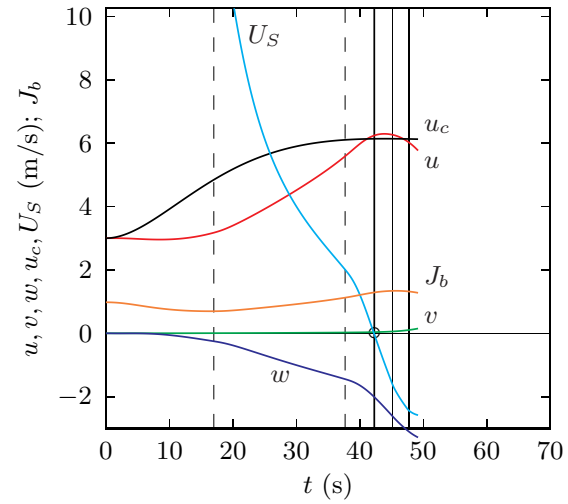

a) *Velocity and propulsion states.*

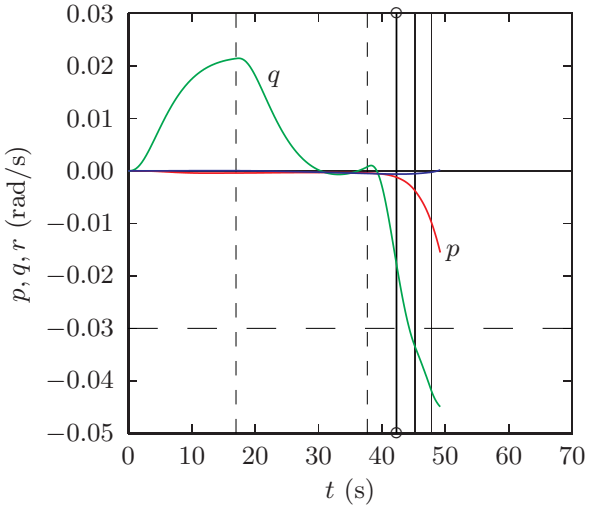

b) *Rotational velocity states.*

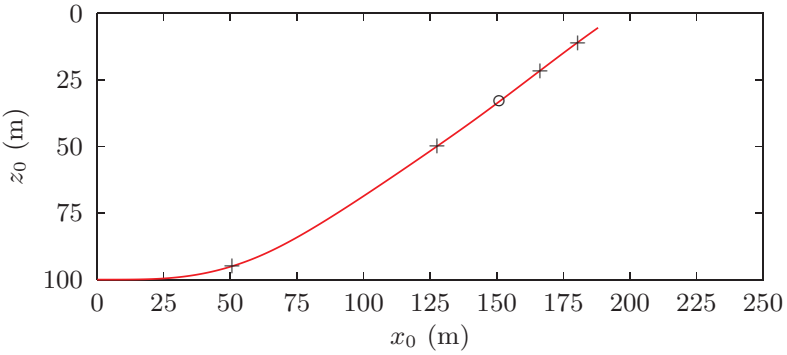

c) *Trajectory, elevation view.*

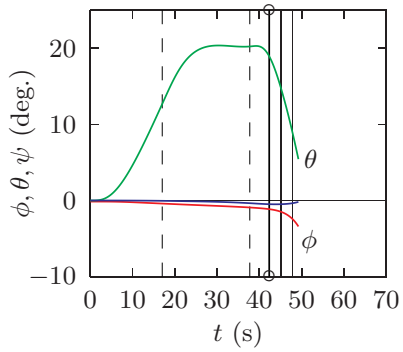

d) *Euler angles.*

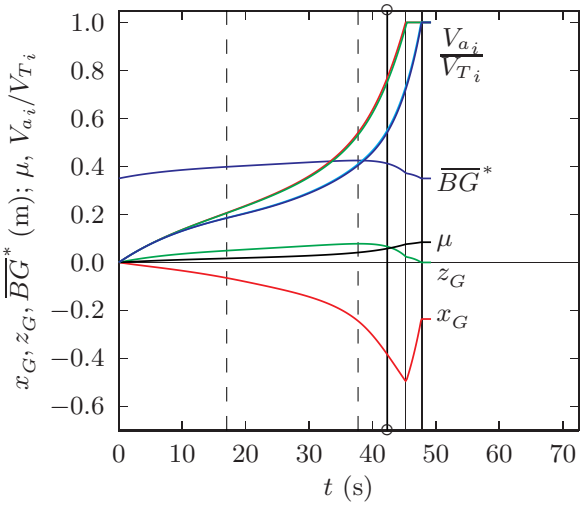

e) *Mass and blow characteristics.*

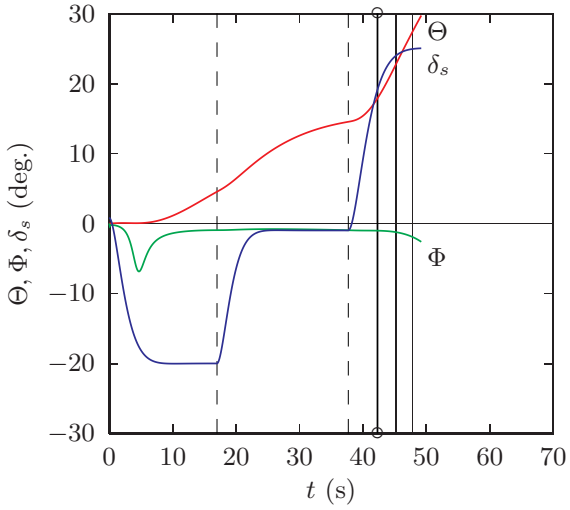

f) *Incidence and sternplane deflection.*

Figure C6 *Simulation 6: The same as S1 except the sternplanes are used to curtail the pitch (once 50 m depth is achieved) so the boat surfaces with a pitch angle under 10 degrees.*

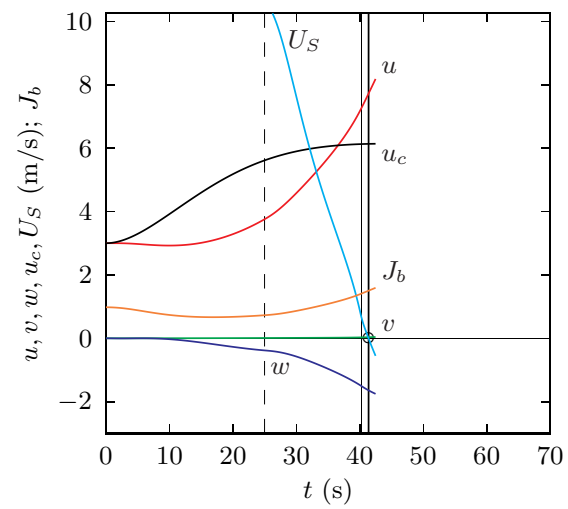

a) *Velocity and propulsion states.*

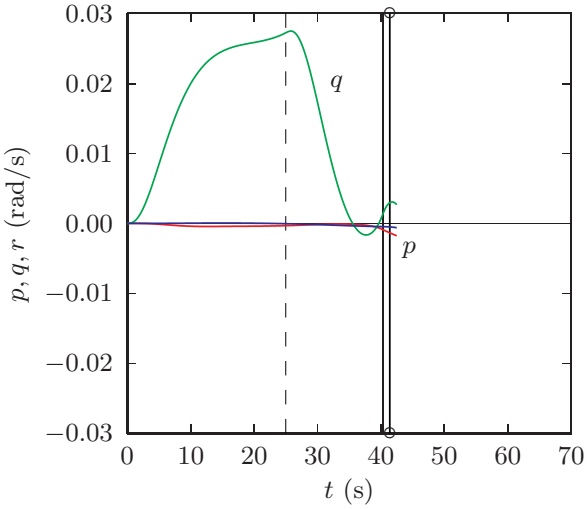

b) *Rotational velocity states.*

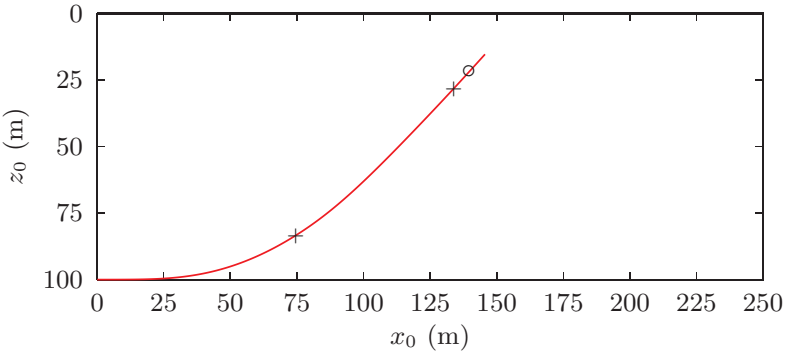

c) *Trajectory, elevation view.*

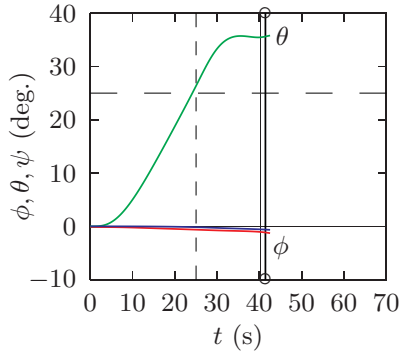

d) *Euler angles.*

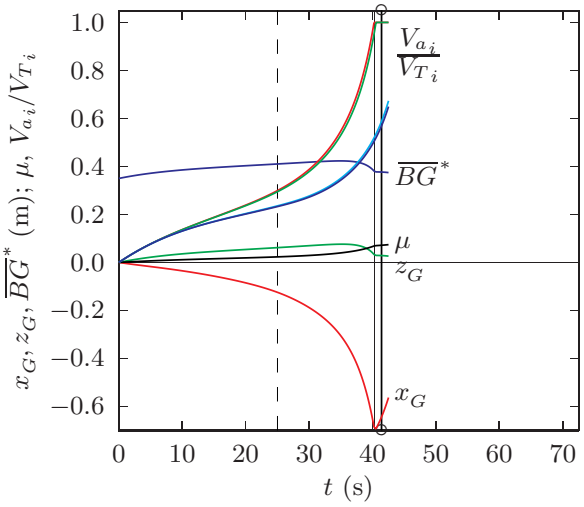

e) *Mass and blow characteristics.*

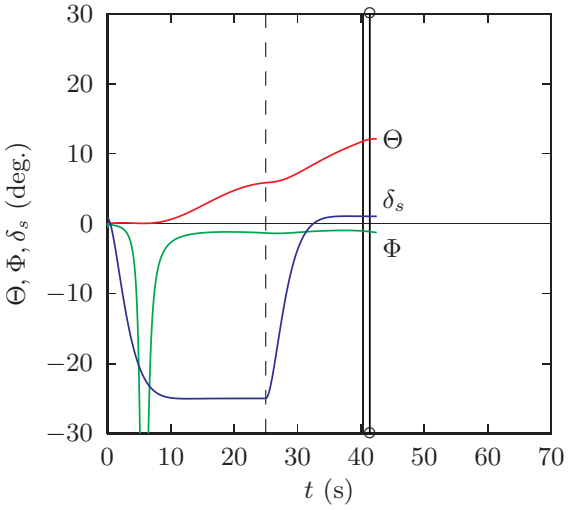

f) *Incidence and sternplane deflection.*

Figure C7 *Simulation 7: The same as S1 except the pitch angle is allowed to increase to 35 degrees.*

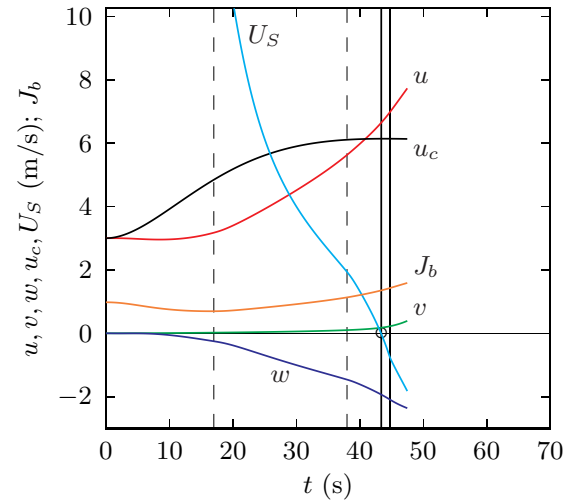

a) *Velocity and propulsion states.*

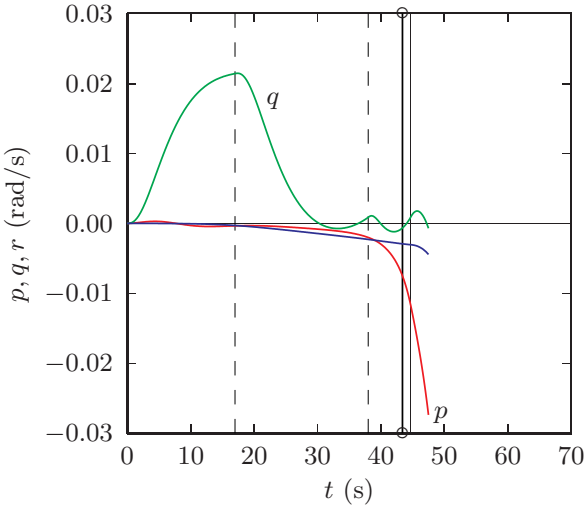

b) *Rotational velocity states.*

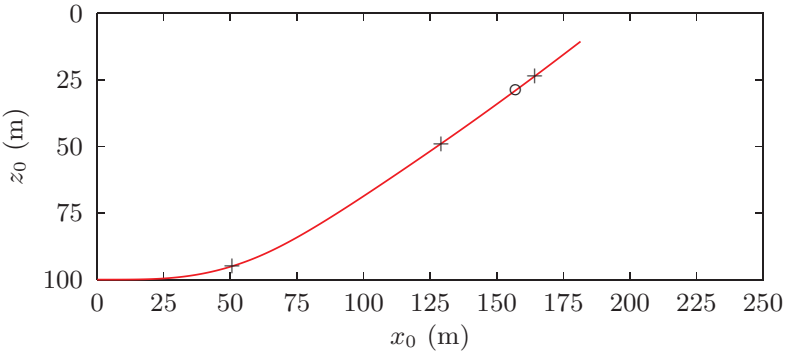

c) *Trajectory, elevation view.*

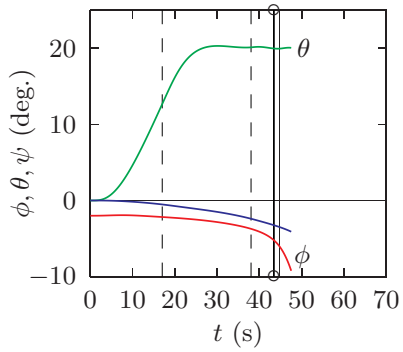

d) *Euler angles.*

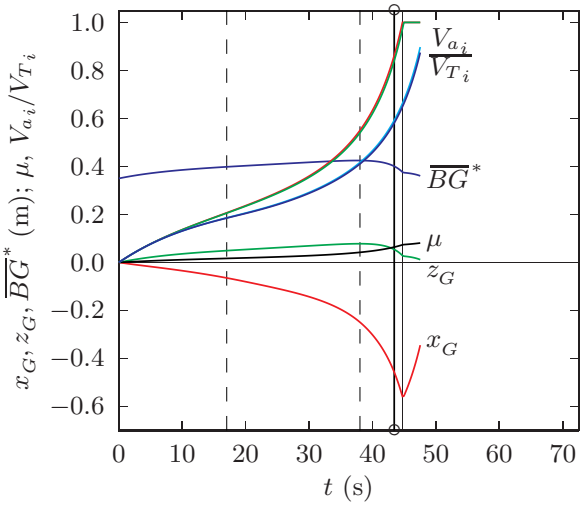

e) *Mass and blow characteristics.*

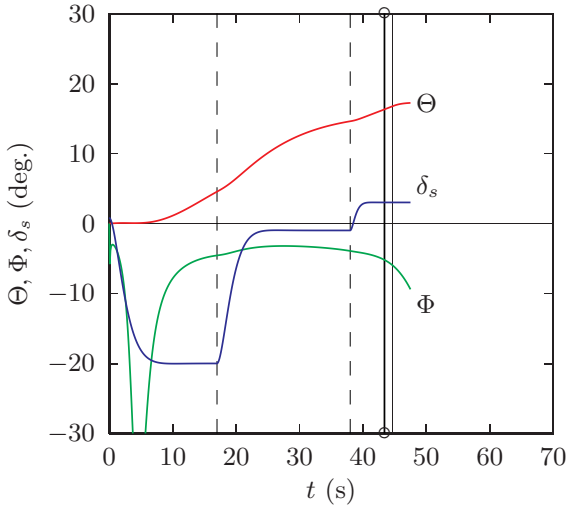

f) *Incidence and sternplane deflection.*

Figure C8 *Simulation 8: The same as S1 except the initial roll angle is increased to 2 degrees by setting y_{G_o} (normally 0) to –11 cm.*

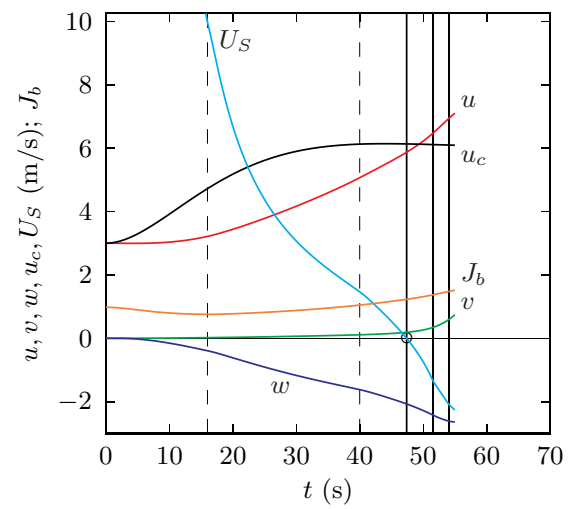

a) *Velocity and propulsion states.*

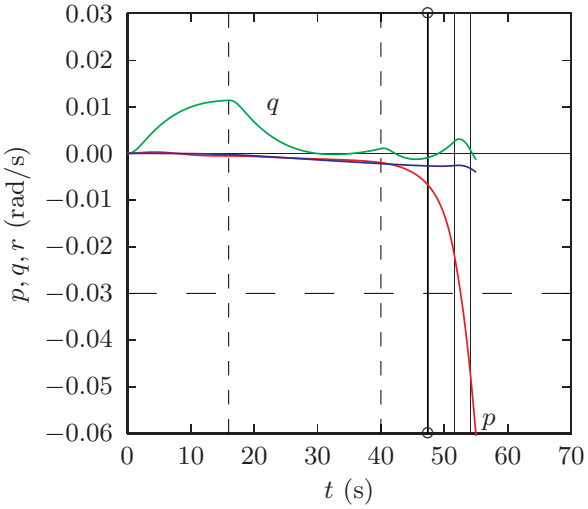

b) *Rotational velocity states.*

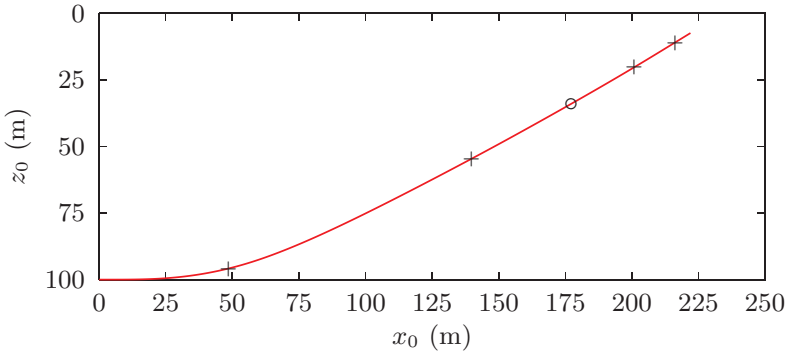

c) *Trajectory, elevation view.*

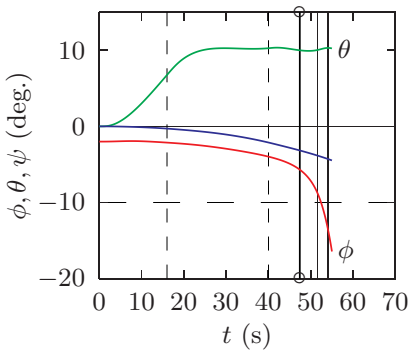

d) *Euler angles.*

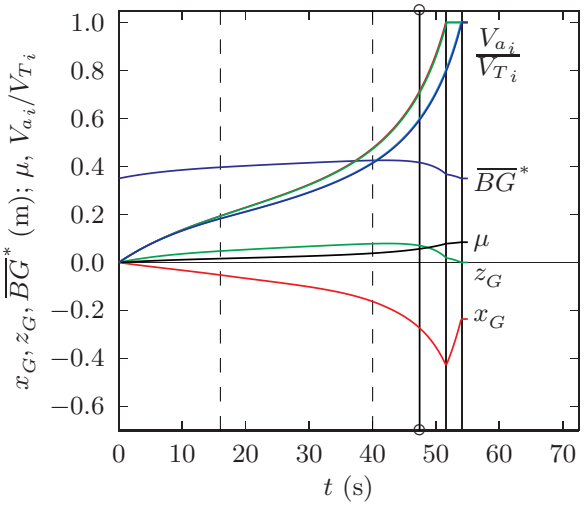

e) *Mass and blow characteristics.*

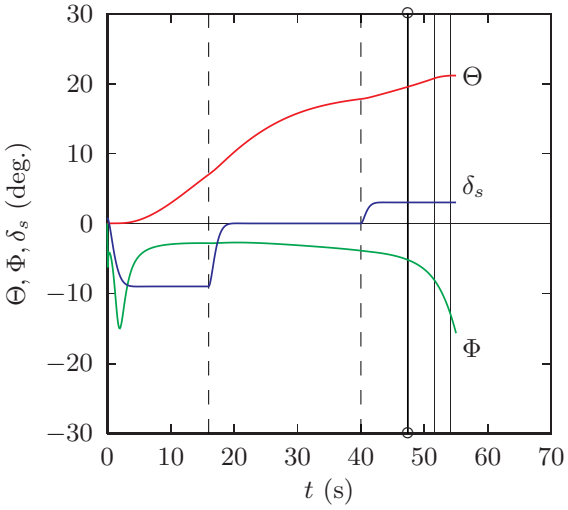

f) *Incidence and sternplane deflection.*

Figure C9 *Simulation 9: The same as S8 except the sternplanes are used to limit the pitch angle to 10 degrees throughout the maneuver.*

This page intentionally left blank.

DOCUMENT CONTROL DATA

(Security classification of title, body of abstract and indexing annotation must be entered when the overall document is classified)

1. ORIGINATOR (the name and address of the organization preparing the document. Organizations for whom the document was prepared, e.g. Centre sponsoring a contractor's report, or tasking agency, are entered in section 8.)

DRDC Atlantic

2. SECURITY CLASSIFICATION (overall security classification of the document including special warning terms if applicable).

UNCLASSIFIED

3. TITLE (the complete document title as indicated on the title page. Its classification should be indicated by the appropriate abbreviation (S,C,R or U) in parentheses after the title).

Modelling and Simulating Unsteady Six Degrees-of-Freedom Submarine Rising Maneuvers

4. AUTHORS (Last name, first name, middle initial. If military, show rank, e.g. Doe, Maj. John E.)

George D. Watt

5. DATE OF PUBLICATION (month and year of publication of document)	6a. NO. OF PAGES (total containing information Include Annexes, Appendices, etc).	6b. NO. OF REFS (total cited in document)
February 2007	67	17

7. DESCRIPTIVE NOTES (the category of the document, e.g. technical report, technical note or memorandum. If appropriate, enter the type of report, e.g. interim, progress, summary, annual or final. Give the inclusive dates when a specific reporting period is covered).

DRDC Atlantic Technical Report

8. SPONSORING ACTIVITY (the name of the department project office or laboratory sponsoring the research and development. Include address).

Defence R&D Canada – Atlantic
PO Box 1012
Dartmouth, NS, Canada B2Y 3Z7

9a. PROJECT OR GRANT NO. (if appropriate, the applicable research and development project or grant number under which the document was written. Please specify whether project or grant).	9b. CONTRACT NO. (if appropriate, the applicable number under which the document was written).
Project 11GP03	

10a ORIGINATOR'S DOCUMENT NUMBER (the official document number by which the document is identified by the originating activity. This number must be unique to this document.)	10b OTHER DOCUMENT NOs. (Any other numbers which may be assigned this document either by the originator or by the sponsor.)
DRDC Atlantic TR 2007-008	

11. DOCUMENT AVAILABILITY (any limitations on further dissemination of the document, other than those imposed by security classification)

(X) Unlimited distribution
( ) Defence departments and defence contractors; further distribution only as approved
( ) Defence departments and Canadian defence contractors; further distribution only as approved
( ) Government departments and agencies; further distribution only as approved
( ) Defence departments; further distribution only as approved
( ) Other (please specify):

12. DOCUMENT ANNOUNCEMENT (any limitation to the bibliographic announcement of this document. This will normally correspond to the Document Availability (11). However, where further distribution (beyond the audience specified in (11) is possible, a wider announcement audience may be selected).

13. ABSTRACT (a brief and factual summary of the document. It may also appear elsewhere in the body of the document itself. It is highly desirable that the abstract of classified documents be unclassified. Each paragraph of the abstract shall begin with an indication of the security classification of the information in the paragraph (unless the document itself is unclassified) represented as (S), (C), (R), or (U). It is not necessary to include here abstracts in both official languages unless the text is bilingual).

DRDC Atlantic is collaborating with ANSYS Canada and the University of New Brunswick to develop an unsteady, six degrees-of-freedom, Reynolds Averaged Navier-Stokes (RANS) submarine maneuvering simulation capability. Initially, this is being used to evaluate emergency rising maneuvers. During these maneuvers, high negative angles of attack can occur which result in a roll instability not previously predicted by quasi-steady modelling. The objective of the RANS simulation is to reproduce the instability and investigate mitigation strategies.

Models for weight and buoyancy when blowing, high incidence propulsion, and appendage and propulsion activation are presented and tested. A high incidence, quasi-steady, coefficient based hydrodynamic model used in previous stability analyses is also presented. These models are used for evaluating stability, testing the system models, and investigating different maneuvering scenarios in preparation for carrying out the computationally intensive RANS simulations. These preliminary investigations suggest the initial roll angle prior to blowing ballast, coupled with the roll instability and low pitch angles, plays an important role in the emergence roll angle.

14. KEYWORDS, DESCRIPTORS or IDENTIFIERS (technically meaningful terms or short phrases that characterize a document and could be helpful in cataloguing the document. They should be selected so that no security classification is required. Identifiers, such as equipment model designation, trade name, military project code name, geographic location may also be included. If possible keywords should be selected from a published thesaurus. e.g. Thesaurus of Engineering and Scientific Terms (TEST) and that thesaurus-identified. If it not possible to select indexing terms which are Unclassified, the classification of each should be indicated as with the title).

submarine hydrodynamics
maneuvering
simulations
six degrees-of-freedom
rising stability
blowing ballast
propulsion
high incidence

This page intentionally left blank.

Defence R&D Canada

Canada's leader in defence
and National Security
Science and Technology

R & D pour la défense Canada

Chef de file au Canada en matière
de science et de technologie pour
la défense et la sécurité nationale

www.drdc-rddc.gc.ca